



3 4456 0055347 0

ORNL/Sub/83-43374/1/V4

# ornl

**OAK RIDGE  
NATIONAL  
LABORATORY**

**MARTIN MARIETTA**

**STUDY TO ASSESS THE EFFECTS OF NUCLEAR  
SURFACE BURST ELECTROMAGNETIC PULSE  
ON ELECTRIC POWER SYSTEMS**

**PHASE I  
FINAL REPORT**

OAK RIDGE NATIONAL LABORATORY  
CENTRAL RESEARCH LIBRARY  
CIRCULATION SECTION  
4508 ROOM 111  
**LIBRARY LOAN COPY**  
DO NOT TRANSFER TO ANOTHER PERSON  
If you wish someone else to see this  
report, send in name with report and  
the library will arrange a loan.

**LIBRARY  
PROGRAM**

OPERATED BY  
MARTIN MARIETTA ENERGY SYSTEMS, INC.  
FOR THE UNITED STATES  
DEPARTMENT OF ENERGY

Printed in the United States of America. Available from  
National Technical Information Service  
U.S. Department of Commerce  
5285 Port Royal Road, Springfield, Virginia 22161  
NTIS price codes—Printed Copy: A07 Microfiche A01

This report was prepared as an account of work sponsored by an agency of the United States Government. Neither the United States Government nor any agency thereof, nor any of their employees, makes any warranty, express or implied, or assumes any legal liability or responsibility for the accuracy, completeness, or usefulness of any information, apparatus, product, or process disclosed, or represents that its use would not infringe privately owned rights. Reference herein to any specific commercial product, process, or service by trade name, trademark, manufacturer, or otherwise, does not necessarily constitute or imply its endorsement, recommendation, or favoring by the United States Government or any agency thereof. The views and opinions of authors expressed herein do not necessarily state or reflect those of the United States Government or any agency thereof.

ORNL/Sub/83-44374/1/V4  
Dist. Category UC-97 a,b,c

Energy Division

STUDY TO ASSESS THE EFFECTS OF NUCLEAR SURFACE  
BURST ELECTROMAGNETIC PULSE ON  
ELECTRIC POWER SYSTEMS  
PHASE I  
FINAL REPORT

J. R. Legro  
N. C. Abi-Samra  
A. R. Hileman  
F. M. Tesche

Date Published - September 1985

Prepared for the U.S. Department of Energy, Assistant  
Secretary for Conservation and Renewable Energy, Office  
of Energy Storage and Distribution, Electric Energy  
Systems Program.

Report Prepared By

Westinghouse Electric Corporation  
Advanced Systems Technology  
777 Penn Center Blvd.  
Pittsburgh, PA 15235  
under  
Subcontract 19X-43374C

for

P. R. Barnes, Project Manager  
Power Systems Technology Program  
Energy Division  
Oak Ridge National Laboratory  
Oak Ridge, Tennessee 37831  
operated by  
MARTIN MARIETTA ENERGY SYSTEMS, INC.  
for the  
U.S. DEPARTMENT OF ENERGY  
under Contract No. DE-AC05-84OR21400



3 4456 0055347 0



## FOREWORD

The Division of Electric Energy Systems (EES) of the United States Department of Energy (DOE) has formulated a program for the research and development of technologies and systems for the assessment, operation, and control of electric power systems when subjected to electromagnetic pulse (EMP). The DOE/EES EMP program plan is documented in a DOE report entitled, "Program Plan for Research and Development of Technologies and Systems for Electric Power Systems Under the Influence of Nuclear Electromagnetic Pulses," DOE/NBB-003, May, 1983. The research documented in this Oak Ridge National Laboratory (ORNL) report was conducted under program plan elements E1, "EMP Surge Characterization and Effects" and E2, "EMP Assessment Methodology Development and Testing."

The research documented in this volume considers electric power system models and methodology applicable to explore the interaction between nuclear surface burst electromagnetic pulse (SREMP) and civilian electric utility systems. The results of this work will be used in subsequent phases of the research program to simulate such interaction, to assess the possible consequences and to explore relevant mitigation techniques.

All data pertaining to SREMP environments have been obtained from public domain documents and unclassified source materials. Such information is presented herein for illustrative purposes only and does not represent actual weapon characteristics or maximum threat environments.

This document is Volume 4 of a four volume series that describes an EMP assessment methodology for civilian electric power systems. Volume 1 is an Executive Summary, Volume 2 discusses high-altitude EMP (HEMP), Volume 3 discusses MHD-EMP, and Volume 4, this document, discusses nuclear surface burst, source region EMP (SREMP).

## ACKNOWLEDGEMENTS

The research for this report was sponsored by the Division of Electrical Energy Systems, United States Department of Energy, under contract DE-AC05-84OR21400 with Martin Marietta Energy Systems, Inc. as operator of the Oak Ridge National Laboratory. The work was performed by Westinghouse Advanced Systems Technology under subcontract 19X-43374C with Martin Marietta Energy Systems, Inc.

The authors wish to acknowledge and thank Mr. K. W. Klein of the United States Department of Energy, Mr. P. R. Barnes and Mr. P. A. Gnadl of the Oak Ridge National Laboratory. Thanks are also expressed to Ms. C. Brown, Ms. B. Ayers, and Mr. J. E. Lokay of Westinghouse Advanced Systems Technology for their assistance in the preparation of this document.

## CONTENTS

	<u>Page</u>
FOREWORD.....	iii
ACKNOWLEDGMENTS.....	iv
LIST OF FIGURES.....	vii
LIST OF TABLES.....	x
ABSTRACT.....	xi
1. INTRODUCTION.....	1
2. SURFACE BURST EFFECTS.....	5
2.1 Introduction.....	5
2.2 Blast Craterization.....	6
2.3 Fireball and Thermal Radiation.....	8
2.4 Blast Wave Phenomena.....	11
2.5 Source Region Spatial Characterization.....	16
2.6 Summary.....	19
3. SREMP ENVIRONMENTAL DESCRIPTION.....	24
3.1 Introduction.....	24
3.2 Compton Current and Air Conductivity.....	24
3.3 Symmetric Source Region SREMP Field Characterization.....	31
3.4 Surface Burst Source Region SREMP Field Characterization.....	34
3.5 Summary.....	36
4. SREMP COUPLING TO POWER SYSTEMS.....	62
4.1 Introduction.....	62
4.2 Electromagnetic Field Coupling Within The Source Region.....	63
4.3 Radiated Field Coupling Outside The Source Region.....	68
4.4 Summary.....	82
5. SREMP ASSESSMENT METHODOLOGY.....	84
5.1 Introduction.....	84
5.2 Assessment Initial Conditions.....	87
5.3 SREMP Radiated Field Analysis.....	91
5.4 Source Region Surge Assessment.....	93
5.5 System Stability Analysis.....	96
5.6 Summary.....	96

CONTENTS (Cont'd)

	<u>Page</u>
6. SREMP COMPUTER CODES AND MODELS.....	99
6.1 Introduction.....	99
6.2 Simulation Codes.....	100
6.3 Simulation Models.....	101
6.4 Summary.....	112
7. CONCLUSIONS AND RECOMMENDATIONS.....	114
8. BIBLIOGRAPHY.....	117

## LIST OF FIGURES

<u>Figure</u>	<u>Page</u>
1 Physical dimensions of interest due to surface burst craterization effects.....	7
2 Time dependence for the fireball rate of emission for thermal radiation.....	9
3 Fireball surface temperature variation as a function of time.....	10
4 Air shock wave dynamics for a surface nuclear burst.....	13
5 Air shock wave orientation for a surface nuclear burst.....	14
6 Spatial relationship of ejected material, fireball and shock wave radial contours.....	18
7 Conjecture of nominal source region spatial characterization and select peak overpressure distances as a function of weapon yield.....	20
8 Conjecture of source region composite spatial characterization and $2.4 \times 10^4$ N/m <sup>2</sup> (3.5 psi) for weapon yields from 100 kilotons to 10,000 kilotons.....	21
9 Approximate spatial relationship of selected weapon effects distances for a one-megaton surface burst.....	23
10 The Compton Process.....	26
11 Charge separation model illustrating the creation of the radial electric field ( $E_r$ ) via the Compton Process.....	27
12 Charge separation model for a perfectly symmetric source region.....	33
13 Spherical coordinate system for source region field characterization.....	37
14 Source region characterization during diffusion stage.....	39
15 General time waveform for $E_r$ and $B_\phi$ in the surface burst source region.....	42
16 Longmire calculation of transient phenomena due to 10-KT weapon (nominal).....	43
17 Longmire calculation of transient phenomena due to 10-KT weapon (nominal).....	44
18 Longmire calculation of transient phenomena due to 1-MT weapon (nominal).....	45
19 Longmire calculation of transient phenomena due to 1-MT weapon (nominal).....	46
20 Source region model depicting region boundary and characterization of vertically polarized electric field in the radiated "far" region.....	48
21 Ratio of horizontal to vertical SREMP radiated electric field components.....	51
22 Hypothetical time domain waveforms for the $E_z$ radiated field component based on Bell parameters.....	53

23	Calculated time domain waveforms for the $E_x$ radiated field component based on Bell parameters.....	54
24	Frequency domain plot for hypothetical $E_z$ and $E_x$ radiated field components based on Bell parameters.....	55
25	Typical time domain waveform of Radasky and Smith for SREMP radiated $E_z$ field.....	57
26	Typical time domain waveforms for $E_z$ radiated field component for the Radasky shape and $Z$ Bell parameters.....	58
27	Typical time domain waveforms for $E_x$ radiated field component for the Radasky shape and $X$ Bell parameter for $\sigma_g=0.01$ mhos/meter.....	59
28	Typical time domain waveforms for $E_x$ radiated field component for the Radasky shape and $X$ Bell parameter for $\sigma_g=0.001$ mhos/meter.....	60
29	Longwire example of transient surge current for a overhead line and an underground cable, each 1000 meters in length, in a nuclear surface burst source region.....	66
30	Graham calculation of transient surge current into a 0.1 ohm load located at the end of a 2500 meter long overhead line in a nuclear surface burst source region.....	67
31	Representation of the current surge formed within the source region on an overhead line by a Norton equivalent source located at the source region boundary.....	69
32	Physical geometry and electrical equivalent circuit for an overhead line excited by SREMP.....	71
33	Orientation of an arbitrary overhead line located outside the source region (plan view).....	78
34	Geometry of an arbitrarily orientated, straight, overhead line outside the source region.....	81
35	Overview of methodology for SREMP assessment for civilian electric utility systems.....	86
36	Conjecture of nuclear surface burst source region (solid circle), non-SREMP initial damage (shaded circle) and radiated field assessment area superimposed on an arbitrary power system grid.....	88
37	Overview of source region surge assessment methodology.....	94
38	Overview of system stability assessment methodology.....	97
39	Typical surge voltage transferred through the transformer.....	104
40	Electrostatic model for a transformer for the analysis of the radiated field effects.....	104
41	Complete model of a transformer for the analysis of the radiated field effects.....	105
42	Model for a three winding transformer for the analysis of the source region surge effects.....	105
43	Models used for distribution loads.....	108
44	Model for a SiC arrester.....	108
45	Effect of wavefront on switching CFO.....	111

46	Comparison of lightning and switching CFO.....	111
47	Comparison of CFO and withstand voltage ( $V_3$ ).....	113
48	Graphic depiction of stress-strength analysis used to determine the probability of flashover.....	113

## LIST OF TABLES

<u>Table</u>		<u>Page</u>
1	Approximate Crater Depth, Radius and Ejected Material Radius for Nuclear Surface Burst.....	7
2	Approximate Fireball Radius and Elapsed Time to Maximum Surface Temperature as a Function of Yield.....	11
3	Peak Overpressure, Dynamic Pressure and Maximum Wind Velocity in Air at Sea Level for Ideal Shock Front.....	15
4	Radial Distance, Arrival Time and Duration for Select Peak Overpressure as a Function of Weapon Field.....	17
5	Approximate average energies and effective absorption lengths in air of gammas source components.....	25
6	Bell Parameters for a Vertically Polarized Electric Field ( $E_z$ ) at a Source Region Boundary.....	52
7	Parameters for Overhead Line Calculation of Open Circuit Voltage Induced by SREMP Radiated Field.....	76
8	Radiated Electric Field Comparison.....	92

STUDY TO ASSESS THE EFFECTS OF NUCLEAR SURFACE BURST  
ELECTROMAGNETIC PULSE ON ELECTRIC  
POWER SYSTEMS

J. R. Legro  
N. C. Abi-Samra  
A. R. Hileman  
F. N. Tesche\*

ABSTRACT

The surface burst of a nuclear device, within the continental United States, can expose nearby portions of the civilian electric utility system to transient, source region electromagnetic pulse (SREMP). This threat is in addition to any coincident, non-SREMP damage to the system due to craterization, fireball, blast wave and radiation. The unique properties of the civilian electric power system, such as its complex electrical interconnection over a vast geographic area, strongly suggests that a separate SREMP assessment methodology should be prepared with specific focus on the power system.

This volume documents a preliminary research effort to: (1) investigate the nature and coupling of the SREMP environment to electric power systems, (2) define the attributes of system response, and (3) document the development of a unified methodology to assess equipment and systematic vulnerability.

The research, to date, does not include an attempt to quantify power system performance in an SREMP environment. This effort has been to develop the analytical tools and techniques necessary to perform such assessments at a later time. It is anticipated that the SREMP methodology will be incorporated into a comprehensive EMP assessment process to investigate total system risk.

---

\*LuTech, Incorporated, Lafayette, CA



## 1. INTRODUCTION

In recent years, there has been a growing awareness on the part of the electric utility industry and relevant government agencies concerning the potential impact of electromagnetic pulse (EMP) on the civilian electric power system. The concern has primarily focused on the impact of very early-time transient electromagnetic fields produced by the burst of a nuclear weapon outside the earth's atmosphere. The EMP phenomena is not limited to this high-altitude burst scenario. Spatially local EMP signals are also produced in and around the surface burst of a nuclear weapon. This type of electromagnetic transient has been defined under the term: source region electromagnetic pulse (SREMP).

Since the United States electric power network of generation, transmission and distribution may be exposed to SREMP phenomena, it is of critical importance to national security that a methodology be developed to assess the vulnerability of electric power systems to this unique, externally imposed, electromagnetic transient environment. The creation of such an assessment technique would enable all interested parties to quantify the potential SREMP risk to existing systems and explore mitigating strategies. SREMP assessments have been performed for other types of electrical systems such as found in military weapon and communication facilities. The unique properties of the civilian electric power system, such as its complex electrical interconnection over a vast geographic area strongly indicates that a separate SREMP assessment methodology should be prepared with specific focus on the electric power system. All EMP methodology developments begin with an appreciation of the nuclear source region.

An elementary definition of the "source (deposition) region" is: that space related to or surrounding a nuclear burst where an electromagnetic pulse (EMP) is produced. Within the source region, the initial EMP generation mechanism can be understood from the Compton process. This physical model is dominated by the production of gamma radiation ( $\gamma$ -radiation) from the weapon itself and from weapon produced neutrons

and their interaction with air and ground materials. The collision of gamma photons and air molecules liberates high-energy free Compton (recoil) electrons moving away from their parent ions. Additional interactions between the Compton electrons and the atmospheric environment creates an electrically conductive medium of low-energy (secondary) electrons and positive/negative ion pairs. The result of large-scale charge separation is the creation of a strong radial non-radiated electric field within the source region.

Any asymmetry of the source region, due to environmental parameters, will result in a net radiated EMP transient. These transient fields, created by the charge motion within the source region, will also exist outside the region. Such asymmetry can be produced by 1) an air/earth boundary (surface bursts), 2) variations in atmospheric density (mid-altitude bursts) and 3) the space/atmospheric interface in combination with the earth's geomagnetic field (high-altitude bursts).

The assessment of risk to the electric utility power system due to EMP must initially consider the threat to power system components located within the source region and that threat associated with power system components located outside the source region but exposed to the radiated EMP transient fields. For a nuclear weapon burst whose origin is essentially outside of the earth's atmosphere, the source region is created at an altitude between 20 and 40 kilometers above the earth's surface. Since none of the electric power system is located in this source region, the system threat is limited to the radiated EMP fields. The initial transient phenomena associated with the above radiated fields has been defined as early-time "high-altitude electromagnetic pulse" (HEMP). This initial HEMP is immediately followed by an intermediate-time HEMP due to scattered gamma photons and inelastic gammas from weapon neutrons. At much later times, the quasi-static transient of the same event has been defined as "magnetohydrodynamic-electromagnetic pulse" (MHD-EMP). Assessment methodologies required to investigate the impact of HEMP and MHD-EMP on electric power systems are presented in separate volumes of this report.

For a nuclear burst whose origin is located within the earth's atmosphere, where the source region does not intersect the surface and/or the electric power system, the threat to the electric power system is also limited to a radiated EMP field. The greater symmetry of this source region results in a relatively weak radiated field when compared to high-altitude and near-surface burst locations. In this research effort, the EMP threat associated with a mid-altitude (air) burst will not be considered since: 1) the source region and the power system location are not coincident and 2) the radiated EMP field is significantly less than those associated with high-altitude or surface burst events.

It is in the case of a surface (or near-surface) contact burst that portions of the electric power system can physically exist within the source region while the remainder of the system, to some distance, will be exposed to the corresponding radiated EMP transient. Thus, for the purpose of this report, source region definition shall be limited to that associated with the surface burst of a nuclear weapon.

In contrast to high-altitude bursts, wherein the HEMP may constitute the only threat aspect to the electric power system, surface bursts will cause massive physical damage to system equipment located near the origin in addition to any SREMP exposure. Section 2 of this report briefly discusses major surface burst effects other than SREMP in order to place the spatial extent of each effect in perspective and introduces a concept known as "balanced survivability" for power system assessment. Phenomena known as "nuclear lightning" and its potential impact on electric power systems is outside the present scope of investigation and is not considered in this report.

Section 3 presents an overview of the physical models associated with the production of an EMP within the source region. The spatial and time dependent characteristics of the Compton current density ( $J_r^C$ ) and air conductivity ( $\sigma$ ) are developed as a prelude to field descriptions via Maxwell's equations. Within the source region, the total field definition is shown to be a function of a radial electric field ( $E_r$ ), a

vertically polarized electric field ( $E_{\theta}$ ) and an azimuthally-orientated magnetic field ( $H_{\phi}$ ). At the source region spatial boundary, the radial electric field produced within the source region is small enough so that the radiated field beyond the boundary can be defined as a vertically polarized electric field and an associated magnetic field propagating in air over a lossy ground.

In Section 4, the coupling of SREMP transient fields to power system lines and facilities is explored. Knowledge of the coupling mechanisms allows for definitions of the transient overvoltage/over-current surges induced on illuminated conductors within and outside of the source region. It is shown that surges induced within SREMP illuminated areas can propagate via transmission and distribution networks to affect equipment beyond the illumination boundary.

A comprehensive methodology is documented in Section 5 to assess the impact of SREMP on electric power systems. The methodology contains a recommended format for surface burst effects environmental definition and includes the potential impact of non-SREMP threats as well as potential SREMP equipment damage and system operational upset.

In Section 6, power system models and analysis techniques, relevant to surface burst/SREMP assessment, are presented. This section also includes a description of digital computer codes needed to perform a system-wide study.

The report concludes with a summary of recommended areas of additional research to refine both the environmental definition and assessment methodology.

The investigation, to date, does not include any attempt to quantify power system performance in a surface burst/SREMP environment. This Phase I effort has been directed to the development of tools and techniques necessary to perform such assessments in subsequent phases. The development of a validated methodology is the prerequisite to consistent and meaningful risk assessment.

## 2. SURFACE BURST EFFECTS

### 2.1 Introduction

In the event of a surface (or near surface) burst of a nuclear weapon, those elements of the electric power system near the burst point will receive massive physical damage in addition to illumination by transient source-region EMP (SREMP) fields. Any realistic assessment of the SREMP threat to power systems must place this singular aspect of the burst in the context of the entire range of threats.

This section of the report briefly discusses the major initial damage aspects of the surface burst. In addition to the spatial characterization of the source region, parameters of interest include:

- Spatial extent of craterization
- Fireball and thermal radiation
- Blast wave phenomena

This report does not attempt to quantify the physical damage to affected portions of the power system due to the above parameters. The potential spatial extent of such damage is presented in order to place the spatial aspects of SREMP illumination into context. The primary reference for burst effects, as discussed, is The Effects of Nuclear Weapons-1977 [1]. Parameters are calculated by use of the nuclear bomb effects slide-rule computer provided with the above reference.

For those facilities and systems designed to withstand the total range of nuclear surface burst effects, the principle of "balanced survivability" is an important concept. Briefly stated, this principle requires that the subject system is hardened to withstand all weapon threats, including SREMP, to a level at which the system will continue to perform its intended function(s). The civilian power system, as presently constituted, has not been specifically designed to withstand the blast effects of a surface nuclear weapon. Within some radial distance from the burst, the power system will be destroyed and/or

otherwise damaged to the point where the impacted section can no longer perform its intended function(s). The SREMP threat becomes significant only for that area outside of the damage zone, where SREMP constitutes the major mechanism for additional damage and/or system operation upset. The methodology developed in this report will use the principle of "balanced survivability" to bound the spatial limits of SREMP risk assessment for electric utility systems.

## 2.2 Blast Craterization

The surface (or near surface) burst of a nuclear weapon will cause significant craterization in the earth directly beneath, and to some distance away from, the burst point. This physical effect is enhanced by a larger radius of ejected material surrounding the crater. As a first approximation, the extent of craterization is a function of:

- height of burst
- weapon yield
- soil conditions

The craterization is maximum for a burst at the surface of the earth. The depth and radius of the crater will be greatest for wet soil (wet soft rock) and least for dry hard rock.

As illustrated in Figure 1 and tabulated in Table 1, for a given height of burst and soil conditions, the amount of craterization is a function of weapon yield. The data presented in Table 1 assumes an intermediate soil condition and a surface burst at sea level.

An obvious conclusion can be drawn; that elements of the power system resident at a distance less than or equal to the radius of ejected material ( $R_E$ ) will be completely destroyed by this effect alone.

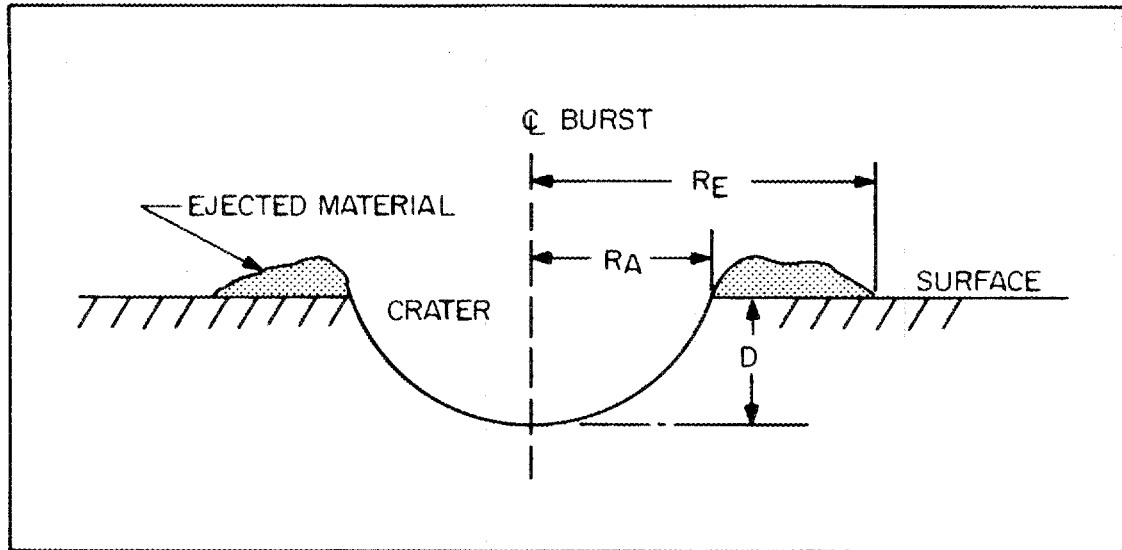


Fig. 1. Physical dimensions of interest due to surface burst craterization effects.

Table 1

APPROXIMATE CRATER DEPTH, RADIUS AND EJECTED MATERIAL RADIUS FOR NUCLEAR SURFACE BURST

Weapon Yield (kt)	Crater Depth (D) (Meters)	Crater Radius ( $R_A$ ) (Meters)	Material Radius ( $R_E$ ) (Meters)
1.0	8.1	19.3	40.3
10.0	16.1	35.4	77.3
100.0	32.2	67.6	153.0
500.0	51.5	112.7	241.5
1000.0	61.2	135.2	289.8
10,000.0	125.6	281.8	644.0
20,000.0	151.3	354.2	772.8

### 2.3 Fireball and Thermal Radiation

Surface burst damage to systems proximate to the point of burst will also occur due to the formation of the fireball and the effects of thermal radiation. The physics associated with this phenomena is a complex issue; but as a first approximation, the extent of physical damage is a function of:

- height of burst
- weapon yield
- atmospheric conditions
- combustion properties of materials

For the surface burst, the prompt source of thermal radiation is in the form of X-rays which are absorbed within a very short distance from the burst point. The energy is then re-emitted from the fireball as a secondary thermal radiation in the ultraviolet, visible, and infrared spectra. As a function of time, the interior temperature of the fireball decreases steadily while the surface temperature initially decreases and then increases for a period of time before it continuously falls. Thus, there are two surface temperature pulses. The second pulse contains almost all of the thermal energy. The relationship of these two thermal pulses is shown as Figure 2.

Extreme temperatures are developed at the surface of the fireball. An example of the temperature variation as a function of time is shown as Figure 3. The data is taken from a 20-kiloton weapon yield.

Of direct interest in our investigation is the maximum radius of the fireball and the time to maximum surface temperature of the second pulse. Table 2 depicts this information as a function of weapon yield.

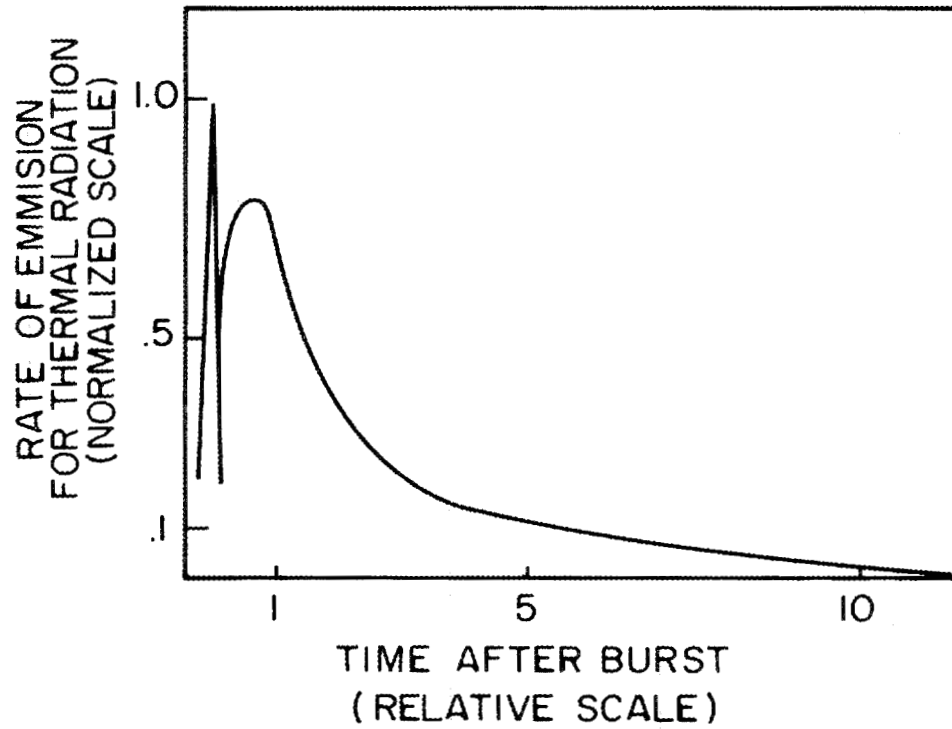


Fig. 2. Time dependence for the fireball rate of emission for thermal radiation [1].

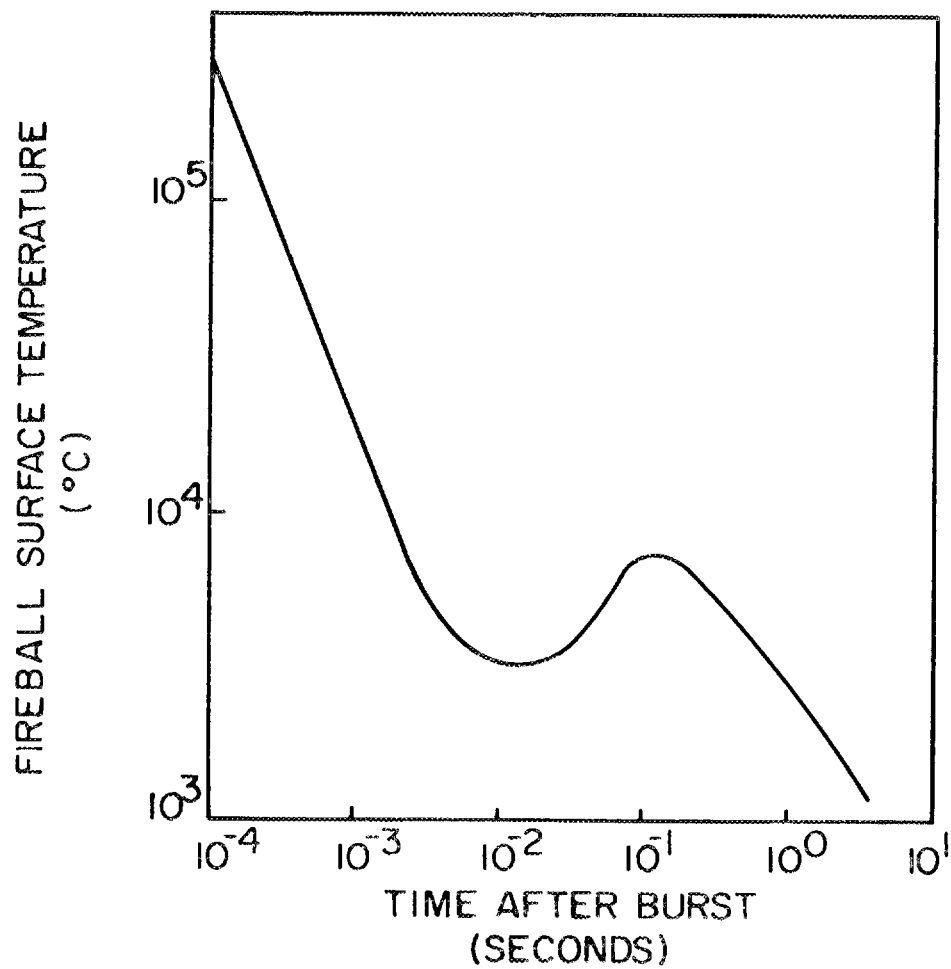


Fig. 3. Fireball surface temperature variation as a function of time [1].

Table 2

APPROXIMATE FIREBALL RADIUS AND ELAPSED TIME TO  
MAXIMUM SURFACE TEMPERATURE AS A FUNCTION OF YIELD

<u>Weapon Yield (kt)</u>	<u>Fireball Radius (Meters)</u>	<u>Elapsed Time (seconds)</u>
1	90	0.043
10	220	0.13
100	550	0.30
500	1030	0.60
1000	1370	0.80
10,000	3380	2.10
20,000	4500	2.80

As with the craterization parameter, surface power system components within or near the fireball radius will suffer complete destruction. Any direct, incremental damage due to SREMP, for components in this location, is not considered.

#### 2.4 Blast Wave Phenomena

The surface burst physical effect that can result in the largest area of damage to power system elements is the blast wave phenomena. The expansion of hot gases in the fireball causes a shock wave to form in air and propagate outward from the burst point. For any structure, a difference in air pressure on separate surfaces of that structure can produce a force and thus, a damaging or destructive effect. The blast wave effect can be quantified as the variation in time and distance of the overpressure as a function of weapon yield.

At the shock front, the maximum value of the phenomena is defined by the term maximum (peak) overpressure expressed in units of Newton/meter<sup>2</sup> (N/m<sup>2</sup>). For many structural types, the degree of damage depends on the drag force associated with the strong winds accompanying the passage of the shock wave. This effect is defined by the term dynamic pressure expressed in the same units. The dynamic pressure is proportional to the square of the wind velocity and to the density of the air behind the shock wavefront.

In order to illustrate time dependent concepts associated with the blast wave, one can consider an observer location at some distance from the burst point. As shown in Figure 4, for some period of time before the shock wall arrives, pressure remains at atmospheric steady-state conditions. At the time of arrival, the relative value of atmospheric pressure and the magnitude of dynamic pressure can be modelled by a step increase. This positive phase is characterized by a strong wind blowing away from the burst point.

At some later time, the wind ceases to blow away from the burst and changes direction such that a negative overpressure (suction) phase is experienced. Still later in time, a change in wind direction again occurs and wind blows away from the blast. This last effect may be due to the expansion of air caused by an increase of temperature at this time.

It is important to note that the magnitude of the dynamic pressure always remains positive since, by definition, this pressure is an absolute force, a measure of the kinetic energy of a certain volume of air behind the shock front.

Another important aspect of the shock wave associated with the surface burst is that the incident wave and reflected wave are always merged such that a single shock wave is formed as shown in Figure 5. Near the surface, the wave front is essentially vertical; the transient winds behind the front will blow in a horizontal direction.

Damage to power system components as a result of the blast wave phenomena will occur due to the overpressure (dynamic pressure) of the event and debris carried along with the event by the wind. A first approximation as to the spatial extent of damage can be obtained from the quantification of maximum dynamic pressure and maximum wind velocity as a function of peak overpressure. This information is tabulated for select values in Table 3.

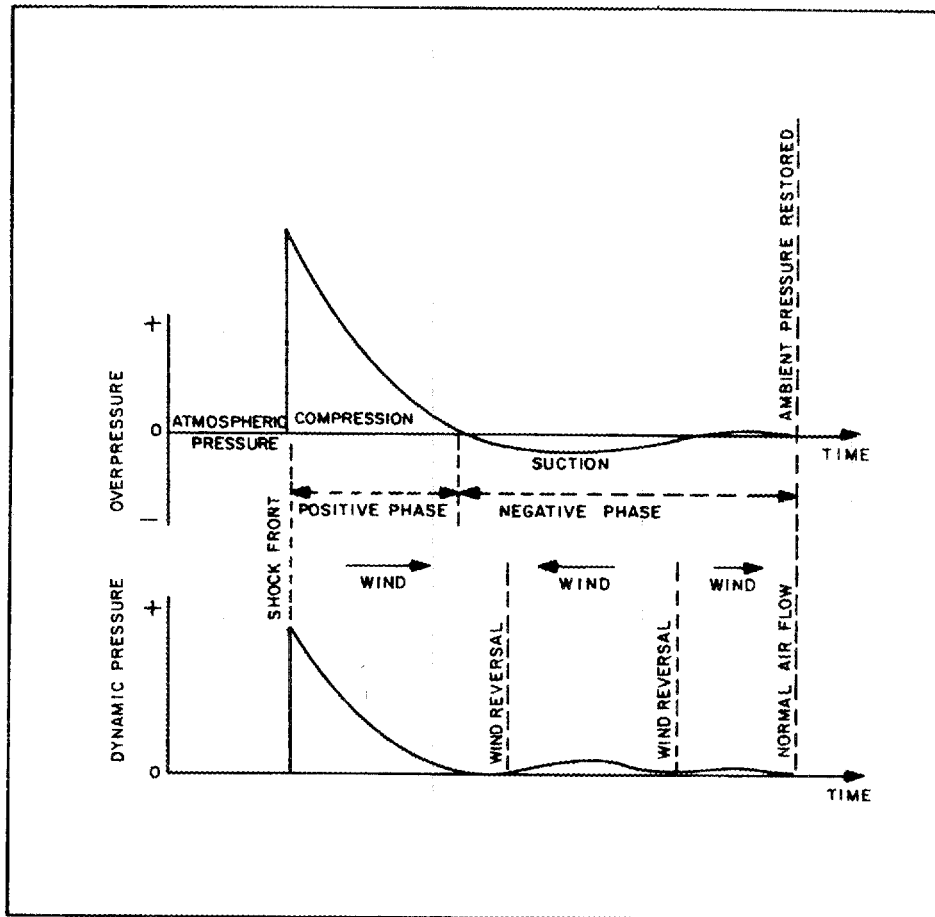


Fig. 4. Air shock wave dynamics for a surface nuclear burst [1].

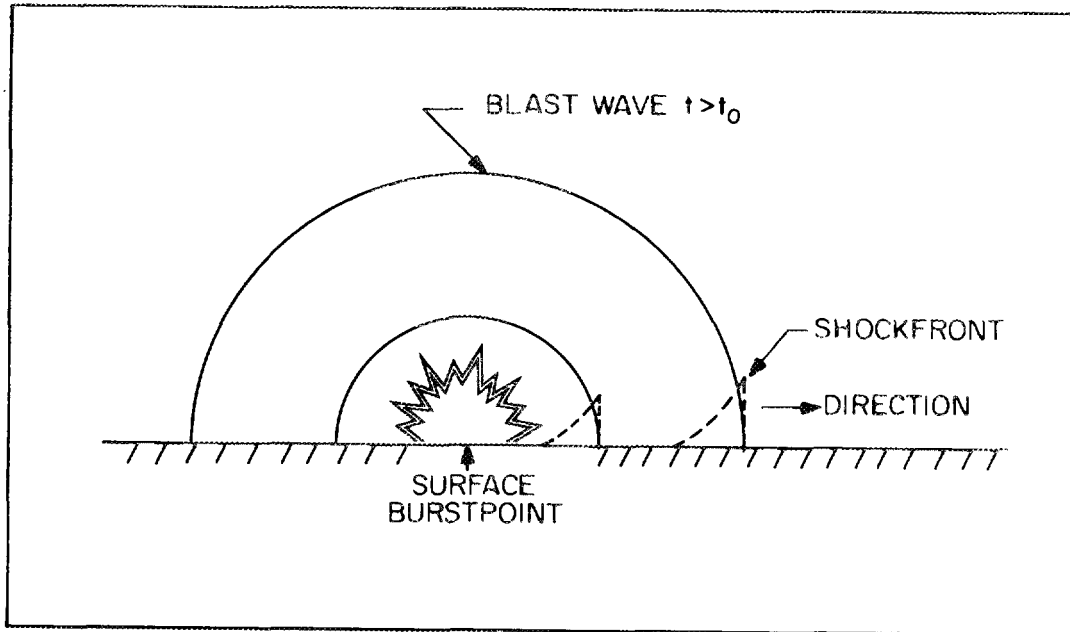


Fig. 5. Air shock wave orientation for a surface nuclear burst [1].

Table 3

PEAK OVERPRESSURE, DYNAMIC PRESSURE AND MAXIMUM  
WIND VELOCITY IN AIR AT SEA LEVEL FOR IDEAL  
SHOCK FRONT

Peak Overpressure (N/m <sup>2</sup> ) (psi)		Peak Dynamic Pressure (N/m <sup>2</sup> ) (psi)		Maximum Wind Velocity (km/hour) (miles/hour)	
1.379x10 <sup>6</sup>	200.0	2.275x10 <sup>6</sup>	330.0	3,346	2,078
6.895x10 <sup>5</sup>	100.0	8.481x10 <sup>5</sup>	123.0	2,278	1,415
6.895x10 <sup>4</sup>	10.0	1.517x10 <sup>4</sup>	2.2	473	294
3.448x10 <sup>4</sup>	5.0	4.137x10 <sup>3</sup>	0.6	262	163
2.413x10 <sup>4</sup>	3.5	2.069x10 <sup>3</sup>	0.3	193	120
1.379x10 <sup>4</sup>	2.0	6.895x10 <sup>2</sup>	0.1	113	70

From the parameters shown in Table 3, it is reasonable to conclude that power system equipment, located at or above the surface of the earth, which experiences a peak overpressure greater than or equal to  $3.5 \times 10^4 \text{ N/m}^2$  (5 psi) will almost certainly sustain some damage such that the equipment will no longer perform its intended function(s). This conclusion is supported by test data obtained in 1955 at the Nevada Test Range [1].

In the Nevada test(s) a 69-kV substation and a distribution line of some fourteen wooden poles was placed at the  $3.5 \times 10^4 \text{ N/m}^2$  (5 psi) distance expected from a 30-kiloton weapon burst. Recorded damage included: 1) the collapse of the 69-kV subtransmission tower, 2) down and damaged wooden distribution poles, lines, distribution transformers and 3) damage to substation batteries, housing, 4-kV regulators and other equipments. At that time, the damage restoration time was assessed at a few days using material normally stocked by an electric utility. It is interesting to note that this estimate seems to assume a radiation fallout level low enough such that the work could be performed in a safe manner.

It seems reasonable to assume that as the peak overpressure seen by the power system decreases, the probability of damage will also decrease. Based on system design parameters for transmission and

distribution systems [2,3], an argument can be made that, for a radial distance from the burst where the peak overpressure is greater than  $2.4 \times 10^4 \text{ N/m}^2$  (3.5 psi) and corresponding winds of 193 km/hour (120 miles/hour) or greater, any above ground components, in total, will be damaged such that the system will no longer operate. A reasonable estimate for the largest radial distance where any damage can occur may be the  $1.4 \times 10^4 \text{ N/m}^2$  (2 psi) pressure ring.

For the surface burst, the radial distance of equal peak overpressure, the arrival time of that pressure and the duration are strong functions of weapon yield. These parameters, for select values of peak overpressure, are tabulated in Table 4.

Review of the above data indicates that, regardless of weapon yield, the  $3.4 \times 10^4 \text{ N/m}^2$  (5 psi) radial contour is always significantly greater than the corresponding fireball radius and the extent of ejected material from the crater. Thus, the spatial area of direct damage can be understood from the peak overpressure data and distances for above-ground systems. This concept is graphically depicted as Figure 6.

## 2.5 Source Region Spatial Characterization

The spatial extent of the nuclear surface burst source region is an important parameter for power system assessment. In the open literature, general limits have been described [6,7] which place a lower bound, expressed as the radial distance from the burst, at three kilometers (low-yield weapon) and an upper bound between five and six kilometers (high-yield weapon).

It is important to note that, for any SREMP assessment, the "size" of the source region has practical meaning only in the context of a specific problem and physical assumptions. Boundary estimates may be derived from SREMP physical arguments based on: 1) the radial distance at which the electrical conductivity of air ( $\sigma$ ) does not rise beyond a certain magnitude, 2) the radial distance at which the peak Compton current density ( $J_r^C$ ) has a maximum lower limit, or 3) the radial

Table 4

RADIAL DISTANCE, ARRIVAL TIME AND DURATION FOR  
SELECT PEAK OVERPRESSURES AS A FUNCTION OF  
WEAPON FIELD

Weapon Yield (Kt)	Peak Overpressure (N/m <sup>2</sup> ) (psi)		Radial Distance (Km)	Arrival Time (seconds)	Duration (seconds)
1	3.4x10 <sup>4</sup>	5.0	0.443	0.8	0.3
1	2.4x10 <sup>4</sup>	3.5	0.547	1.4	0.4
1	1.4x10 <sup>4</sup>	2.0	0.773	1.7	0.5
10	3.4x10 <sup>4</sup>	5.0	0.934	2.7	0.6
10	2.4x10 <sup>4</sup>	3.5	1.159	3.0	0.8
10	1.4x10 <sup>4</sup>	2.0	1.642	3.7	1.0
100	3.4x10 <sup>4</sup>	5.0	2.013	3.6	1.3
100	2.4x10 <sup>4</sup>	3.5	2.496	6.0	1.5
100	1.4x10 <sup>4</sup>	2.0	3.542	8.0	2.0
500	3.4x10 <sup>4</sup>	5.0	3.462	6.0	2.3
500	2.4x10 <sup>4</sup>	3.5	4.267	10.0	2.6
500	1.4x10 <sup>4</sup>	2.0	6.118	14.0	3.5
1000	3.4x10 <sup>4</sup>	5.0	4.347	8.0	2.8
1000	2.4x10 <sup>4</sup>	3.5	5.313	14.0	4.0
1000	1.4x10 <sup>4</sup>	2.0	7.728	17.0	4.5
10,000	3.4x10 <sup>4</sup>	5.0	9.338	15.0	5.8
10,000	2.4x10 <sup>4</sup>	3.5	11.750	30.0	9.0
10,000	2.4x10 <sup>4</sup>	2.0	16.905	35.0	10.0
20,000	3.4x10 <sup>4</sup>	5.0	11.914	20.0	7.5
20,000	2.4x10 <sup>4</sup>	3.5	14.813	35.0	12.0
20,000	1.4x10 <sup>4</sup>	2.0	20.930	45.0	14.0

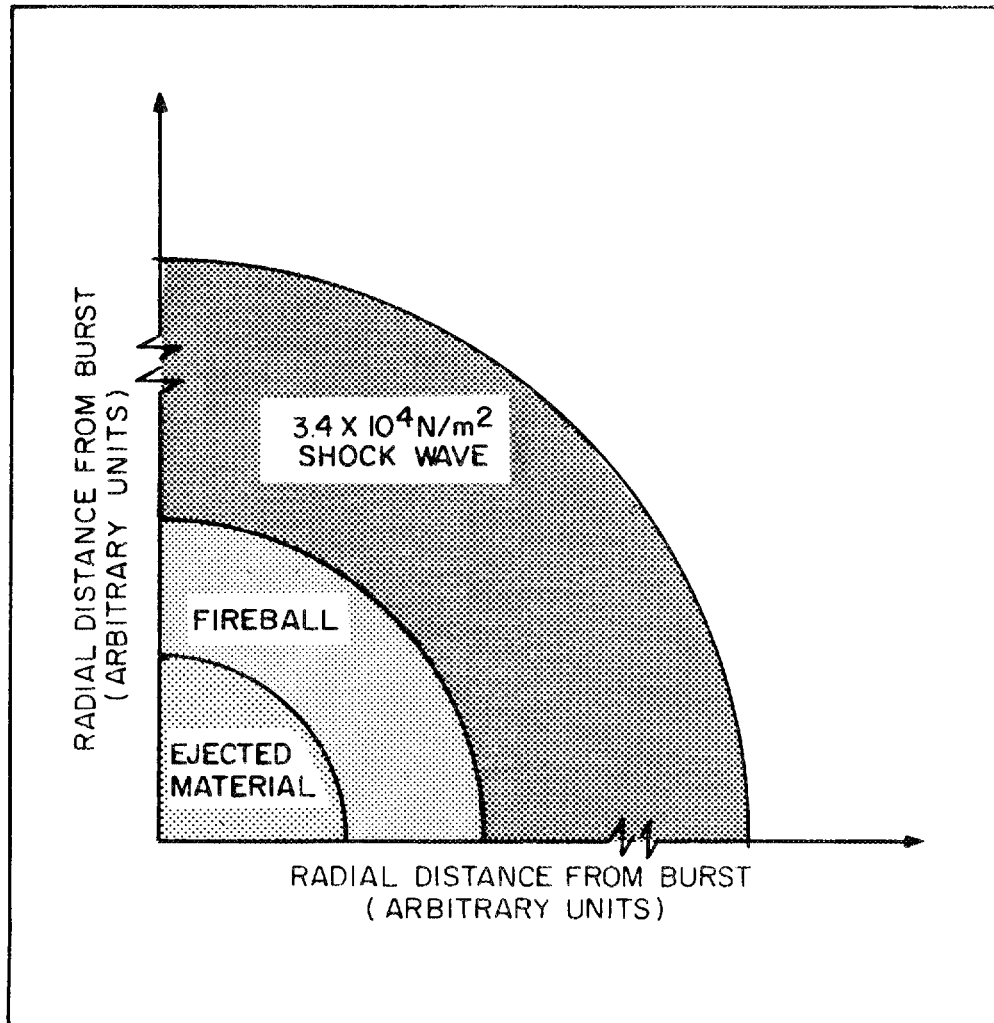


Fig. 6. Spatial relationship of ejected material, fireball and shock wave radial contours.

distance ( $r_0$ ) beyond which the peak magnitude of the transient electric field ( $E_{pk}$ ) decreases as a ( $r^{-1}$ ) function. These physical phenomena are discussed in Section 3 of this report.

Based on information obtained from Jones [15], and certain assumptions of Peak Compton current and air conductivity, a number of source region boundary estimates, are plotted as Figure 7. The plot includes select contours of peak overpressure as a function of weapon yield. The indicated distances for the source region should be considered as nominal ranges. Review of this data set suggests that, for yields above 10 kilotons, alternate physical assumptions tend to result in similar estimates of distance for a given yield.

In order to explore the relationship between peak overpressure contours and source region distances, Figure 8 was constructed showing a composite conjecture of source region spatial characterization and  $2.4 \times 10^4 \text{ N/m}^2$  (3.5 psi) peak overpressure for yields from 100 kilotons to 10,000 kilotons. In this range, the available data strongly suggests that the source region radial distance is always less than the peak overpressure distance and the separation between the two effects may tend to increase in some relationship directly proportional to yield.

## 2.6 Summary

In this section, a select group of nuclear surface burst weapon's effects have been presented to place the spatial extent of the EMP source region in some perspective. Based on the principle of "balanced survivability," it may not be constructive to assess the direct threat due to SREMP alone in those geographic areas where the electric power system will ultimately suffer massive damage due to other weapon's effects. The corresponding assessment methodology will require, as an input, knowledge of the following spatial parameters:

- Geographic location of the burst
- Crater radius
- Ejected material radius

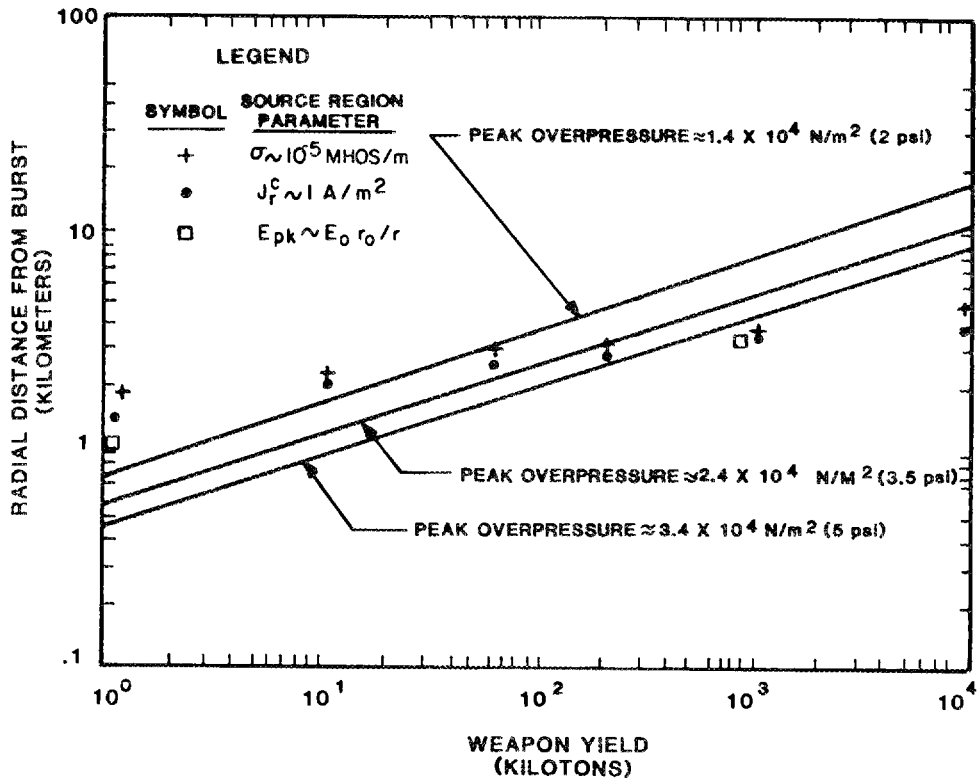


Fig. 7. Conjecture of nominal source region spatial characterization and select peak overpressure distances as a function of weapon yield.

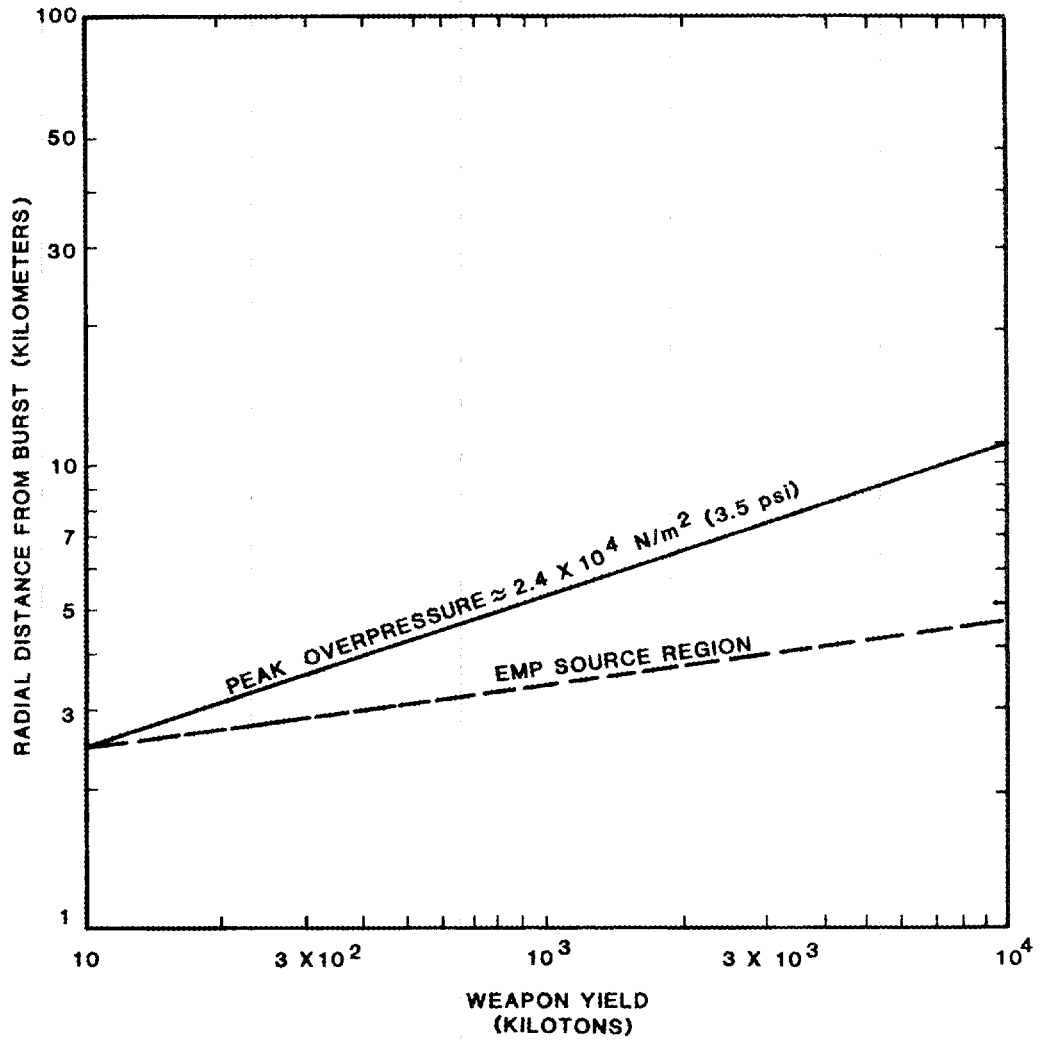


Fig. 8. Conjecture of source region composite spatial characterization and  $2.4 \times 10^4$  N/m<sup>2</sup> (3.5 psi) for weapon yields from 100 kilotons to 10,000 kilotons.

- Fireball radius
- EMP source region radius
- Select peak overpressure radii

To illustrate the use of the above parameters in an assessment methodology for civilian electric utility systems, the approximate spatial relationships for a one-megaton surface burst are shown as Figure 9. The geographic location of the burst will define those elements of the power system directly affected. For above-ground components, the approximate radial distance of non-SREMP damage could be determined by the distance associated with the peak overpressure radii. In this example, the source region radial distance is less than the  $3.4 \times 10^4 \text{ N/m}^2$  (5 psi) peak overpressure. As discussed in Section 4 of this report, the SREMP threat may then be expressed, for overhead lines penetrating or traversing the source region boundary, as an induced surge, formed on the line within the region and propagating outside the region. The SREMP radiated field may then be used to determine additional interaction with power system elements located outside the source region.

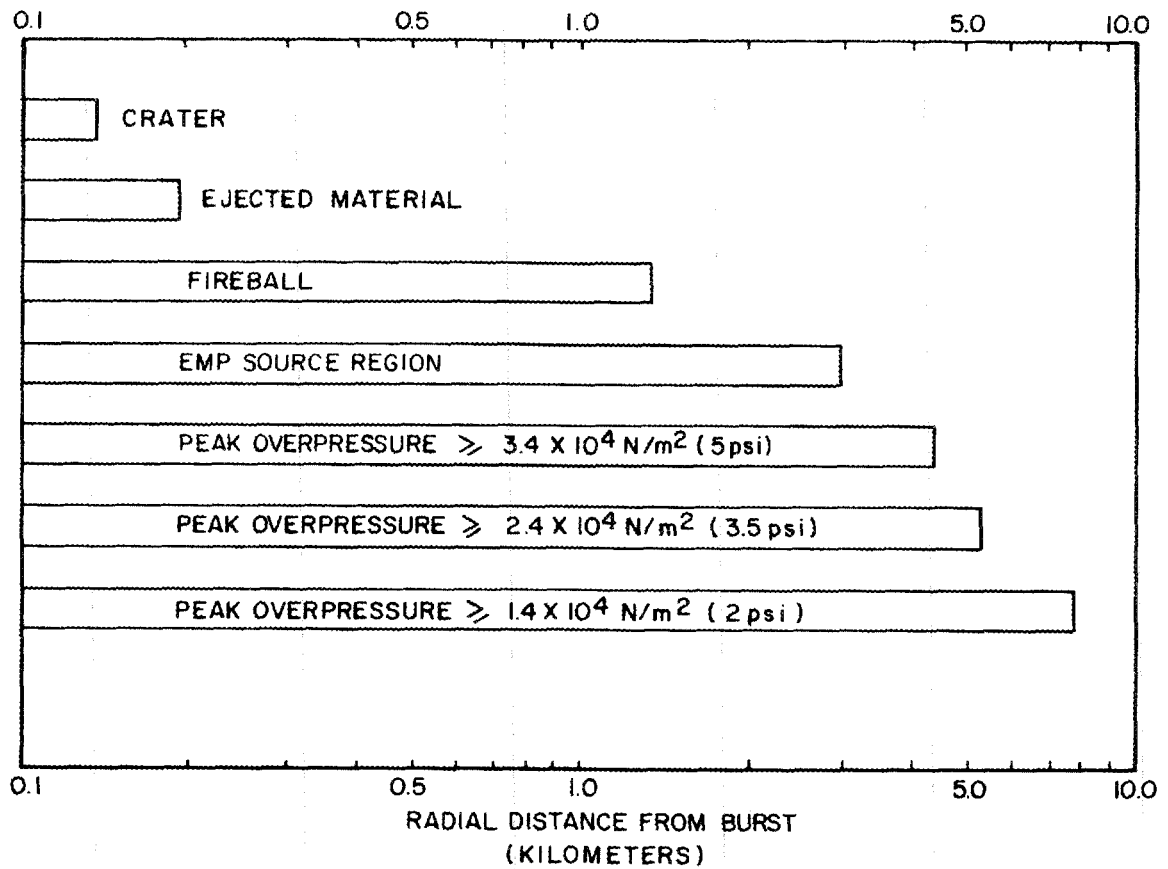


Fig. 9. Approximate spatial relationship of selected weapon effects distances for a one-Megaton surface burst.

### 3. SREMP ENVIRONMENTAL DESCRIPTION

#### 3.1 Introduction

The development of SREMP environmental conditions necessarily begins with the physics associated with gamma radiation ( $\gamma$ -radiation) and weapon neutrons produced in the nuclear burst and concludes with an understanding of the non-radiated fields within the region and the radiated fields outside the region. Concepts of the Compton process are discussed in order to explore the spatial and time characteristics of the Compton current and air conductivity. These parameters serve as variables for Maxwell's equations whereby the natures of a radial electric field, polar electric field and corresponding azimuthal magnetic field are defined.

The field characterization of a symmetric source region is initially developed as a prelude to discussion of the surface burst, asymmetric source region of interest. The physical geometry is based upon a spherical coordinate system of independent variables  $r$ ,  $\theta$ , and  $\phi$ . By convention, the  $r = \text{constant}$  surface is a hemisphere, in the air, centered at the burst origin, the  $\theta = \text{constant}$  surface is a cone and the  $\phi = \text{constant}$  surface is a plane. The base vectors ( $\hat{r}$ ,  $\hat{\theta}$ ,  $\hat{\phi}$ ) are defined as mutually orthogonal unit vectors perpendicular to the respective constant surfaces and point in the direction of increasing coordinate values.

Unless otherwise noted, the development contained herein is strongly based upon the theory of Longmire documented in THE EMP INTERACTION HANDBOOK [8] as issued by the Air Force Weapons Laboratory (AFWL). The discussion concludes with a summary of important field issues necessary to understand coupling to power systems.

#### 3.2 Compton Current and Air Conductivity

The SREMP environment begins with the physics associated with gamma radiation emission from the weapon. This prompt gamma pulse, in the radial direction out of the burst, has a rise time of several nano-

seconds (ns) and decays in a few tens of nanoseconds. Additional gammas are formed by neutron emission from the burst. These neutrons interact with the air or ground to produce inelastic gammas and capture gammas. In addition, fission product gammas are emitted by weapon debris following the beta decay of fission fragments. Table 5 shows the approximate average energies and effective absorption lengths, in air, of gamma source components beyond 200 meters from the burst origin [8].

Table 5  
APPROXIMATE AVERAGE ENERGIES AND EFFECTIVE  
ABSORPTION LENGTHS IN AIR OF GAMMA SOURCE COMPONENTS

<u>Component</u>	<u>Energy (MeV)</u>	<u>Absorption Length (gm/cm<sup>2</sup>)</u>
Prompt	1.5	40
Air Inelastic	4.0	52
Ground Capture	3.0	38
Air Capture	6.0	58
Fission Fragment	1.0	37

The burst emission of gammas interacting with air molecules is the primary mechanism of free electron production and is defined by the term Compton Process. As shown in Figure 10, an incident gamma ray can strike an air molecule producing a positive (parent) ion and a Compton (recoil) free electron(s). The once-incident gamma is scattered while the Compton electron(s) lose energy via collisions with other air molecules. At sea level, this electron energy loss will bring the Compton electron to rest within a distance of a few meters. In the process, secondary electron/air collisions have produced many secondary electron/ion pairs ( $\approx 34$  MeV per ion pair).

The movement of Compton electrons is defined as the Compton current density ( $J_{\gamma}^C$ ). The charge separation generates an electromagnetic field ( $E_{\gamma}$ ). This concept is illustrated in Figure 11. The charge-separation model depicts the nonradiated (radial) electric field produced by positive and negative charges separated by the Compton Process. At

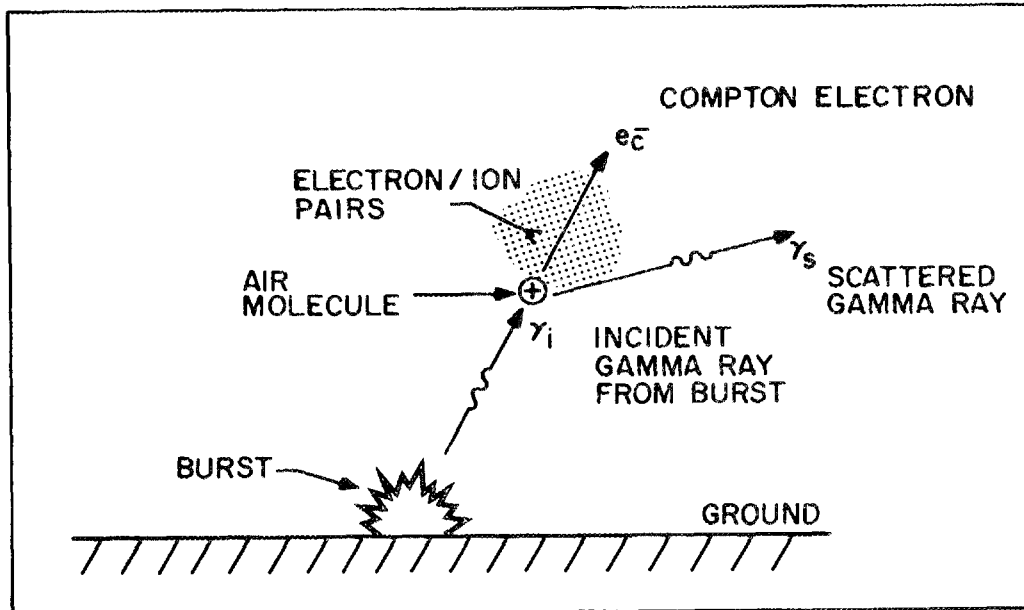


Fig. 10. The Compton Process.

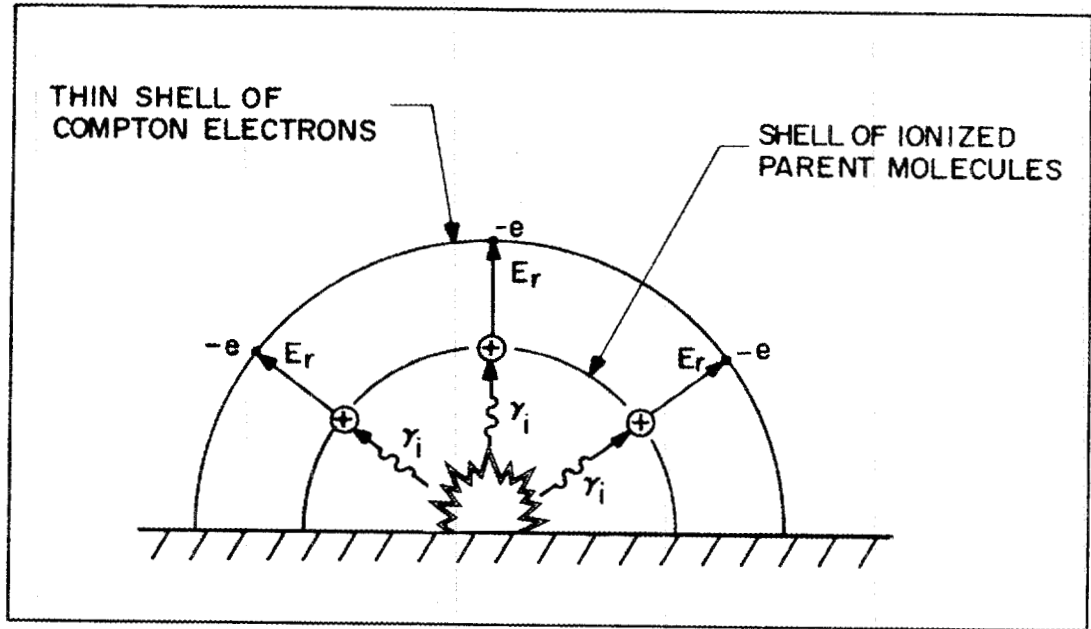


Fig. 11. Charge separation model illustrating the creation of the radial electric field ( $E_r$ ) via the Compton Process.

early times, the heavier, positively charged parent ions remain almost stationary while the Compton electrons form a thin shell at some radial distance away from the burst.

The quantification of the Compton current density ( $J_r^C$ ) in the radial direction, at a distance ( $r$ ) from the burst, can be developed from an estimate of the gamma number flux ( $\dot{\phi}_\gamma$ ) at this distance as:

$$\dot{\phi}_\gamma \sim \frac{e^{-r/\lambda_a}}{4\pi r^2} \quad (1)$$

where:

- $\dot{\phi}_\gamma$  = gamma number flux (gammas per unit area per unit time)
- $\lambda_a$  = absorption length
- $r$  = radial distance from burst

In conformance with the model, it is evident that a steady gamma number flux ( $\dot{\phi}_\gamma$ ) will produce a steady number flux of Compton electrons ( $\dot{\phi}_e$ ) in the same radial direction by the relation:

$$\dot{\phi}_e \approx \dot{\phi}_\gamma R_{mf}/\lambda_s \quad (2)$$

where:

- $\dot{\phi}_e$  = electron number flux (electrons per unit area per unit time)
- $R_{mf}$  = mean forward range of the electron(s)
- $\lambda_s$  = scattering mean free path of the gammas

By definition, the Compton current density ( $J_r^C$ ) is equal to the electron number flux  $\dot{\phi}_e$  such that:

$$J_r^C = q \dot{\phi}_e \approx q \dot{\phi}_\gamma R_{mf}/\lambda_s \quad (3)$$

The Compton current density can also be developed from a concept of gamma energy flux ( $\dot{\phi}_\gamma^*$ ), expressed in units of gamma-MeV/cm<sup>2</sup>-second as:

$$\dot{\phi}_y \sim \dot{\phi}_y^* \quad (4)$$

A radiation dose rate of 1 rad/second approximately corresponds to a gamma energy flux of  $2 \times 10^9$  gamma-MeV/m<sup>2</sup>-second for gamma rays in the 1 to 3 MeV range. Using this value and equation (3), the Compton current density in terms of dose rate ( $\dot{D}_e$ ) can be expressed as:

$$J_r^C \approx 2 \times 10^{-8} \dot{D}_e \quad (5)$$

where:

$$J_r^C = \text{Compton current density (amperes/meter}^2\text{)}$$

$$\dot{D}_e = \text{Dose rate (rads/second)}$$

Thus, a relationship can be established between the magnitude of the Compton current density and the weapon and neutron produced gammas. Since, at sea level, the effective lifetime of a Compton electron is a few nanoseconds, the waveform of the Compton current density will be approximately the same as the gamma flux.

The earth's geomagnetic field can deflect Compton electrons such that generally there will exist Compton currents in directions other than that of the incident gamma(s). For a surface-burst source region development, this effect is small and has been omitted in most models. This simplification is justified by the fact that at sea-level, the Larmor radius ( $R_L$ ) of Compton electrons in the geomagnetic field is up to 100 meters which is much longer than the corresponding mean free path of the electron ( $R_{mf}$ ) of a few meters. The traverse, geomagnetically deflected Compton current density is:

$$J_t^C \approx J_r^C (R_{mf}/2R_L) \quad (6)$$

It is important to note that this simplification is valid for surface bursts and cannot be made for high-altitude bursts. In fact, in the high-altitude source region (30 kilometers) the deflected (traverse)

Compton current density is the principle source of the HEMP signal. At this altitude, the  $R_{mf}$  approach the  $R_L$  value. The traverse Compton current density is a principle mechanism of HEMP.

As depicted in the Compton process model, Compton electrons can make secondary electron/ion pairs in collisions with other atoms. The pairs result in a time-change of air conductivity within the source region. Characterization of the electron/ion pairs in terms of electric conductivity ( $\sigma$ ) allows for the definition of a conduction current as  $\sigma E_r$  where  $E_r$  is the electric field created by the charge separation model.

The calculation of the air conductivity ( $\sigma$ ) as a function of time is a complex issue since both electrons and ions contribute to the conductivity but the mobility of the electron is much greater than that of the parent ion. Simple approximate relationships have been developed [8] to express electron (ion) densities ( $N_e$ ) in terms of an ionization source ( $S_e$ ) and appropriate production constants ( $K$ ) for a source whose production rate rises as:

$$S_e \sim e^{\alpha t} \quad (7)$$

The electron density, for simple cases, can be described by:

$$N_e = S_e / (\alpha + K) \quad (8)$$

For a source which falls more slowly than  $t^{-2}$ , ( $S_i = e^{-\beta t}$ ), the late time ion densities can be expressed as:

$$N_e \approx N_i \approx \sqrt{S_i / K} \quad (9)$$

The mobility ( $\mu_e$ ) of an electron is defined as the ratio of its drift velocity to the electric field causing the drift. At early times, when the electrons dominate the conductivity, the air conductivity is:

$$\sigma = -e N_e \mu_e \quad (10)$$

where:

$-e$  = electron charge

$\sigma$  = electrical conductivity

If  $N_e$  is defined by Equation (8), it can be shown [8] that electron conductivity is related to the dose rate ( $\dot{D}_e$ ) as:

$$\sigma = \frac{1 \times 10^{-4}}{\alpha + K} \dot{D}_e \quad (11)$$

where:

$\sigma$  = electrical conductivity (mhos per meter)

$\dot{D}_e$  = dose rate (rads/second)

$\alpha$  = rise (+) or decay (-) rate of the ionization  
( $\text{sec}^{-1}$ )

$K$  = electron attachment rate ( $\text{sec}^{-1}$ )

### 3.3 Symmetric Source Region SREMP Field Characterization

In order to understand the nature of the source region radiated and non-radiated electromagnetic fields, the spherically symmetric geometry for a source region can be used to explore the nature of the radial electric field ( $E_r$ ). Knowledge of the Compton process, Compton current density ( $J_r^C$ ) and air conductivity ( $\sigma$ ) allows for the solution of Maxwell's equations expressed as follows:

$$\mu_0 \frac{\partial H_\phi}{\partial t} + \nabla \times E_r = 0 \quad (12)$$

$$-\epsilon_0 \frac{\partial E_r}{\partial t} + \nabla \times H_\phi = J_r^C + \sigma E_r \quad (13)$$

The spherically symmetric geometry is a classic case where, if the magnetic field ( $H_\phi$ ) is initially zero, the term  $\partial H_\phi / \partial t$  of Equation (12) will remain zero if the electric field ( $E_r$ ) is curl-free. In this case:

$$\mu_0 \frac{\partial H_\phi}{\partial t} = \nabla \times E_r = 0 \quad (14)$$

The absence of any magnetic field ( $E_r$  field curl) results in a purely radial E-field within the source region which can be expressed by Equation (13) as:

$$\epsilon_0 \frac{\partial E_r}{\partial t} + \sigma E_r = -J_r^C \quad (15)$$

Outside of the source region ( $J_r^C = 0$ ), no field will exist. This insight is reinforced by an appreciation of the geometry of a total symmetric source region via a charge-separation model. This geometry is shown as Figure 12.

The total time solution to Equation (15) can be understood if elapsed time is divided into three segments for investigation. At very early times, the value of the conduction current term ( $\sigma E_r$ ) is small and may be neglected. In this time region, the solution to (15) is:

$$E_r(t) = -1/\epsilon_0 \int_{-\infty}^t J_r^C dt \quad (16)$$

Since the Compton current ( $J_r^C$ ) exhibits an exponentially rising function with respect to time, Equation (16) indicates that the radial electric field ( $E_r$ ) behaves in a like manner.

At some mid-time, the conduction current term may become comparable to the displacement current term. After this time, when the displacement current term is so small that it may be neglected, the solution of Equation (15) approximates:

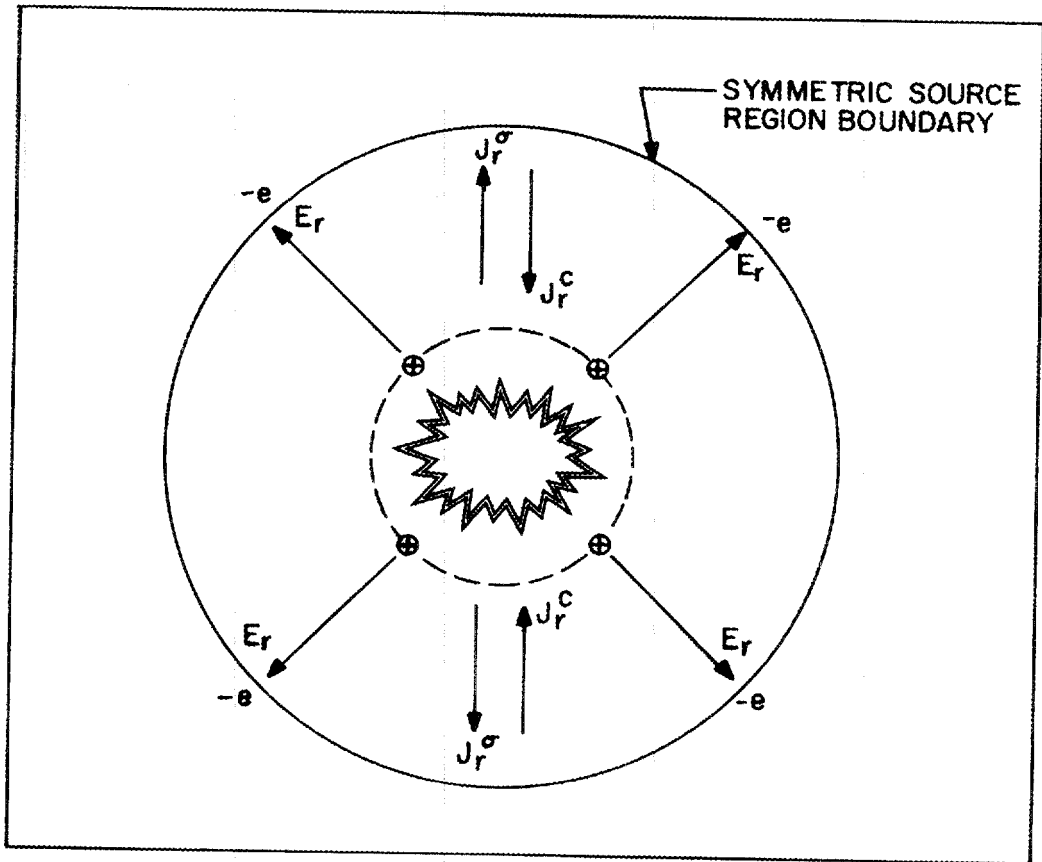


Fig. 12. Charge separation model for a perfectly symmetric source region.

$$E_r \approx - \frac{J_r^C}{\sigma} = E_s \quad (17)$$

Saturation occurs,  $E_r$  becomes constant at some value  $E_s$ . For a Compton current defined by Equation (5) and an air conductivity defined by Equation (11) one obtains:

$$E_s \approx \frac{2 \times 10^{-8} \dot{D}_e (\alpha + K_1)}{10^{-4} \dot{D}_e} \quad (18)$$

$$E_s \approx 2 \times 10^{-4} (\alpha + K_1) \quad (19)$$

The field is expressed in volts per meter. For most cases of interest  $K < \alpha$ , therefore:

$$E_s \approx 2 \times 10^{-4} \alpha \quad (20)$$

At later times, the displacement current remains neglectable. The  $E_r$  field follows  $E_s$ . The increasing dominance of ion conductivity results in a decay of  $E_s$  approximately as  $\sqrt{S_e}$ .

### 3.4 Surface Burst Source Region SREMP Field Characterization

Precise solutions for the transient electric and magnetic fields within and outside of the surface-burst source region demand the use of complex, multi-dimensional finite difference codes to solve Maxwell's equations for all points in a volume around the burst. In addition to the physical models necessary to define the Compton current density, other significant issues include 1) spatial and time dependent nature of air conductivity, 2) lossy ground effects, and 3) magnetic turning effects due to the surface magnetic field ( $H_\phi$ ). Fundamental work by

Longmire [9] has resulted in a set of analytic expressions for SREMP produced by the surface burst. This physical model consists of three main phases. The initial (wave) phase has some similarity to the symmetric source region at early times before saturation.

This is followed by a diffusion phase and a quasi-static phase. Crevier and Pettus [10] have combined Longmire's phases in a single expression for approximate calculations. Additional work by Crevier and Kalasky [11] has produced a single-dimension code (MODEL C) to calculate fields at any point on the earth's surface for times up to 10 microseconds. The MODEL C code also includes approximate correctional terms for lossy ground and magnetic turning effects.

In order to assess SREMP effects on electric power systems, field characterization can be divided into three main issues, 1) the spatial and time dependence of the non-radiated fields within the source region, 2) the spatial boundary of the source region, and 3) the spatial and time dependence of the radiated fields beyond the source region boundary.

The following subsections explore these issues.

### 3.4.1 Field Characterizations Within the Source Region

As indicated previously, the electromagnetic fields of interest within the source region are 1) the radial electric field ( $E_r$ ), 2) the polar electric field ( $E_\theta$ ), and 3) the magnetic field ( $H_\phi$ ). In order to present the mathematical development, it is convenient to adopt a spherical coordinate system. Above the surface, Maxwell's equations become:

$$\mu_0 \frac{\partial H_\phi}{\partial t} = \frac{-1}{r} \frac{\partial}{\partial r} (rE_\theta) + \frac{1}{r} \frac{\partial}{\partial \theta} E_r \quad (21)$$

$$\epsilon_0 \frac{\partial E_\theta}{\partial t} + \alpha E_\theta + J_\theta^c = \frac{-1}{r} \frac{\partial}{\partial r} (rH_\phi) \quad (22)$$

$$\epsilon_0 \frac{\partial E_r}{\partial t} + \sigma E_r + J_r^c = \frac{1}{r \sin \theta} \frac{\partial}{\partial \theta} (\sin \theta H_\phi) \quad (23)$$

This coordinate system is shown in Figure 13, where the angle  $\theta$  is exaggerated for graphic clarity. The concept of an outgoing field (F), an incoming field (G) and a retarded time ( $\tau$ ) are also defined such that:

$$F = r(E_\theta + c B_\phi) \quad (24)$$

$$G = r(E_\theta - c B_\phi) \quad (25)$$

$$\tau = t - r/c \quad (26)$$

In Equations (24), (25) and (26), the constant "c" denotes the speed of light.

Previous investigations [8,11] have made the following assumptions at early times, when the magnitude of air conductivity is less than ground conductivity:

$$J_\theta^c \ll J_r^c \quad (27)$$

$$G \ll F \quad (28)$$

$$\sin \theta \approx 1 \quad (29)$$

Based on the above assumptions, Equations (21) and (23) simplify to become:

$$\frac{\partial F}{\partial r} + \frac{1}{2} Z_0 \sigma F = \frac{\partial E_r}{\partial \theta} \quad (30)$$

$$\frac{1}{c} \frac{\partial E_r}{\partial \tau} + Z_0 \sigma E_r = -Z_0 J_r^c + \frac{1}{2r^2} \frac{\partial F}{\partial \theta} \quad (31)$$

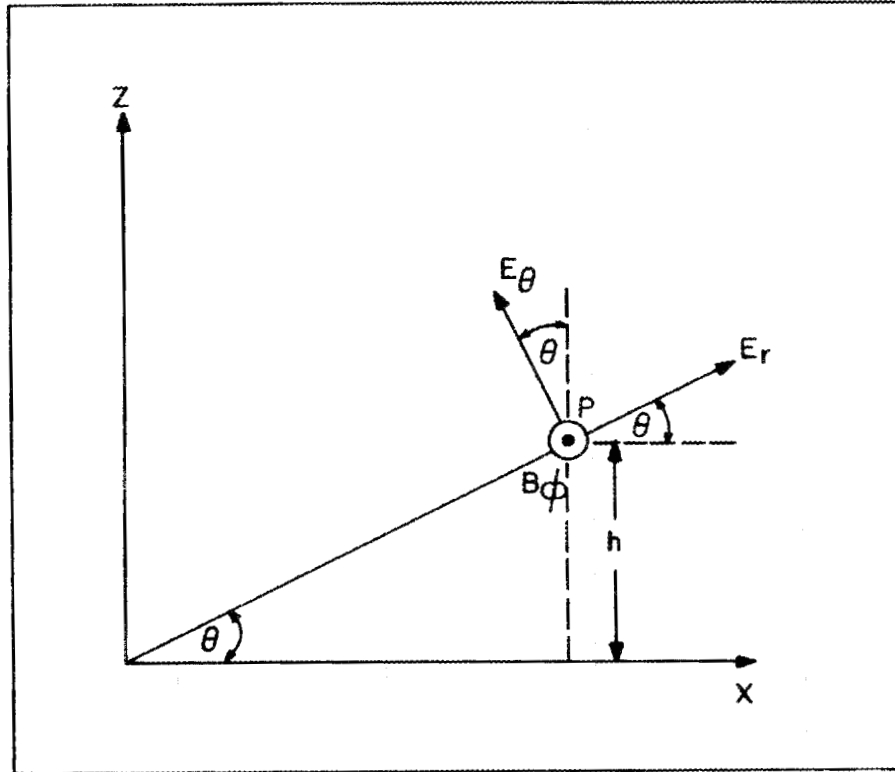


Fig. 13. Spherical coordinate system for source region field characterization.

$$Z_0 = \sqrt{\mu_0/\epsilon_0} = 377 \text{ ohms} \quad (32)$$

If one assumes, in a manner similar to the symmetric source region case, that the conduction term ( $Z_0 \sigma E_r$ ) is very small compared to the displacement term [8], equation (31) further reduces to:

$$\frac{1}{c} \frac{\partial E_r}{\partial \tau} = -Z_0 J_r^c + \frac{1}{2r^2} \frac{\partial F}{\partial \theta} \quad (33)$$

The physical interpretation of Equations (30) and (33) is that the F field is located near the earth's surface and spreads upward as it propagates outward.  $E_r$  has the same physical interpretation as the symmetric source region case.

It has been shown [11] that Equations (30) and (31) can be written in the form of a diffusion equation where the outgoing field F is related to the integral of  $J_r^c$  weighted by the diffusion of the sources over distance. When air conductivity reaches the same magnitude as ground conductivity, the G field can no longer be neglected. It has been shown that the G field, at this time may be approximated as:

$$\frac{1}{c} \frac{\partial G}{\partial \tau} + \frac{1}{2} Z_0 \sigma (F+G) = -\frac{1}{2} \frac{\partial (F-G)}{\partial r} - Z_r J_\theta \quad (34)$$

A set of equations has now been developed to solve for F and G(or, equivalently, for  $E_\theta$  and  $B_\phi$ ) on the surface at a distance r from the burst point.

In the diffusion phase, the conduction current far from the ground tends to flow radially back to the burst point opposite the Compton current. Near the ground, except in those regions where the air conductivity is higher than the ground conductivity, the conduction current tends to flow into the ground and then back to the burst point. Thus, in this phase, the surface current is just equal to the Compton current flowing at some distance  $\delta_a$  from the surface.  $\delta_a$  can be thought

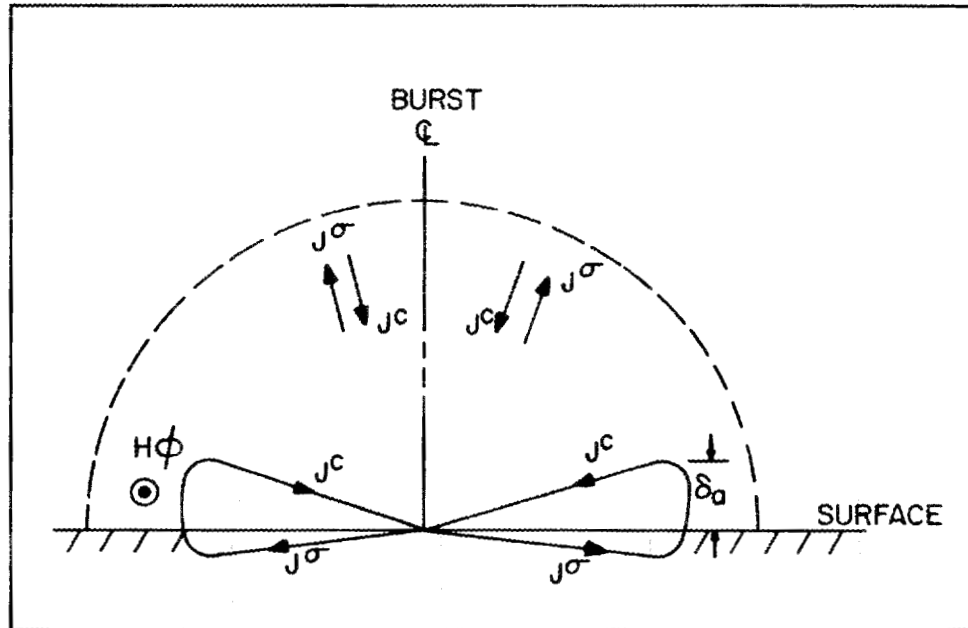


Fig. 14. Source region characterization during diffusion stage.

of as an air "skin depth." A graphic representation of this phase is shown as Figure 14.

For this diffusion phase, it has been shown [11] that the skin depth can be expressed as:

$$\delta_a = 2 \sqrt{\beta \sigma_a \mu_0} \quad (35)$$

$$\beta = J_r^C / \int J_r^C d\tau \quad (36)$$

The magnetic field becomes:

$$B_\phi = \mu_0 J_r^C \delta_a \quad (37)$$

If one assumes that, in this phase, the displacement current term can be neglected and that  $\sigma E_r$  is uniform over  $\delta_a$ , the surface magnetic field can be obtained directly from Maxwell's Equation (12) as:

$$B_\phi \approx \mu_0 (J_r^C + \sigma E_r) \delta_a \quad (38)$$

The above equation is for a lossy ground condition. If the ground was perfectly conducting ( $E_r = 0$ ) Equation (38) reduces to Equation (37). The physical interpretation of lossy ground is that the surface current is modified by the presence of the conduction current in air that tends to cancel part of the Compton Current.

At radial distances close to the burst, a self-consistent complexity is introduced by the fact that the strength of the surface magnetic field may be such to "turn" a Compton electron from a radial path and thus introduce a traverse ( $\theta$ ) component in the Compton current. Previous investigators have shown [11] that a first order correction can be made where the  $\theta$ -component is modelled as:

$$J_\theta = J_r^C (B/B_g) \quad (39)$$

where:

B = magnetic field in Telsa

B<sub>g</sub> = magnetic field at which the forward electron range and electron Larmor radius are approximately equal

A generalized time waveform for a surface burst radial electric field (E<sub>r</sub>) and the corresponding azimuthal magnetic field (B<sub>φ</sub>) is shown as Figure 15. The shape of the E<sub>r</sub> field has similarity to the symmetric source region case. The time to peak may be on the order of 50 nanoseconds. The magnitude of E<sub>r</sub> may vary from 10<sup>4</sup> to 10<sup>6</sup> volts per meter. At early times, the shape of the B<sub>φ</sub> field can be approximated as:

$$B_{\phi} \sim e^{\alpha t/2} \quad (40)$$

The peak will occur near the peak of the Compton current. At later times, the B<sub>φ</sub> field may vary only as the square root of the gamma flux.

The time and spatial characterization of parameters of interest within the source region are complex issues. Longmire [21] has presented computational results of 1) air conductivities, 2) azimuthal magnetic fields, 3) vertical electric fields and 4) radial electric fields for nominal ten kiloton and one megaton weapons. The relevant graphs are depicted as Figure 16 to Figure 19 of this report. The calculations of Longmire should not be interpreted as "hard data" but are presented here solely to illustrate the nature of the transient phenomena.

EMP investigators often fit analytic approximations to simulated results to facilitate subsequent research such as field coupling to conductors within the source region. An example of this technique can be found in Graham [12] where the object was to calculate the induced surge formed on an above-ground distribution line.

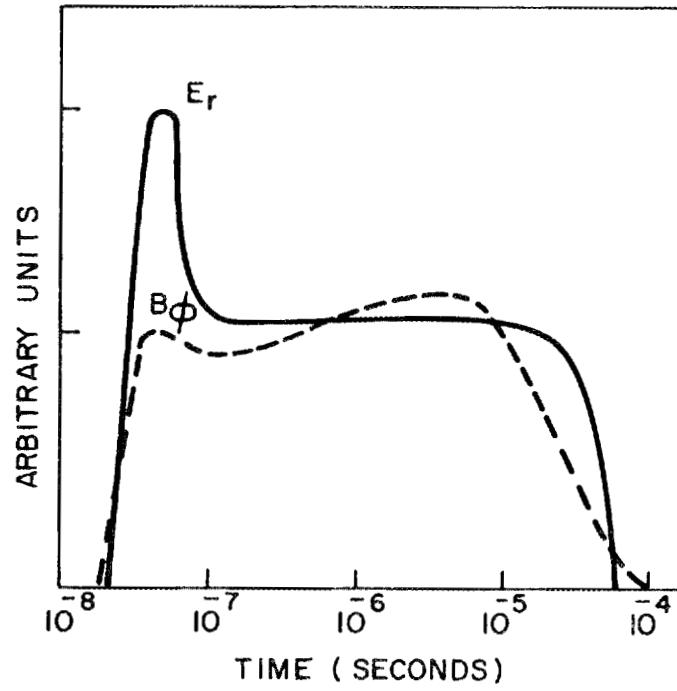
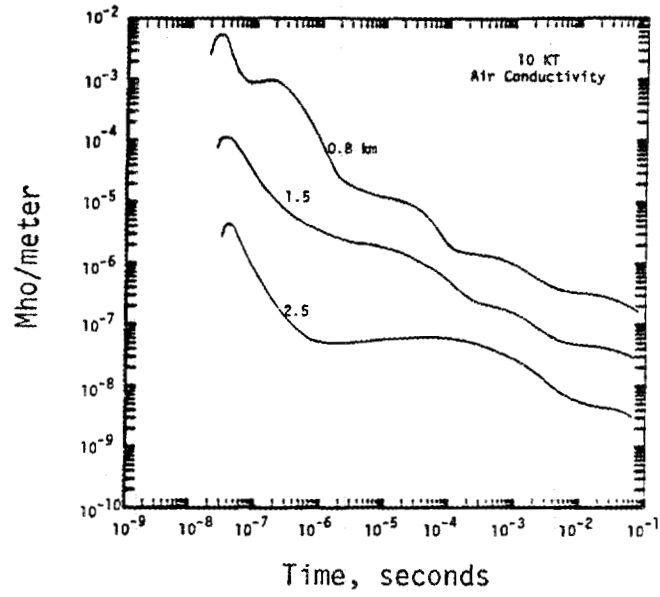
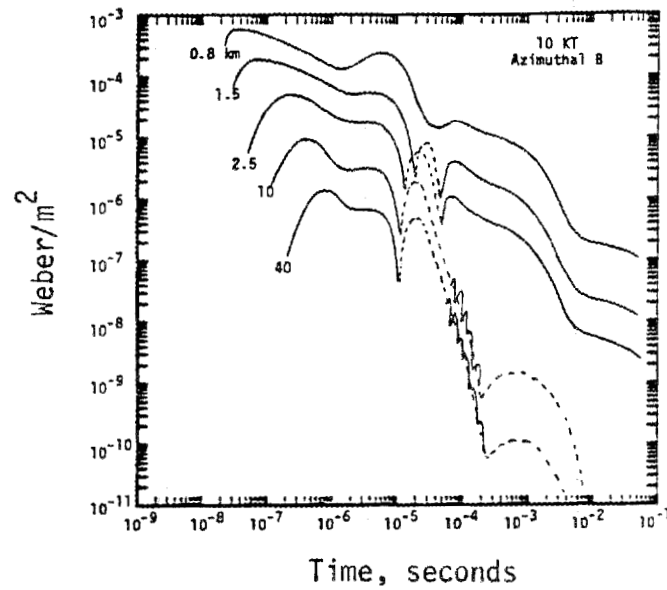


Fig. 15. General time waveform for  $E_r$  and  $B_\phi$  in the surface burst source region.

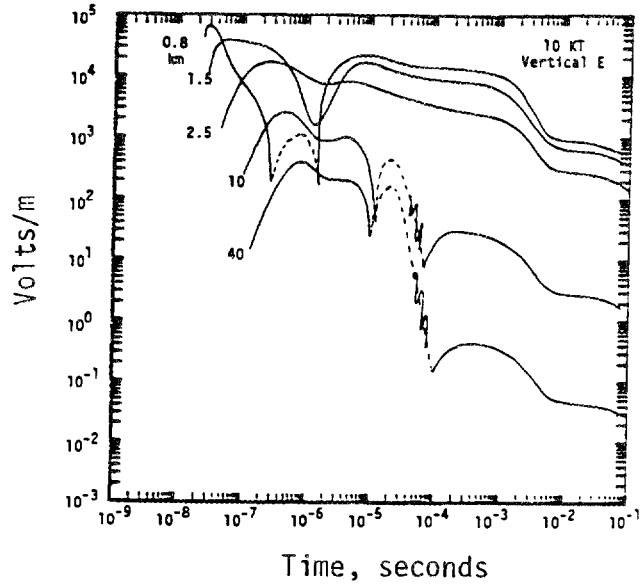


a) Air Conductivity

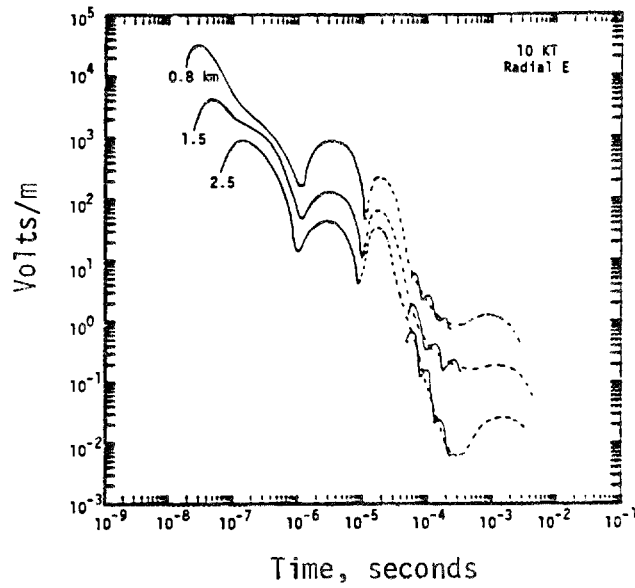


b) Magnetic Field

Fig. 16. Longmire [21] calculation of transient phenomena due to 10-kT weapon (nominal).

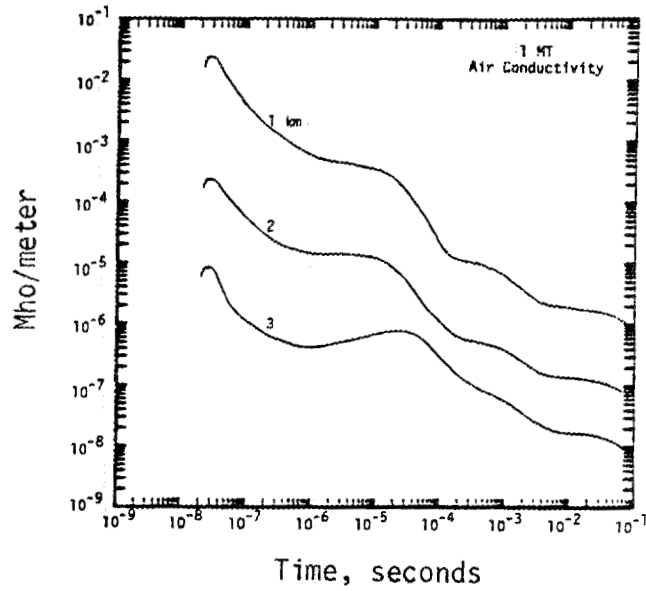


a) Vertical Electric Field

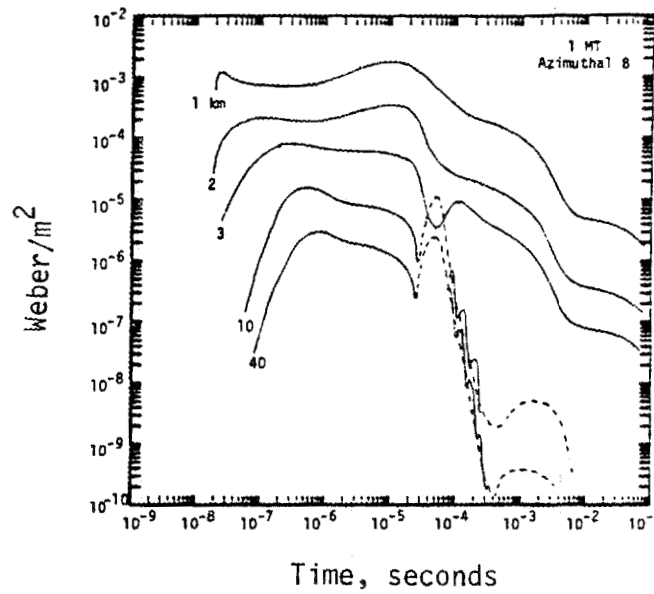


b) Radial Electric Field

Fig. 17. Longmire [21] calculation of transient phenomena due to 10-kT weapon (nominal).

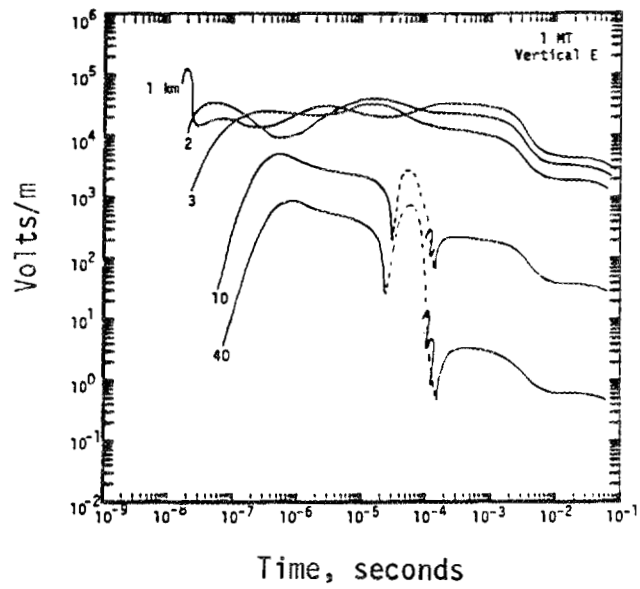


a) Air Conductivity

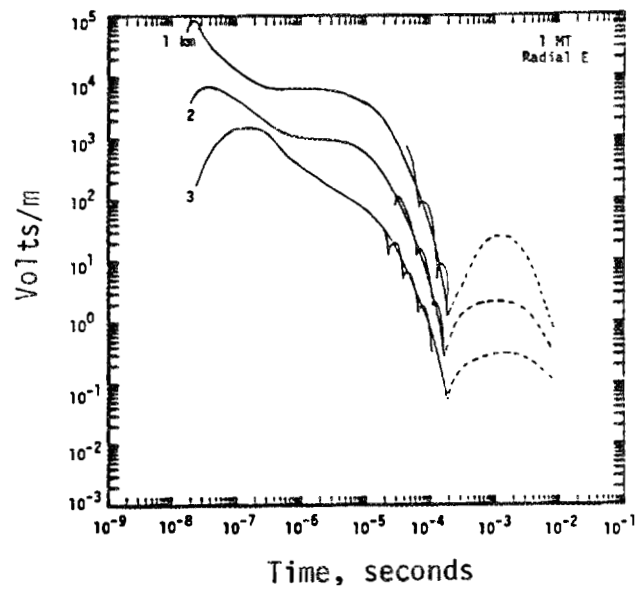


b) Magnetic Field

Fig. 18. Longmire [21] calculation of transient phenomena due to 1-MT weapon (nominal).



a) Vertical Electric Field



b) Radial Electric Field

Fig. 19. Longmire [21] calculation of transient phenomena due to 1-MT weapon (nominal).

### 3.4.2 Source Region Spatial Boundary

Within the source region for a given weapon yield, the field magnitudes decrease as a function of distance from the burst point. This effect can be observed in the Longmire data. At some boundary, the magnitude of the radial electric field is such that field characterization beyond this point is described as a radiated "far" field. A model of this concept is shown as Figure 20. At elevations on or above the earth's surface, where the height of interest is much less than the boundary radius, previous investigators have depicted the radiated electric field as a polar field ( $E_\theta$ ) whose orientation is parallel to the z-axis ( $\theta=0$ ), having a corresponding azimuthal magnetic field ( $B_\phi$ ) with a direction of propagation ( $n$ ) parallel to the x-axis outward from the burst. For a perfectly conducting ground, field magnitude in the radiated region is set to decrease linearly with increasing distance from the boundary.

It is obvious that the above selection of a source region boundary distance is somewhat arbitrary since the radial electric field does not suddenly go to a zero value. Such a boundary may be established by arguments based on some level of air conductivity or dose production of the weapon. The value of such a model for system analysis is that the two distinct areas can be evaluated by techniques more applicable to each. As discussed in Section 2.6, the boundary concept is very useful in comparing the total spatial extent of threat for a variety of surface weapon effects.

### 3.4.3 Radiated Field Characterization

In the previous subsection, the radiated "far" field has been discussed as a vertically polarized electric field ( $E_\theta$ ) propagating outward from the burst. This field can be expressed in a rectangular coordinate system as  $E_z$  with propagation in a positive x direction. The coordinate  $x_0$  is the source region boundary. If the wave in air is assumed to propagate as though the earth was a perfect conductor,  $E_z$  can be expressed in the frequency domain as:

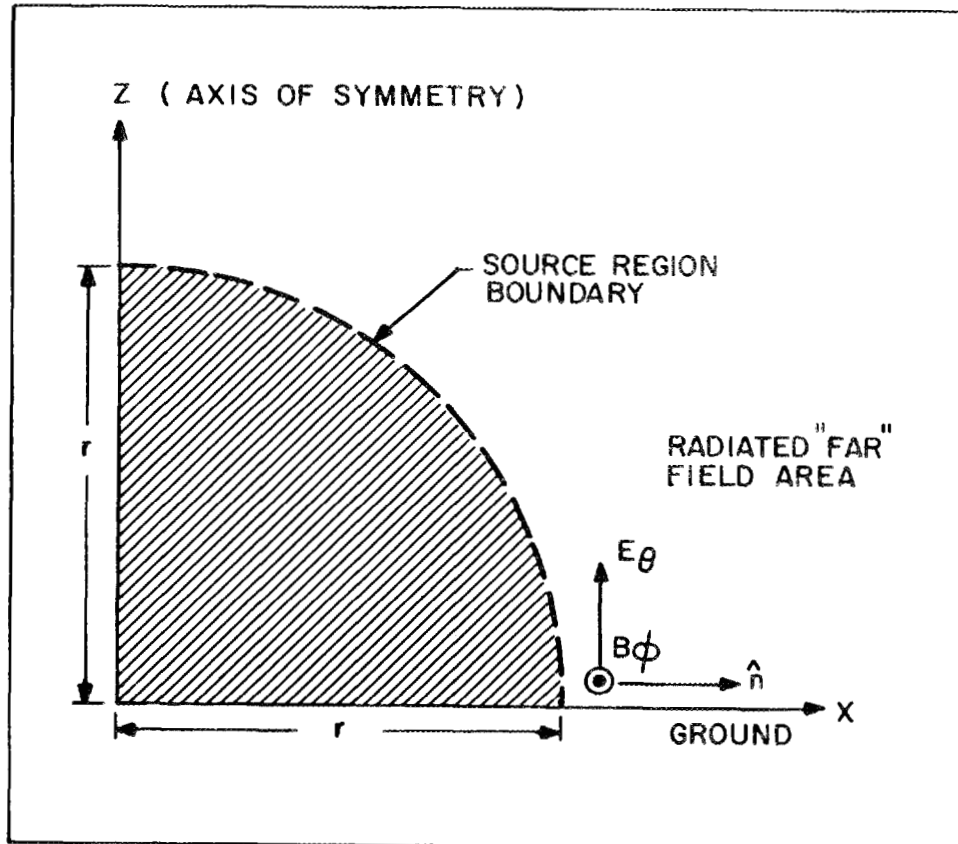


Fig. 20. Source region model depicting region boundary and characterization of vertically polarized electric field in the radiated "far" region.

$$E_z(x, \omega) = A_0(\omega) \frac{e^{-jkx}}{x} \quad (41)$$

where:  $A_0(\omega)$  is a frequency dependent function and  $x > x_0$ .

This approximation is conservative since a finite (lossy) conducting ground will cause attenuation as a function of propagational distance. This effect has been examined by Lee [13] but is not incorporated in this characterization.

For the purpose of this report, the presence of a finitely conducting ground will give rise to a horizontal ( $E_x$ ) component of the radiated field whose value at the surface is related to the tangential magnetic field ( $H_y$ ) through the surface impedance as:

$$E_x(x, h=0, \omega) = Z_s H_y(x, h=0, \omega) \quad (42)$$

$$Z_s = \sqrt{\frac{j\omega\mu}{\sigma + j\omega\epsilon}} \approx \sqrt{\frac{j\omega\mu}{\sigma}} \quad (43)$$

Noting that  $H_y = E_z/Z_0$ , we have:

$$E_x(x, 0, \omega) = \frac{Z_s}{Z_0} A_0(\omega) \frac{e^{-jkx}}{x} \quad (44)$$

where  $Z_0$  is the impedance of free space. It can be shown that, for a horizontal field at a height ( $h$ ) where  $h$  is much less than the radius of the source region ( $x_0$ ), the  $E_x$  field component at  $h$  can be expressed as:

$$E_x(x, h, \omega) = \left[ \frac{Z_s}{Z_0} - \frac{h}{x} \right] A_0(\omega) \frac{e^{-jkx}}{x} \quad (45)$$

One could now look at the ratio of the horizontal to vertical field components expressed as:

$$\frac{E_x(x, h, \omega)}{E_z(x, \omega)} = \left[ \sqrt{\frac{j\omega\epsilon}{\sigma}} - \frac{h}{x} \right] \quad (46)$$

The results of Equation (46) are plotted as Figure 21 for three values of ground conductivity. Also included in this figure is a plot of Equation (46) where the  $(\sigma + j\omega\epsilon)$  term is used. In both cases the relative dielectric constant is set at a value of 10. At frequencies below one megahertz, where  $\sigma \gg \omega\epsilon$  this change is inconsequential. Above this frequency, the difference is evident. However, since the present form of Equation (46) permits easier computations in the time domain, the approximation of  $\sigma + j\omega\epsilon \approx \sigma$  is kept with the knowledge that field waveform components above one megahertz, are at best, approximate values.

Equations (41) and (45) develop the relationships between the vertical and horizontal components of the electric field. If the  $E_z$  field at the source region boundary is known, the field components at an arbitrary distance  $x > x_0$  can be developed from the expressions:

$$E_z(x, \omega) = \frac{x_0}{x} E_{oz}(x_0, 0, \omega) e^{-jk(x-x_0)} \quad (47)$$

$$E_x(x, \omega) = \frac{x_0}{x} \left[ \sqrt{\frac{\epsilon}{j\omega\sigma}} j\omega E_z(x_0, 0, \omega) - \frac{h}{x} E_z(x_0, 0, \omega) \right] e^{-jk(x-x_0)} \quad (48)$$

Since the exponential term in the above equation accounts only for a shift of time origin, the equations in the time domain become:

$$E_z(x, t) = \frac{x_0}{x} E_{oz}(x_0, 0, t) \quad (49)$$

$$E_x(x, t) = \frac{x_0}{x} \left[ \frac{\epsilon}{\sigma\pi} \int_0^t \frac{1}{\sqrt{t-t'}} \frac{\partial E_z}{\partial t'}(x_0, 0, t') dt' - \frac{h}{x} E_z(x, t) \right] \quad (50)$$

In order to examine the above mathematical concepts for radiated electric field components, a public domain description of an  $E_z$  field at a source region boundary was constructed from information available in

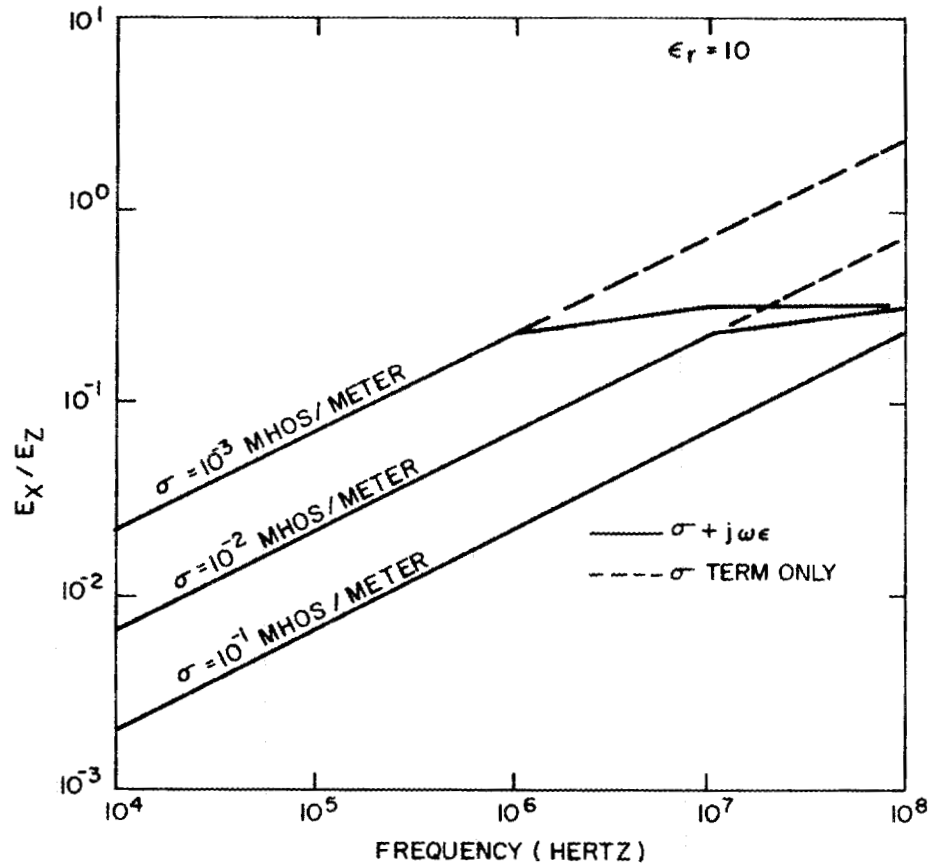


Fig. 21. Ratio of horizontal to vertical SREMP radiated electric field components.

Bell Systems research [7]. The applicable parameters for this example are shown in Table 6.

Table 6

BELL PARAMETERS FOR A VERTICALLY POLARIZED ELECTRIC FIELD ( $E_z$ ) AT A SOURCE REGION BOUNDARY

<u>PARAMETER</u>	<u>DESCRIPTION</u>
Peak Magnitude	$E_p = 1600$ volts/meter
Time Domain Waveform	Figure 22
Source Region Boundary	$x_0 = 6000$ meters
Height Above Ground	$h = 10$ meters
Ground Conductivity	$\sigma_g = 0.01$ mhos/meter
Relative Dielectric Constant	$\epsilon_r = 10.0$

Given the above data, the magnitude and time domain waveform for the  $E_z$  and  $E_x$  components of the radiated electric field can be calculated for distances greater than or equal to the source region boundary ( $x_0$ ). Figure 22 depicts the  $E_z$  time domain waveform at 6,000 meters ( $x_0$ ) and 10,000 meters. As expected, the waveforms exhibit an  $x_0/x$  dependence with increasing distance from the burst. Figure 23 depicts the corresponding  $E_x$  component at the same spatial locations. As indicated by Equation (50),  $E_x(t)$  exhibits a very sharp spike at early times due to the  $\partial E_z/\partial t$  term, but the magnitude is much less than the corresponding  $E_z(t)$ . Figure 24 presents the frequency content of the time domain waveforms of the previous two figures.

A second examination was made using an unclassified nominal radiated ground-burst EMP waveform offered by Radasky and Smith [14]. This arbitrary waveform, shown as Figure 25, was scaled with the Bell parameters [7] for peak magnitude and zero crossing. Ground conductivity was kept at 0.01 mhos/meter. The resulting  $E_z$  and  $E_x$  time domain waveforms, at 6,000 and 10,000 meters, are shown as Figures 26 and 27.

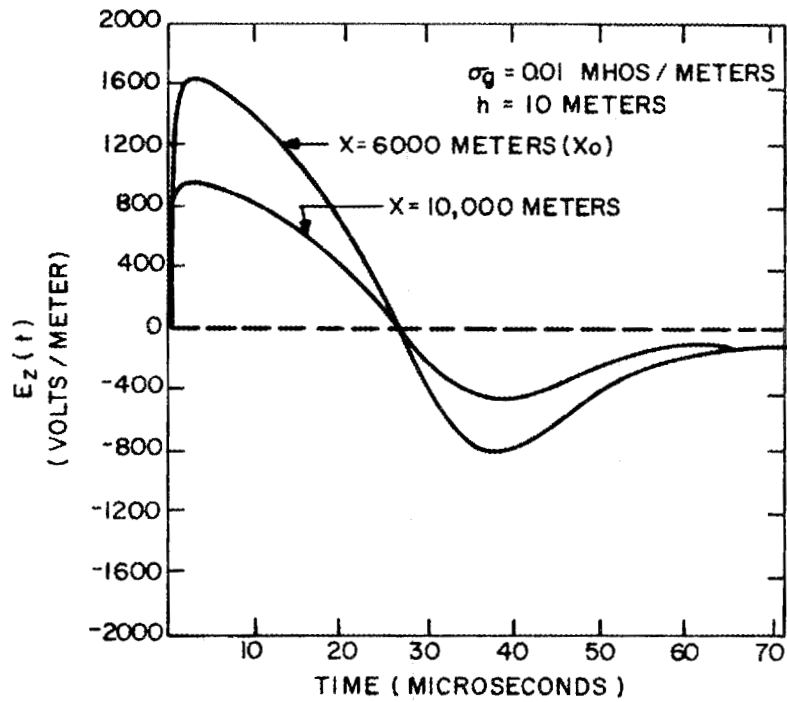


Fig. 22. Hypothetical time domain waveforms for the  $E_z$  radiated field component based on Bell parameters [7].

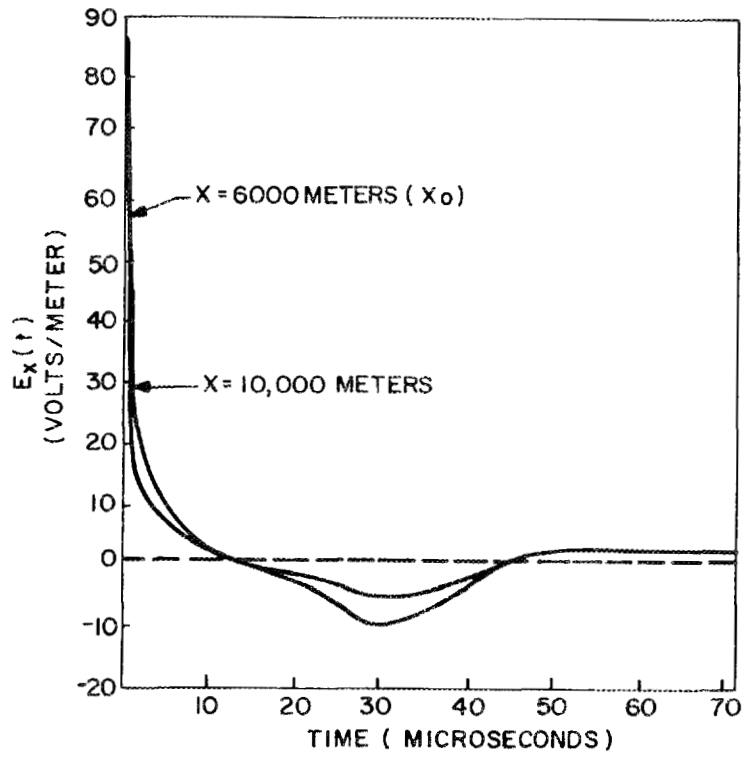


Fig. 23. Calculated time domain waveforms for the  $E_x$  radiated field component based on Bell parameters [7].

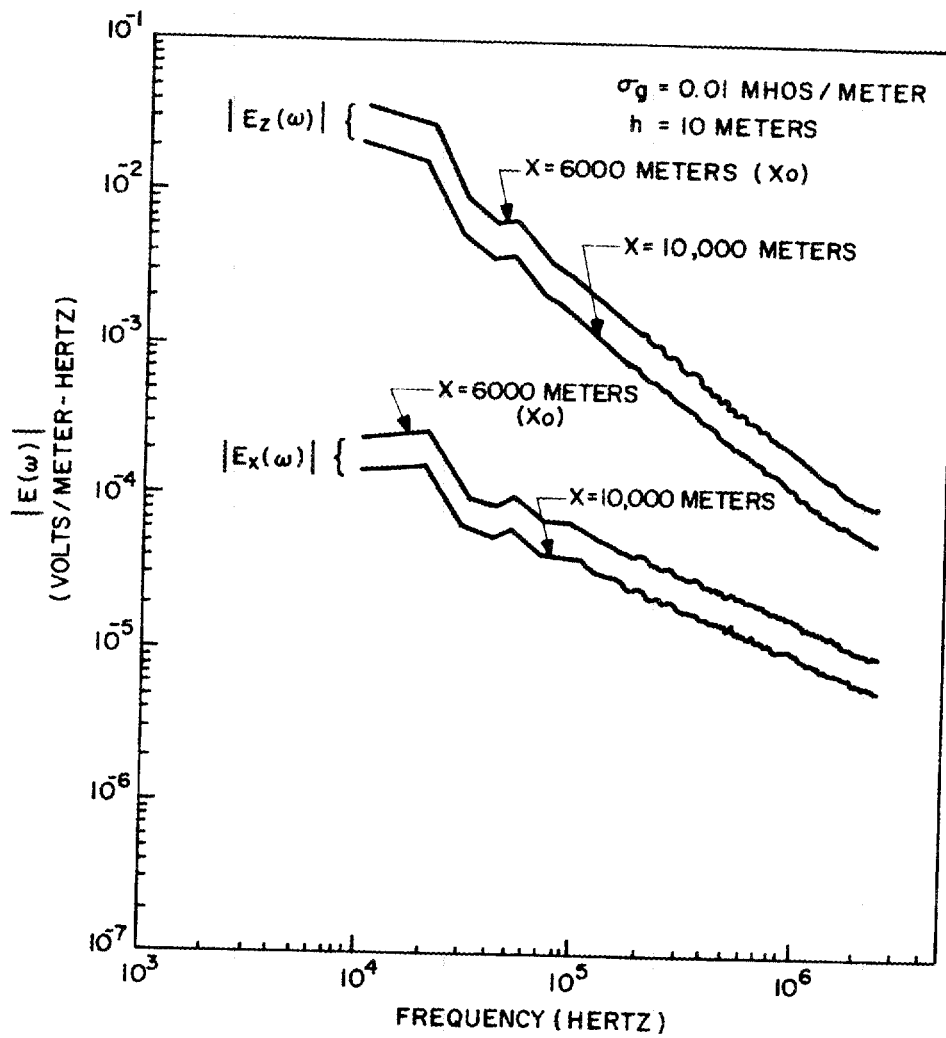


Fig. 24. Frequency domain plot for hypothetical  $E_z$  and  $E_x$  radiated field components based on Bell parameters [7].

In order to explore the sensitivity of the  $E_x$  component to ground conductivity, the Radasky time domain waveform was used for  $\sigma_g=0.001$  mhos/meter. The result is shown as Figure 28. It is important to note that the order-of-magnitude change in ground conductivity resulted in a three-fold increase in the  $E_x(t)$  peak magnitude when compared to the 0.01 mhos/meter case.

The above use of a vertical electric field peak magnitude of 1,600 volts per meter should not be construed as an expected value nor an upper bound on this parameter. The Longmire calculation, shown as Figure 19(b) indicates a peak magnitude exceeding 5,000 volts per meter at a distance of 10,000 meters. Extreme care must be taken to quantify the temporal and spatial definition of the radiated field under well defined scenarios.

### 3.5 Summary

As discussed in this section, SREMP descriptions result from an extremely complex interaction between specific weapon yield and the local physical environment. Knowledge of weapon gamma production and the Compton process can be used to develop the transient field characterizations of interest.

Typical SREMP characterizations divide the SREMP field environment into two distinct areas separated at a spatial boundary. Within the source region boundary, the SREMP fields are considered to be non-radiating and consist of radial and polar electric fields and azimuthal magnetic fields defined under a spherical coordinate system. These fields will couple with power system circuits and equipment located above and below the earth's surface. Accurate estimation of the fields at all spatial locations requires the use of complex, multi-dimensional finite difference codes operating on Maxwell's equations.

The spatial boundary of the source region becomes an extremely important parameter since, at and beyond this distance, SREMP fields can be characterized by a vertically polarized electric field propagating

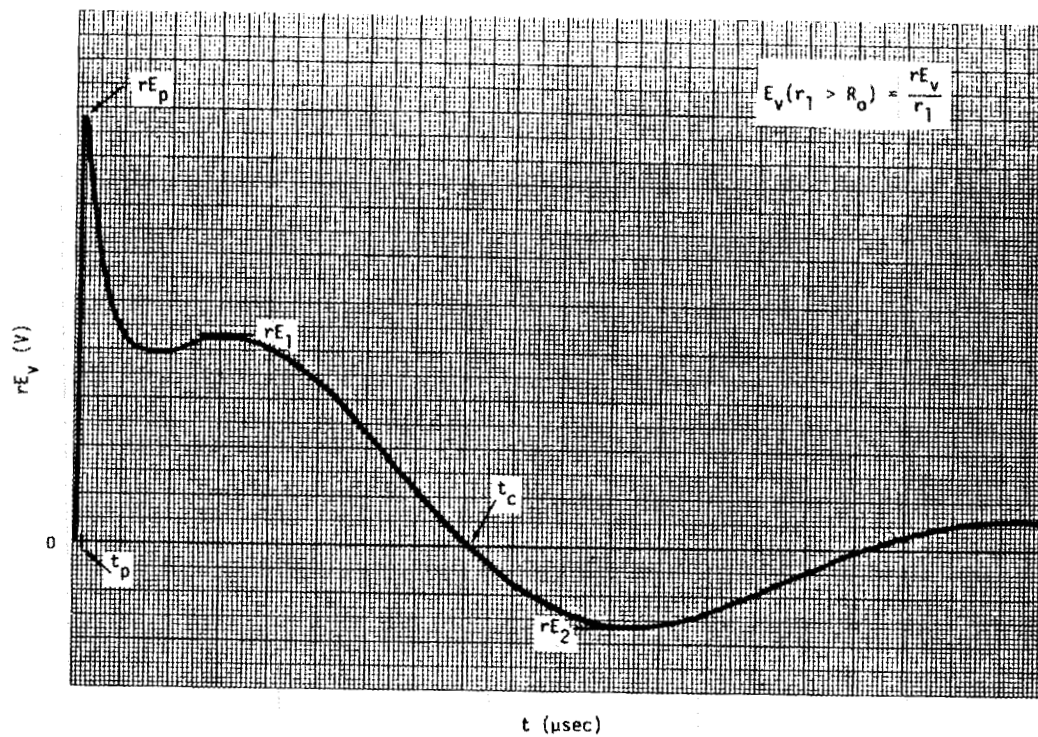


Fig. 25. Typical time domain waveform of Radasky and Smith [14] for SREMP radiated  $E_z$  field.

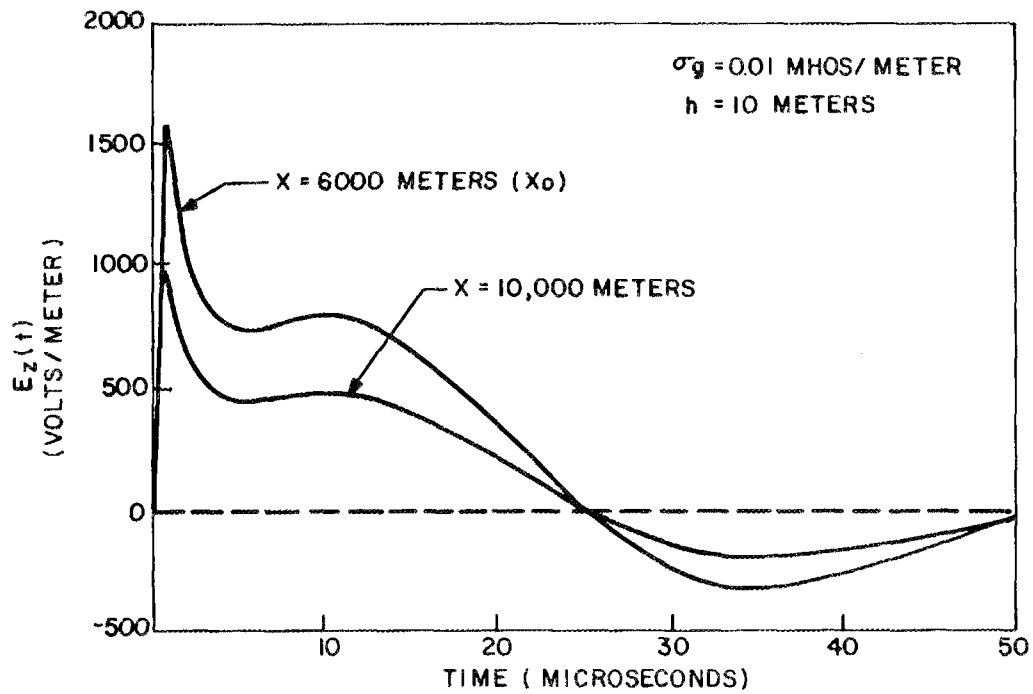


Fig. 26. Typical time domain waveforms for  $E_z$  radiated field component for the Radasky [14]<sup>2</sup> shape and Bell parameters.

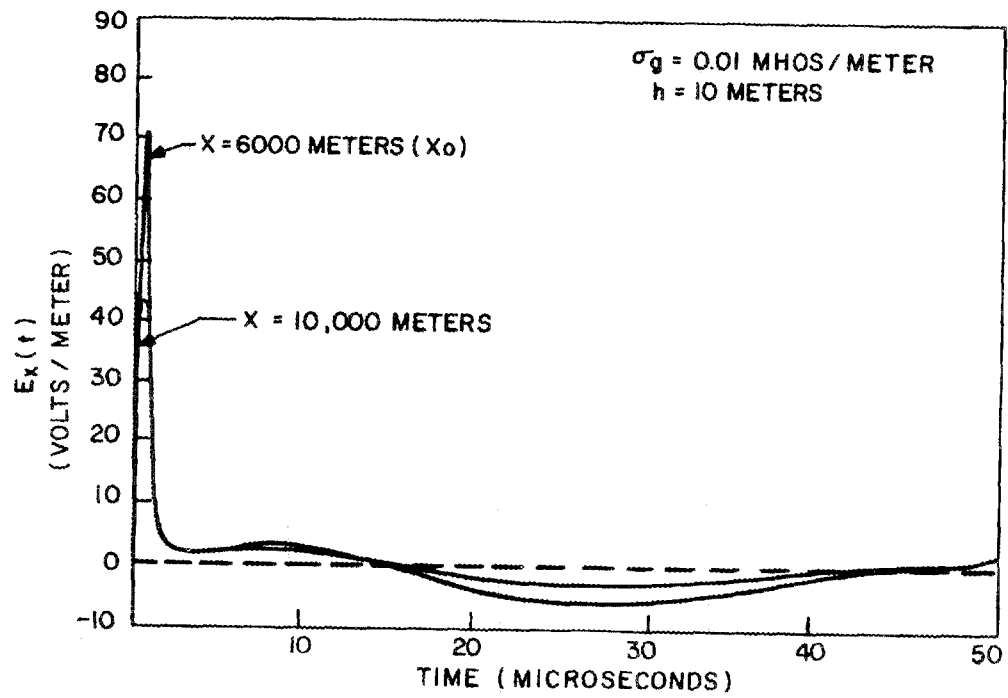


Fig. 27. Typical time domain waveforms for  $E_x$  radiated field component for the Radasky shape and Bell parameter for  $\sigma_g = 0.01$  mhos/meter.

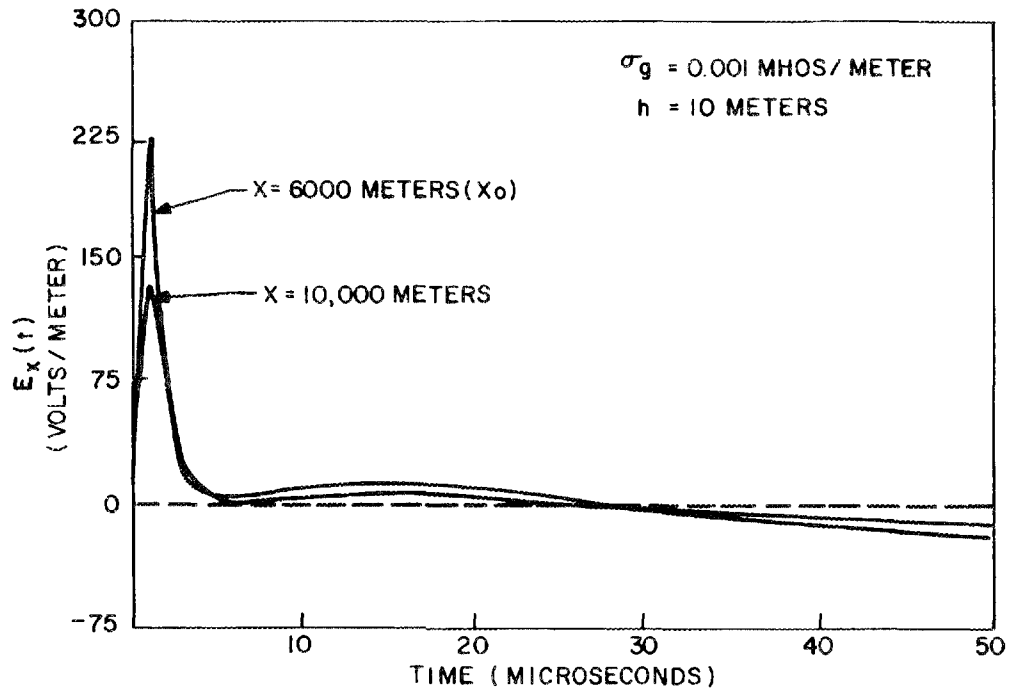


Fig. 28. Typical time domain waveforms for  $E_x$  radiated field component for the Radasky shape and Bell parameter for  $\sigma_g = 0.001$  mhos/meter.

away from the burst attenuating at least as the inverse of the radial distance. Lossy ground creates a surface tangential component of this radiating field. Both the vertical and horizontal components may excite power systems circuits and components located at some distance beyond the source region boundary.

It is important to note that, unlike HEMP characterization, there are no public domain "canonical" transient field descriptions ascribed to SREMP. Rigorous coupling analysis requires weapon specific, multi-dimensional field descriptions within the source region and at least, a complete description of the radiated field at the source region boundary. In the next section, discussion of SREMP coupling to the power system explores the relevant set of required field and induced surge parameters for civilian power system assessments.

## 4. SREMP COUPLING TO POWER SYSTEMS

### 4.1 Introduction

In the previous section, an overview of the transient electromagnetic fields associated with surface burst SREMP has been presented. Power system assessment requires a different perspective than that normally associated with other SREMP evaluations. The vast majority of previous investigations have been concerned with the SREMP threat to military systems. Typical of these investigations, within the source region, is the characterization of surges expected to occur at entry points to a hardened facility or weapon system via underground cables, above ground distribution circuits, and communication antennas. Based on the principle of balanced survivability, quantification of the SREMP threat within the source region is extremely important, since the facility under evaluation is otherwise hardened to perform its intended function for all cases except a direct strike.

This same principle of balanced survivability, applied to civilian electric utility systems, indicates a different set of concerns. Since the system was never designed to survive the weapon effects within a circular radius corresponding to the source region, it is not constructive to evaluate SREMP effects directly on the system within this area. The important issues then become:

- The threat associated with electrical surges formed within the source region and propagating out of that region via overhead and underground lines and cables.
- The threat associated with the SREMP radiated field in the form of surge transients induced on power system elements located outside the source region.
- System operational capability and response due to the physical destruction of power system elements within the spatial radius of direct damage.

Given the above considerations, a logical place to define SREMP induced surges and SREMP radiated field is at a source region spatial boundary applicable for power system assessment.

As a prelude to methodology development, this section discusses representative time and frequency domain characteristics of SREMP induced surges, defined at the source region boundary, for source region penetrations of interest. The discussion continues with an evaluation of surges induced by the radiated field.

The section concludes with a summary of recommendations for the environmental specification of surface burst SREMP and other surface weapons effects necessary to perform power system risk assessment.

#### 4.2 Electromagnetic Field Coupling Within The Source Region

Within the source region, all computational techniques for calculating coupling of SREMP fields to above and below ground power system lines and cables begin with an expression of Maxwell's equations such as Equations (12) and (13) of this report. The specific SREMP environment, in terms of required variable definitions (Compton current, air ionization rate, etc.) necessary to solve the above equations, are normally supplied by the sponsor agency. At this point, the analysis focuses on the selection of a computational method to be used to develop a characterization of the induced surge at a point of interest, based on reasonable assumptions. Specific problems have been solved using: 1) a strict analytical approach as offered by Longmire [16], 2) large, multi-dimensional finite-difference codes operating directly on Maxwell's equations [11,17] and 3) such equations expressed in transmission line form and solved by digital techniques [12]. The applicability of each approach, for a specific problem, continues to be a topic of extensive discussion within the EMP research community.

The discussion is most intense for the analysis of above ground lines physically located deep within the source region. Research by JAYCOR [17] suggests that the early time response (less than a micro-

second) for such lines can be highly dependent on the details of the spatial and time characterization of air conductivity. For this case, transmission line calculations do not agree well with finite difference solutions. Investigations by Graham [12] suggest that his transmission line approach may be a good approximation only when the air conductivity is small, such that the skin depth of the air is greater than the height of the line. In this regard, Graham postulates that, for surges to propagate out of the deep source region, the skin depth must be on the order of the e-folding distance of the air conductivity, typically on the order of hundreds of meters. For the analysis of power system lines, since the e-folding distance may be much greater than the height of any line, surges coupled within highly conducting spatial areas of the source region do not propagate out of this area. Therefore, this stimulus may not affect the characterization of surges predicted by transmission line calculations for those areas where such a technique is valid. Such an area exists for fields coupled near the edge of the source region.

Recent investigation of buried cable systems [19] indicates that solutions obtained by transmission line and finite-difference calculations are much closer in agreement than for the overhead line cases. This agreement may largely be due to the characterization of soil conductivity and the absence of the time and space domain complexity inherent in air conductivity.

In the assessment of civilian electric power systems, the effect of transient, electromagnetic field conditions within the source region can be understood by the characterization of coupled surges on lines and cables penetrating or traversing the region. Such lines and cables constitute the propagational path by which such surges exit the source region prior to system damage/destruction due to other weapon effects. A consistent spatial location characterizing such surges occurs at the source region boundary.

Employing an analytical approach, Longmire [16] has calculated examples of load current surges expected at the entrance of a hardened facility located 1000 meters from the burst point via: 1) a buried power distribution cable and, 2) an overhead line located 10 meters above the surface. The results of these calculations are shown as Figure 29. The scenario under investigation may not be atypical of a large yield weapon event. It is interesting to note that the surge current associated with the overhead line peaks somewhat earlier in time and at a higher magnitude when compared to the buried cable. This effect may be due to the fact that, for the majority of the distance, air conductivity is smaller than ground conductivity. The intense SREMP fields generated close to the source are seen by the overhead line at an earlier time.

Graham [12] has calculated the surge current across a 0.1 ohm impedance at the end of a 2500 meter overhead line located at a height of 10 meters above the surface. His result is shown as Figure 30. In this representation, no line flashover is assumed to occur. For power systems analysis, the significant points of interest of this result are as follows:

- Current surge peak magnitude ( $E_0 = 0$ ) approximately 180 kiloamperes.
- Time to crest greater than 250 microseconds.
- Significant low frequency energy content.

The incorporation of  $E_0$  effects are seen to decrease the peak magnitude of the surface due to field cancellation. Barnes [18] has suggested that the above surge might generally be represented as a double exponential waveform, for some distance greater than 2500 meters, as:

$$I = I_0 (e^{-\tau t} - e^{-\lambda t}) \quad (51)$$

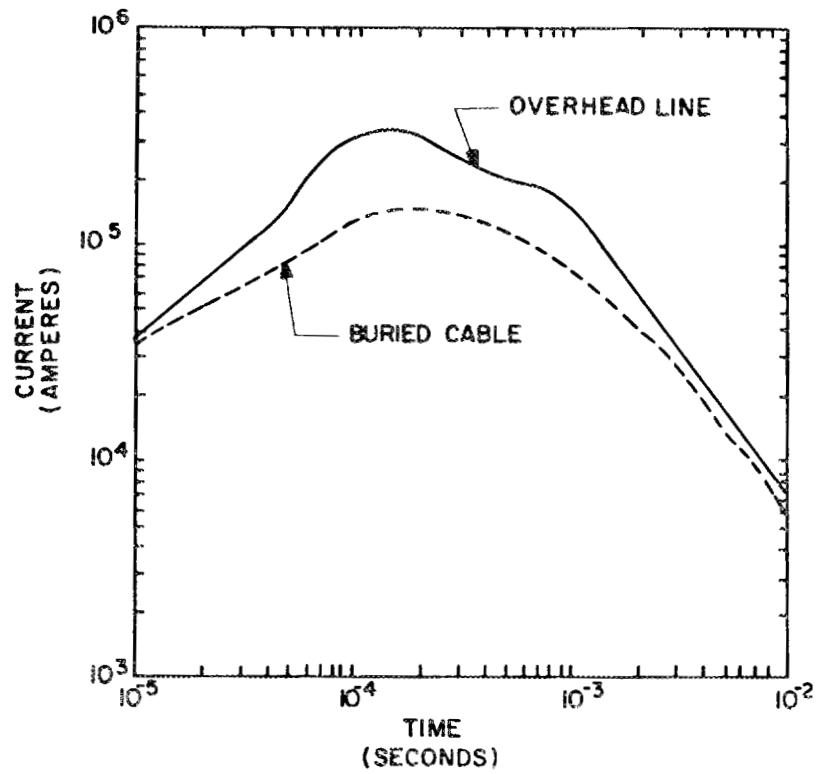


Fig. 29. Longmire example [16] of transient surge current for a overhead line and an underground cable, each 1000 meters in length, in a nuclear surface burst source region.

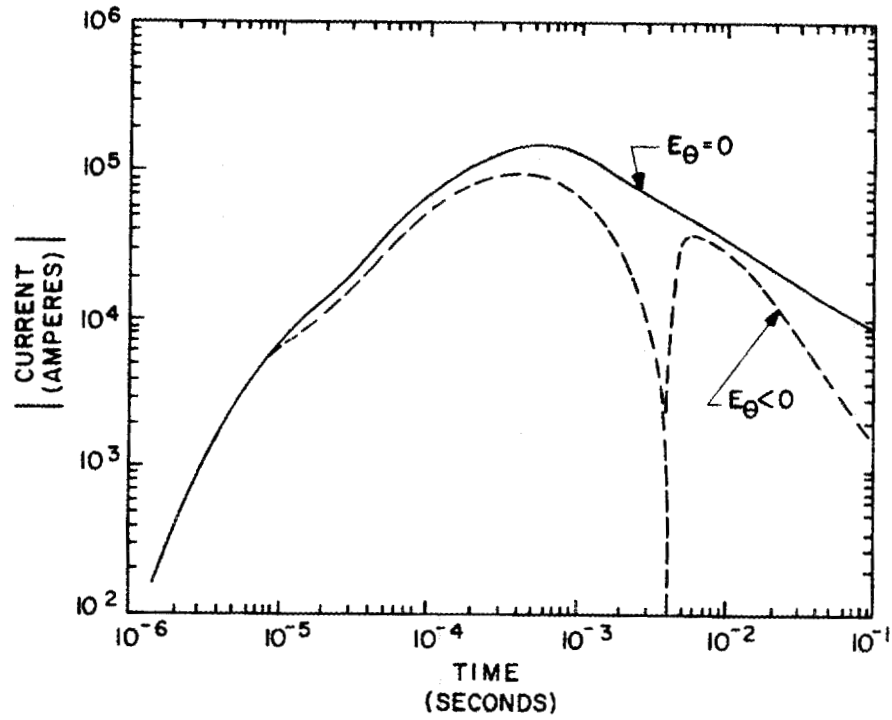


Fig. 30. Graham calculation [12] of transient surge current into a 0.1 ohm load located at the end of a 2500 meter long overhead line in a nuclear surface burst source region.

where

$$I_0 = 180.3 \text{ kiloamperes}$$

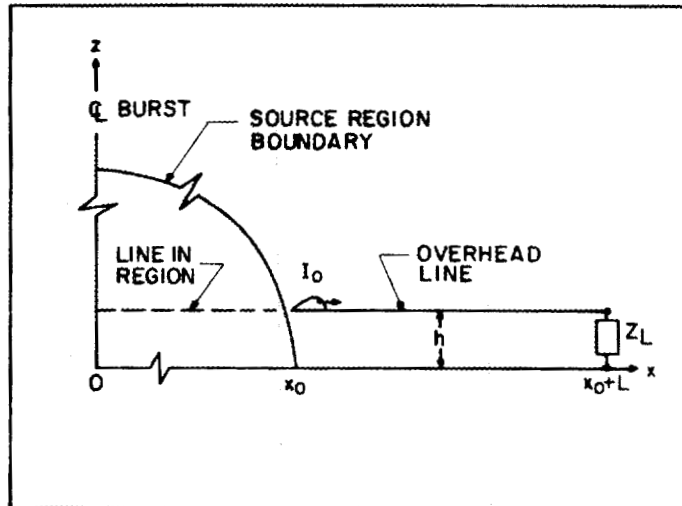
$$\tau = 3.8 \times 10^2 \text{ sec}^{-1}$$

$$\lambda = 2.0 \times 10^3 \text{ sec}^{-1}$$

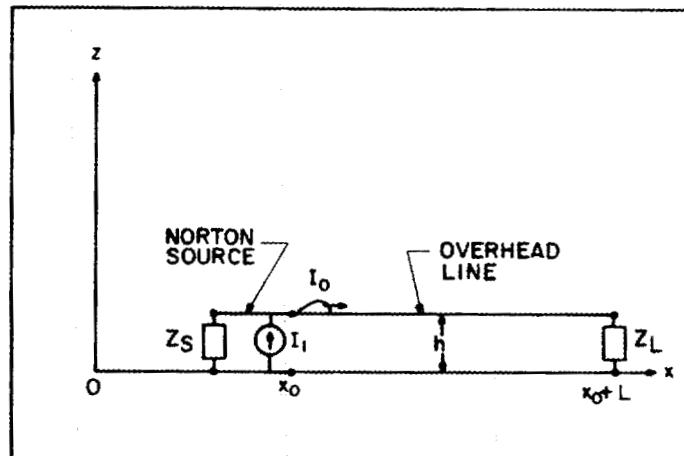
In summary, power system assessment for that portion of the SREMP environmental definition within the source region may be facilitated by the characterization of a "reasonable" worst case surge formed within and propagating out of the region via lines and cables. For these power system elements, the characterization may take the form of a Norton equivalent source placed at the source region boundary. This concept is shown as Figure 31. The question remains as to the value of the source impedance ( $Z_s$ ) applicable to the model. One might reason that, since the air conductivity within the region is high,  $Z_s$  may be represented by a value of a few ohms. This implies that a surge on the line which is incident to the region boundary from the exterior will be reflected with some attenuation and propagate back into the grid. An alternate view is, because the air conductivity in the source region does not change abruptly at the boundary, an incident current surge, once penetrating the region, will perceive a variable line impedance due to the spatial difference in air conductivity. Such variable distributed loading of the line has been noted to minimize reflections in similar problems involving traveling waves on antennas [20]. Thus, a reasonable selection for the source impedance ( $Z_s$ ) may be the characteristic line impedance ( $Z_c$ ). Assumptions of this type should be further explored in subsequent phases of the research effort.

#### 4.3 Radiated Field Coupling Outside The Source Region

As developed in Section 3 of this report, the second major aspect of surface burst SREMP is the illumination of the power system by the SREMP radiated field. Unlike an incident field, in the form of a plane wave, this radiated field has a magnitude which decreases with increasing distances from the event. This indicates that power system excitation by this field becomes weaker as a function of distance.



a) Physical Configuration



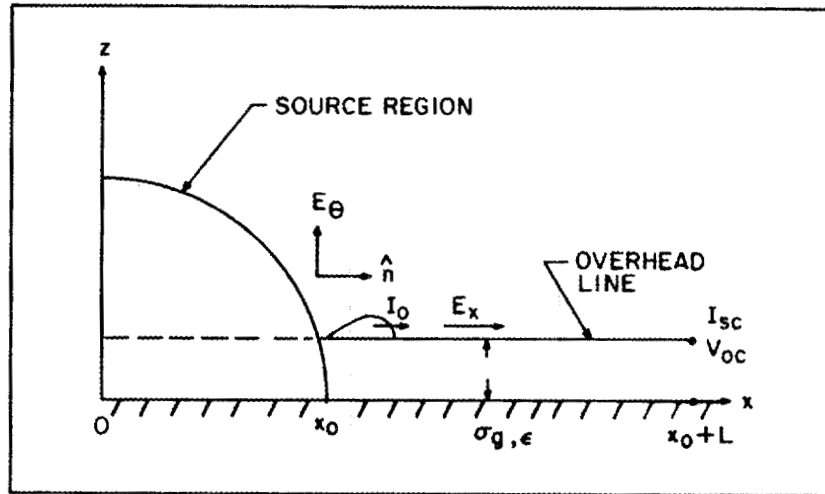
b) Equivalent Model Circuit

Fig. 31. Representation of the current surge formed within the source region on an overhead line by a Norton equivalent source located at the source region boundary.

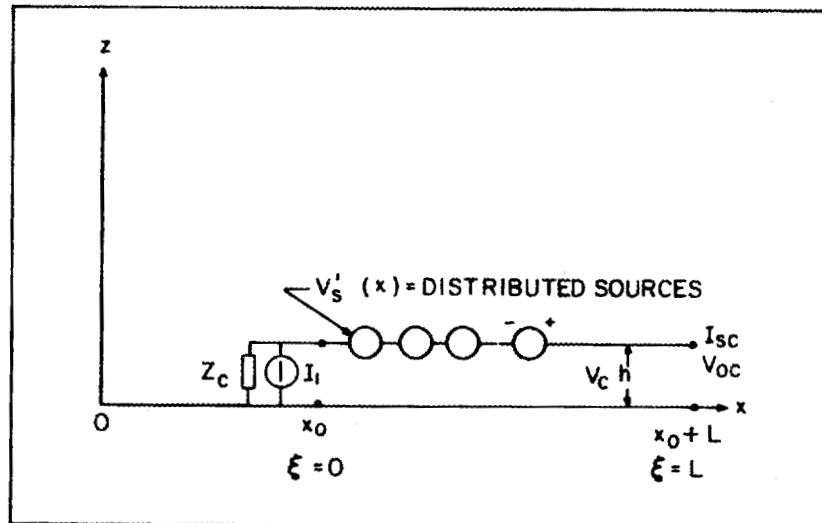
Power system lines and cables penetrating the source region can be excited by both transient field environments, while those power system components located completely outside the source region will be directly excited only by the radiated field.

For the purpose of this report, the development of overhead line response to SREMP radiated fields will begin with an idealized geometry as shown in Figure 32(a). A semi-infinite line of height ( $h$ ) and characteristic impedance ( $Z_c$ ) is assumed to penetrate the source region of a nuclear surface burst. The source region is assumed to extend in a symmetric manner to a distance ( $x_0$ ) meters. The line penetrates the source region at this point; outside the region, the line extends radially away from the burst. The earth is considered to have homogeneous electrical conductivity ( $\sigma_g$ ) mhos/meter and a dielectric constant  $\epsilon = \epsilon_g \epsilon_0$ . The surge current induced on the line segment within the source region is denoted by the term  $I_0$ . The radiated field is assumed to be characterized at the source region boundary ( $x_0$ ) as a vertically polarized transient electric field ( $E_0$ ) propagating radially away from the burst. The vertical component of the radiated electric field is assumed to propagate with the free space propagation constant along the air-earth interface. The excitation of the line by the radiated field is due to the tangential component ( $E_x$ ) along the line, as well as by the vertical electrical field ( $E_z$ ) at both ends of the line. In the present discussion, only the contribution of the horizontal electric field to the line response is considered. In an actual assessment of SREMP effects on a power system, both components of the electric field must be considered.

The physical configuration of the above example is translated into an equivalent circuit as shown in Figure 32(b). The source region has been modelled by a Norton source of magnitude  $I_1$  located at the boundary ( $x_0$ ). The source impedance is assumed to be equal to the characteristic line impedance. It is important to note that there is a difference between the short circuit current source  $I_1$  and the surge current denoted as  $I_0$  in Figure 32(a). In this discussion the short circuit current on the line will always be taken as the equivalent source ( $I_1$ ).



a) Physical Configuration



b) Equivalent Model Circuit

Fig. 32. Physical geometry and electrical equivalent circuit for an overhead line excited by SREMP.

As developed in Section 3, the tangential electric field exciting the line outside the source region may be expressed as:

$$E_x(x, \omega) = \frac{x_0}{x} \left[ \sqrt{\frac{\epsilon_0}{j\omega\sigma_g}} j\omega E_z(x_0, 0, \omega) - \frac{h}{x} E_z(x_0, 0, \omega) \right] e^{-\gamma_0(x-x_0)} \quad (52)$$

where  $\gamma_0 = j\omega/c$  and the term  $E_z(x_0, 0, \omega)$  is a known vertical electric field defined at the source region boundary.

The open circuit voltage of a line of length  $L$  excited by a set of distributed voltage sources ( $V'_s(\xi)$ ) along its length may be calculated as:

$$V_{oc}(\omega) = \frac{e^{-\gamma L}}{1 - \rho e^{-2\gamma L}} \int_0^L V'_s(\xi) \left[ e^{\gamma \xi} - \rho e^{-\gamma \xi} \right] d\xi \quad (53)$$

where  $\rho$  is the reflection coefficient at the source end of the line at  $\xi=0$  ( $x=x_0$ ) and  $\gamma$  is the complex propagation constant for the line. For a matched termination, this reflection coefficient is zero and the above expression reduces to:

$$V_{oc}(\omega) = e^{-\gamma L} \int_0^L V'_s(\xi) e^{\gamma \xi} d\xi \quad (54)$$

Since the distributed voltage source  $V'_s(\xi)$  is actually the tangential electric field along the wire, we have:

$$V'_s(\xi) = \frac{x_0}{\xi+x_0} \left[ \sqrt{\frac{\epsilon_0}{j\omega\sigma_g}} j\omega E_z(x_0, 0, \omega) - \frac{h}{\xi+x_0} E_z(x_0, 0, \omega) \right] e^{-\gamma_0 \xi} \quad (55)$$

Note that the exponential phase term accounts for propagation time delays of the incident field along the line, with  $t = 0$  being chosen to occur at  $x = x_0$  (or  $\xi = 0$ ).

The first term in this equation involving the square root accounts for the effects of the lossy earth on the horizontal electric field exciting the line, while the second term takes into account the spherical nature of the radiated field from the surface burst. As mentioned in Section 3, the square root term in Eq. (55) is really only an approximation to a more complicated expression given by:

$$\sqrt{\frac{\epsilon_0}{j\omega(\sigma + j\omega\epsilon)}}$$

Figure 21 shows the ratio of  $E_x/E_z$  computed as a function of frequency from Eq. (52) as a function of frequency both with and without the square root approximation. As may be noted, for frequencies above 10 MHz for conductivities greater than 0.01 mhos/meter, the results are identical. The degree of accuracy of the approximation degrades somewhat for conductivities on the order 0.001 mhos/meter.

In the time domain, the implication of this approximation is that the calculated time domain results will be identical for signals having rise times up to about 0.1  $\mu$ s. Any faster rising SREMP waveform will experience errors in the coupling to the line if the approximate form of the exciting electric field is used. In such cases, the use of the more accurate relation for the field, together with a numerical Fourier transform to obtain time domain data would be needed.

It is interesting to note the effect of the second term in Eq. (52) in relation to the first. From Fig. 21, the smallest ratio of the component of  $E_x/E_z$  due to the ground conductivity effects is on the order of about  $2 \times 10^{-3}$ . Considering a line having a height of 10m and being located at a distance of km from the burst (at the source region boundary), the ratio of  $E_x/E_z$  due only to the second term in the equation is equal to the ratio of the line height to the observation distance, or  $1.6 \times 10^{-3}$ , a value which is less than that for the earth

conductivity component. As the observation point moves away from the source region boundary, this second term becomes even smaller, and may be neglected in relation to the first term in Eq. (52). Of course, as the conductivity of the earth approaches infinity or as the frequency of the electric field spectrum approaches zero, the first term vanishes, and the only component to the horizontal electric field arises from the second term.

For the normal range of parameters considered for the earth, it is possible to neglect the second term in Eq. (55), and the resulting distributed voltage source on the line then becomes:

$$V'_S(\xi) \approx \frac{x_0}{\xi+x_0} E_X(x_0, \omega) e^{-\gamma_0 \xi} \quad (56)$$

For cases where the conductivity and/or frequency do not permit the neglecting of the second term in Eq. (55) or in the simplification of the square root term, a more generalized expression for the distributed voltage source can be developed.

Use of the above expression in Equation (54) yields:

$$V_{oc}(\omega) = e^{-\gamma L} \int_0^L \frac{x_0}{\xi+x_0} E_X(x_0, \omega) e^{-\gamma_0(\xi)} e^{\gamma \xi} d\xi \quad (57)$$

or

$$V_{oc}(\omega) = x_0 E_X(x_0, \omega) e^{-\gamma L} \int_0^L \frac{e^{(\gamma-\gamma_0)\xi}}{\xi+x_0} d\xi \quad (58)$$

Shifting the time origin so that  $t=0$  occurs at the end of the line at  $x=x_0+L$  (or  $\xi = L$ ) by multiplying Equation (58) by  $\exp(\gamma_0 L)$ , the final expression for the open circuit voltage at the end of the line may be expressed as:

$$V_{OC}(\omega) = x_0 E_X(x_0, \omega) \int_0^L \frac{e^{(\gamma - \gamma_0)(\xi - L)}}{\xi + x_0} d\xi \quad (59)$$

Unlike the case of incident plane wave excitation, the above integral cannot be evaluated analytically. Thus, numerical methods must be employed to obtain a solution.

In a similar development, the open circuit voltage ( $V_{OC}$ ) at some distance ( $x_0 + L$ ) down the line caused by the Norton current source ( $I_1$ ) located at  $x = x_0$  can be expressed by assuming a distributed voltage excitation of the form.

$$V'_S(\xi) = Z_C I_1 \delta(\xi) \quad (60)$$

The use of the above expression in Equation (54) yields:

$$V_{OC}(\omega) = Z_C I_1(\omega) e^{-\gamma L} \quad (61)$$

If a simplification is made such that the characteristic impedance of the line ( $Z_C$ ) is assumed to be a constant in the frequency domain, the short circuit current at distance ( $x_0 + L$ ) on the line can be determined by dividing Equation (59) or (61) by the value of the characteristic impedance.

#### 4.3.1 Example of Radiated Field Line Excitation

In order to understand the time domain characteristics of SREMP radiated field induced surges on the overhead line under discussion, Equation (59) was solved numerically to obtain transient open circuit voltages for differing line lengths from 1 kilometer to 200 kilometers. The input data used for this computation are shown in Table 7.

Table 7

PARAMETERS FOR OVERHEAD LINE CALCULATION OF  
OPEN CIRCUIT VOLTAGE INDUCED BY SREMP RADIATED FIELD

<u>Parameter</u>	<u>Description</u>
Vertical Field Peak Magnitude	$E_p = 1600$ volts/meter
Vertical Field Time Domain Waveform	$E_z =$ Figure 26
Horizontal Field Time Domain Waveform	$E_x =$ Figure 27
Source Region Boundary	$X_o = 6000$ meters
Line Length	$L =$ (variable)
Line Characteristic Impedance	$Z_c = 400$ ohms
Line Height Above Ground	$h = 10$ meters
Ground Conductivity	$\sigma_g = 0.001$ mhos/meter

Based on the above parameters, a numerical Fourier transform was taken of the horizontal field time domain waveform (Figure 28) to obtain the excitation spectrum  $E_x(\omega)$  used in Equation (59). The open circuit voltage spectrum  $V_{oc}(\omega)$  was then calculated for several lengths of line. Time domain results  $V_{oc}(t)$  were then calculated by performing an inverse Fourier transform.

The results of the above simulation are summarized as follows:

- The maximum open-circuit voltage did not occur for the longest length of line. In this simulation, the maximum occurred for a line length of 5 kilometers. On a normalized base where 1.0 per-unit is equal to the largest open-circuit voltage crest magnitude the, results are tabulated below:

<u>Line length (Km)</u>	<u><math>V_{oc}</math> Crest Magnitude (per-unit)</u>
1.0	0.4
2.0	0.6
5.0	1.0
10.0	0.7
20.0	0.5
50.0	0.2
100.0	0.1

For shorter lines the temporal waveform of the voltage more closely resembles that of the exciting waveform and is approximately equal to the product of the line length and the incident radiated electric field. As line length increases, the effects of propagation dispersion become increasingly important as does the  $1/r$  attenuation of the local incident field.

- Frequency analysis of the transient overvoltages indicates that the responses for shorter lines appear to be scaled versions of the excitation. As the line becomes longer, higher frequency attenuation occurs and the spectra has more of a lower frequency nature.
- The time to crest of the transient overvoltage is significantly longer than HEMP excitation and is on the order of conventional power system lightning models.

The above results offer direction as to the important criteria to be incorporated in the methodology. For a particular line, the overvoltage profile must be developed for the entire line length to determine the location of the peak value. In addition, estimates of enclosure shielding effectiveness based on high frequency HEMP assumptions must be re-examined in light of the spectral content of the SREMP radiated field.

#### 4.3.2 Arbitrary Line Orientation Outside The Source Region

Up to this point, the development and numeric calculations have assumed a conducting overhead line orientated radially with respect to the source region. The response of such a line is known to provide the worst case estimate of line response due to the fact that there is a progressive build-up of voltage (or current) on the line when the incident field propagates in the same direction as the line. Of some importance is the excitation of arbitrarily orientated lines, located outside the source region, which are excited by the SREMP radiated field. The development geometry for this case is shown as Figure 33. A nuclear surface burst is assumed to be located at the coordinate origin and is described by a source region radius ( $r_0$ ) with a radiated vertical electric field  $E_z(r_0)$  at this point. The overhead line is assumed to start at some point  $P_1$  located at  $[x_1, y_1]$ .

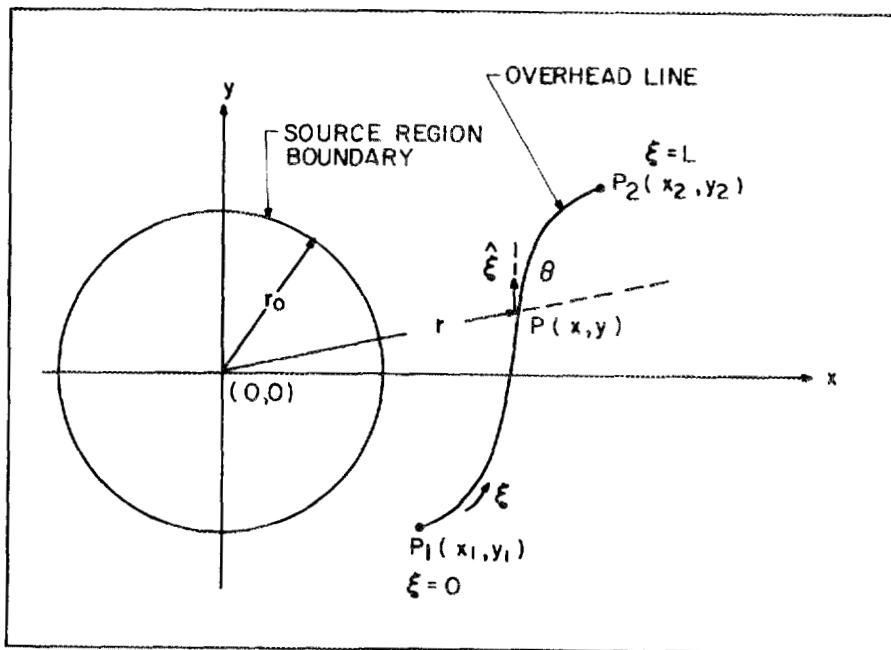


Fig. 33. Orientation of an arbitrary overhead line located outside the source region (plan view).

The other end of the line is at point  $P_2$  located at  $[x_2, y_2]$ . The variable  $\xi$  represents the distance along the line from  $P_1$  to  $P_2$  where  $\xi=L$ , nominally taken to be the "line length." At any point  $P$  on the line, there is a local unit vector  $\hat{\xi}$  in the direction of the line and a radial vector  $r$  from the burst location to point  $P$  on the line. The angle between these two vectors is defined as  $\theta$ .

The open circuit voltage at point  $P_2$  can be obtained by Equation (54). The load impedance at point  $P_1$  is assumed to be equal to the line characteristic impedance. Again, the propagation constant  $\gamma$  for the line is a function of line and ground properties and is a dispersive function of frequency.

The distributed voltage sources required to solve Equation (54) consists of the tangential electric field at any position along the line and may be expressed as:

$$V'_s(\xi) \approx \frac{r_0}{r} \left[ \sqrt{\frac{\epsilon_0}{j\omega\sigma_g}} j\omega E_z(r_0, \omega) e^{-\gamma_0 r} \right] (\hat{r} \cdot \hat{\xi}) \quad (62)$$

The above equation is slightly different from Equation (56) in that radial coordinates have been used in place of the  $x$  spatial coordinates and that there is a  $(r, \xi)$  term to account for the projection of the horizontal (radial) field on the line. Similar to Equation (56), the second term in the distributed source which is directly proportional to the vertical SREMP field is very small and is not included in Equation (62).

In this development, it is convenient to define the time origin ( $t=0$ ) such that it occurs at point  $P_2$ . This is accomplished by multiplying Equation (62) by a phase factor of  $\exp(\gamma_0 r_2)$ , resulting in the following expression for the distributed sources:

$$V'_s(\xi) \approx \frac{r_0}{r} \left[ \sqrt{\frac{\epsilon_0}{j\omega\sigma_g}} j\omega E_z(r_0, \omega) e^{-\gamma_0(r_2-r)} \right] (\hat{r} \cdot \hat{\xi}) \quad (63)$$

Inserting this expression into Equation (54) yields the following relation for the open circuit voltage at  $P_2$ :

$$V_{oc} = r_0 \sqrt{\frac{\epsilon_0}{j\omega\sigma_g}} j\omega E_z(r_0, \omega) \int_0^L \frac{e^{-\gamma_0 [r_2 - r(\xi)]} e^{\gamma(\xi - L)}}{r(\xi)} (\hat{r}(\xi) \cdot \hat{\xi}) d\xi \quad (64)$$

where the dependence of  $r$  on the variable  $\xi$  has been shown explicitly. As before, the integral in Equation (64) cannot be performed analytically, so numerical methods must be used.

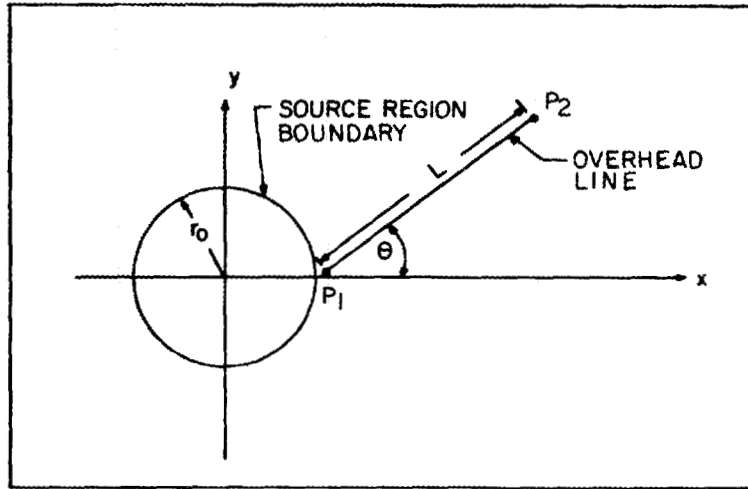
Equation (64) is a general expression for any arbitrarily orientated line. In the case of the radially orientated line where:

$$\begin{aligned} r_0 &= x_0 \\ r_2 &= x_0 + L \\ r &= x_0 + \xi \\ \hat{r} \cdot \hat{\xi} &= 1 \\ r_2 - r(\xi) &= L - \xi \end{aligned}$$

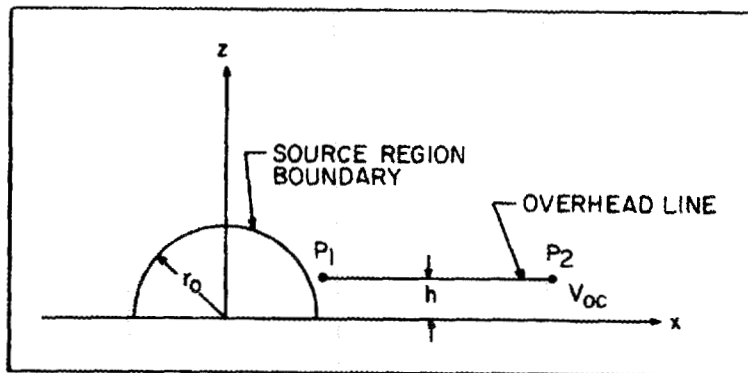
$$\text{and } \sqrt{\frac{\epsilon_0}{j\omega\sigma_g}} j\omega E_z(r_0, \omega) = E_x(x_0, \omega) \quad (65)$$

Equation (64) reduces to a form identical to Equation (54).

In order to illustrate the effects of changing the orientation of the overhead line, the simple case of a straight line of length  $L$ , outside the source region and having an angle of  $\theta$  with the  $x$  axis, was evaluated. This case geometry is shown as Figure 34. The case parameters were the same as the previous examples. Point  $P$ , was taken to be just outside the source region boundary. The results of this simulation are summarized as follows:



a) Plan View



b) Section View

Fig. 34. Geometry of an arbitrarily orientated, straight, overhead line outside the source region.

- For the same length of line, the peak amplitude decreases as  $\theta$  increases due to: 1) the decrease in the tangential component of exciting field along the line (r.ξ term) and 2) the incident field and the voltage waves on the line now have a larger phase difference. On a normalized base, for a line length of 5 kilometers, the results are tabulated below:

<u>Orientation Angle (degrees)</u>	<u>V<sub>OC</sub> Crest Magnitude (per-unit)</u>
0	1.0
30	0.5
60	0.2
90	0.1

- As the angle increased, the maximum peak amplitude occurs at a greater distance from the source region. In all cases, however, this maximum is less than the value obtained on the radially directed line.

Preliminary calculations, to date, support the contention that the case of the radially directed line serves as an upper bound estimate for arbitrary line response.

#### 4.4 Summary

The SREMP associated with a surface nuclear burst is a localized environment with respect to a large interconnected electric utility grid. As developed in this section, coupled surge characterization to overhead lines and underground cables can be calculated from a knowledge of: 1) the transient electromagnetic fields formed within the source region and 2) the time domain waveform of the vertically polarized electric field radiated outside the source region. For the purpose of research concerning the response of civilian electric utility systems to SREMP, environmental definitions are necessary at the spatial location of the source region boundary for both the surge induced within the source region and characterization of the radiated field at the boundary.

Numeric evaluation based on environments obtained from previous research indicate that lines and cables which experience the greatest excitation are those which are spatially orientated radially to the burst and also penetrate (traverse) the source region boundary. These components will experience both the large, relatively low frequency surges propagating out of the source region plus an additional excitation due to the radiated field. The magnitude of the source region contribution may dominate system response.

Power system elements physically located outside the source region boundary will be directly illuminated only by the radiated field. Calculations indicate that there may exist a critical line length for which the radiated field induced surge magnitude is maximum. Orientations other than radial to the burst and increasing distance of the component from the source region boundary will reduce the surge magnitude at a point of interest.

It has been the authors' intent to discuss the nature of SREMP induced surges using only unclassified, public domain information. Such calculations are necessary to understand and develop an applicable methodology to assess the effects of this phenomena. It is recognized, however, that numerical results may constitute a national security issue. For example, pending revisions to security classification guidelines, such as DOD instruction 5210.58 (Rev.) entitled, "Electromagnetic Pulse (EMP) Security Classification Guide (U)" may preclude the use of calculations of the voltage, current and energy induced on lines by surface bursts in the public domain, even when derived from unclassified nuclear sources and non-system-characteristic geometries.

## 5. SREMP ASSESSMENT METHODOLOGY

### 5.1 Introduction

This section discusses the development of a structured process to assess the effects of SREMP on civilian electric utility systems. The nature of a nuclear surface burst is such that, if EMP did not exist, the civilian utility system may still be severely affected by: 1) initial, physical damage to the system near the burst location within tens of seconds, 2) system exposure to high levels of prompt, ionizing radiation, 3) nuclear lightning and 4) long-term operational impairment due to consequential fallout patterns. The methodology contained herein is focused to investigate the additional risk due to electromagnetic pulse associated with the event. Since EMP is a prompt, transient environment occurring within the first second after the burst, simulations evaluated by this methodology encompass an elapsed period of real time not longer than ten seconds into the event. A complete assessment of all effects of nuclear surface burst(s) on the civilian electric utility system is beyond the scope of the EMP research program.

A key assumption embedded in this SREMP methodology is that the spatial extent of the source region formed around the burst origin is contained within the spatial radius of non-EMP physical damage. For civilian power system assessment, this assumption appears to be reasonable for weapon yields above 10 kilotons. Smaller weapons may require the development of a modified methodology to account for a source region larger than the spatial radius of physical damage.

The methodology acknowledges three distinct transient environments produced by the nuclear surface burst. In terms of spatial coverage, the smallest of these environments is the source region. The threat(s) for evaluation are transient electrical surges formed on lines exciting this region. These surges propagate away from the boundary into the grid prior to physical damage to the line. The threat of interest is: 1) consequential damage to equipment and facilities beyond the

source/physical damage region proximate to the burst and 2) system instability caused by system protective reaction to such surges.

The second environment, also spatially local in area, is the region of initial, direct damage. The methodology incorporates this threat by acknowledging: 1) the time-progressive destruction of the power system in this area, 2) the relevant loss of generation and/or load and, 3) the system protective reaction to isolate this damaged portion of the grid from the rest of the system.

The third transient environment, spatially greatest in terms of the nuclear surface burst, is that portion of the system illuminated by the radiated (free) fields outside the source region. The questions and concerns associated with this phenomena are methodologically quite similar to those associated with HEMP investigation.

Preliminary analysis of the nature of these three environments strongly suggest that the order of assessment proceed as follows:

- Investigation of SREMP radiated (free) field interaction with the grid.
- Evaluation of the consequences of surge propagation on lines intersecting the source region boundary.
- Incorporation of non-EMP physical damage in time sequence of events.

An overview of this assessment progression is shown as Figure 35. Recursive power system load flow/stability simulations are incorporated to investigate the magnitude and extent of system disturbance.

The methodology has been intentionally structured to explore the impact of nuclear surface burst EMP on civilian electric utility systems as an unclassified research project. The distinctions drawn between different threat environments and the development of environmental parameters have intentionally been defined with the unclassified objective in place.

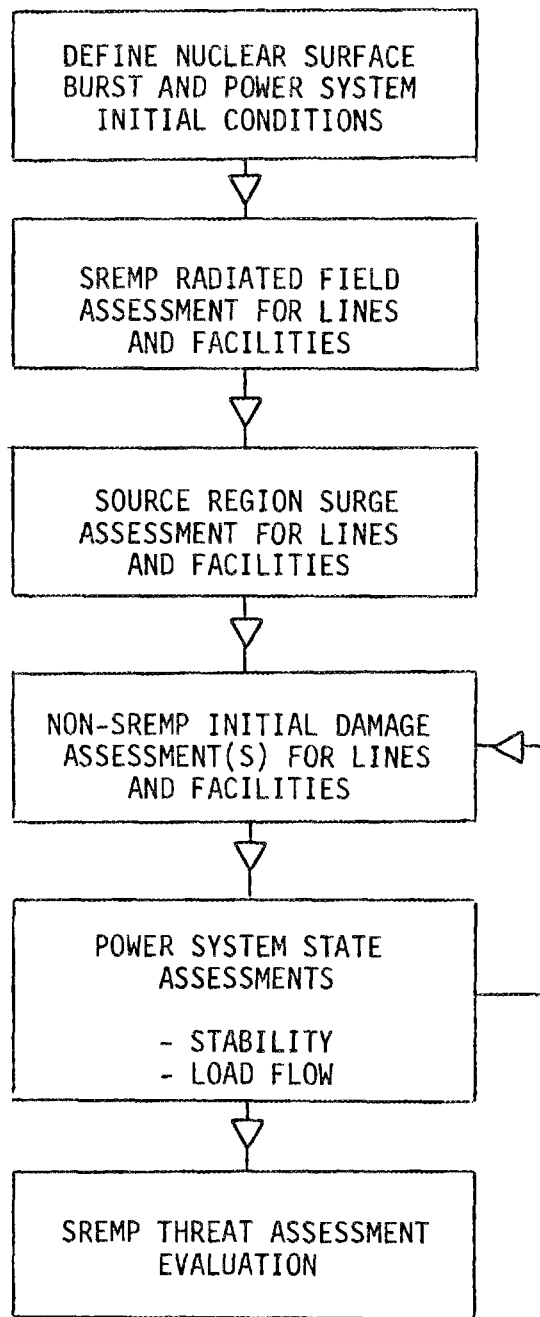


Fig. 35. Overview of methodology for SREMP assessment for civilian electric utility systems.

## 5.2 Assessment Initial Conditions

The methodology must necessarily begin with a definition of the electric utility system of interest and the event. As developed previously in this report, the nuclear surface burst environments are specified as follows:

- Location of the event (burst origin).
- Temporal and spatial characterization of the non-EMP initial damage area, expressed in terms of radial distances from the origin.
- Spatial definition of the applicable source region boundary expressed as a radial distance from the origin.
- Temporal characterization of the induced electrical surges on lines intersecting the source region boundary.
- Temporal characterization of the radiated (free) electric field defined at the source region boundary.

In contrast to transient EMP environments created by high-altitude nuclear events which can directly excite vast areas of the national power system, EMP environments associated with surface nuclear events are local in extent. A spatial shift of a few kilometers in the assumed location of the burst may result in significantly different assessments for otherwise identical scenarios. This dependence on location is illustrated in Figure 36. In this example, a nominal surface burst is assumed to occur near the Phoenix metropolitan area. The solid circle indicates the spatial extent of the source region, the shaded circle indicates the extent of non-SREMP initial damage and the dashed perimeter defines a nominal distance for radiated field assessment. These weapon parameters are shown superimposed on a power system map indicating major transmission lines and generation and facilities.

For the burst location shown, except for local power distribution elements within the shaded circle, the initial excitation of the grid is illumination by the radiated field. A translation of burst location 20

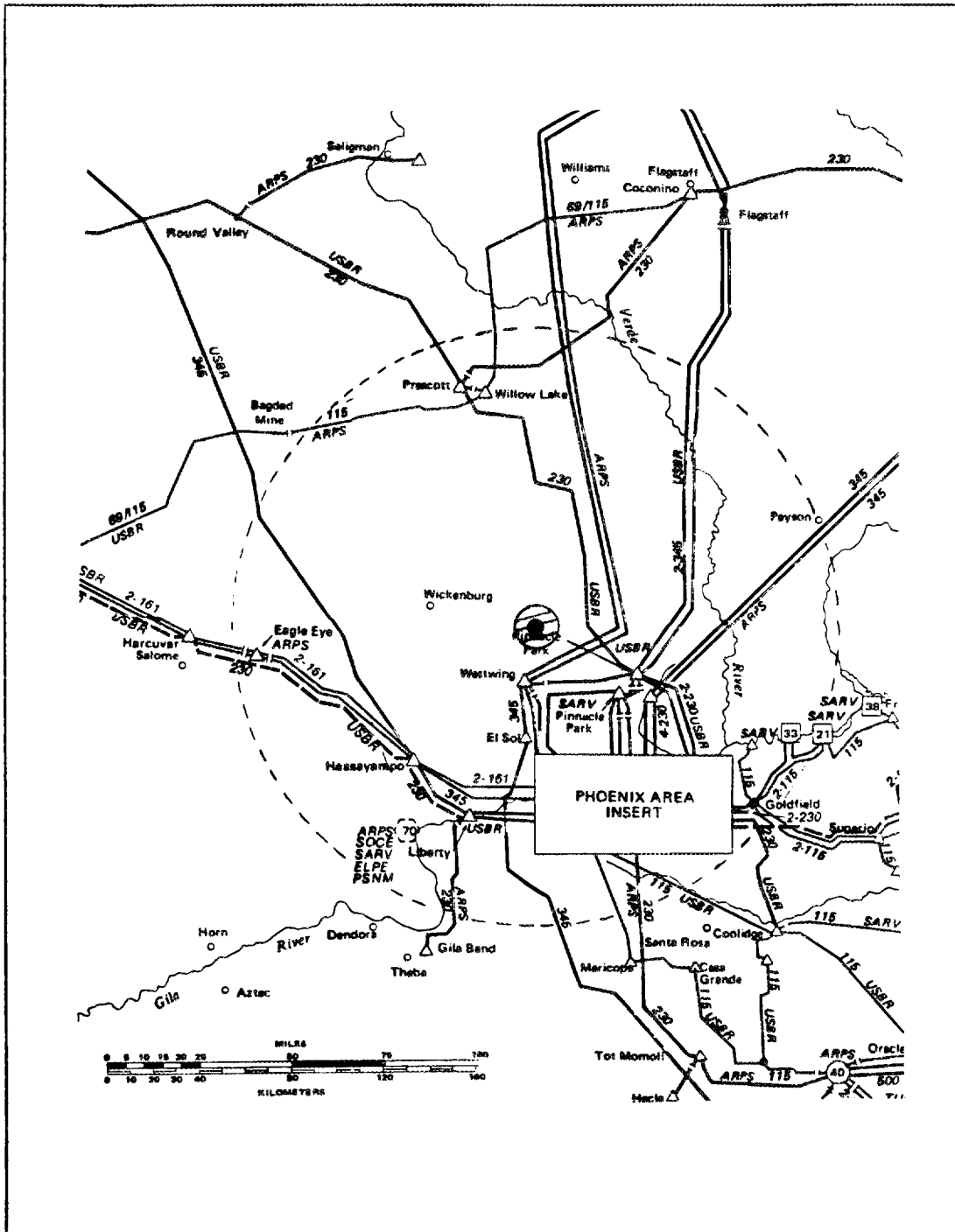


Fig.36. Conjecture of nuclear surface burst source region (solid circle), non-SREMP initial damage (shaded circle) and radiated field assessment area superimposed on an arbitrary power system grid.

kilometers south will place the Westwing 345-kV substation in both the source region and damage area. An alternate shift in location 20 kilometers East has the same impact on the Arizona Public Service (APS) 345-kV transmission circuits and the United States Bureau of Reclamation (USBR) 230-kV circuit. The inclusion of a major transmission circuit and/or facility within the source region may have significant impact on total system response.

For the purpose of this methodology, the spatial and temporal characterization of the initial non-EMP damage are formed from the phenomena of: 1) craterization, 2) fireball formation and 3) propagation of the peak-overpressure shock wave as functions of time and distance from the origin. Phase I research strongly suggests that the maximum spatial extent of such damage is practically established by the 3.5 psi peak-overpressure boundary.

Spatial definition of the applicable source region spatial boundary as a function of weapon yield has been developed in previous sections of this report. This definition is key to the segregation of electromagnetic phenomena as two distinct environments for the purpose of assessment.

Electromagnetic coupling to above ground and underground lines intersecting the source region boundary is represented by the temporal characterization of the formed surge on the line of interest, at the boundary. An individual surge is defined graphically or in closed mathematical form as a time-domain open-circuit voltage and short-circuit current at a node established by the line-boundary intersect. The surge is assumed to exist in common-mode on all individual conductors, propagating away from the boundary into the grid via the conductor(s). For the purpose of unclassified research, such surge definitions may be "canonical" in the sense that the same surge is predicated to exist on each line of interest neglecting the physical orientation or construction of the line within the source region. The research may be facilitated by the development of two "canonical" surge definitions. The first for all above-ground lines and an alternate for all below-surface cables.

As developed previously in this report, a practical location to define the attributes of the radiated (free) field is also at the source region boundary. The definitions take the form of the time domain representation of the vertical electric field at this location. Attenuation is modelled as a function of  $1/r$  where  $r_0$  is the radial distance of the source region boundary and  $r > r_0$ . This definition allows for the conservative estimation of the field at any spatial location of interest.

At this time, it is anticipated that weapon environmental definitions for any scenario will be jointly developed by the Phase II research team and ORNL for discrete assessments. The ability to perform even preliminary assessments is strictly dependent on the sponsoring agencies ability to issue the minimum set of environmental definitions in an unclassified manner.

Once the location and physical parameters of the nuclear surface burst have been defined in any scenario, a systemic description of the utility grid of interest must also be defined. This description includes definition of the load flow and connectivity of the grid just prior to the event. This is the initial, operational "state" of the system. Another key parameter is the size of the grid necessary for assessment. Preliminary investigation suggests that the burst location and thus, that portion of the grid contained within the source region, may be more significant than the effective distance of illumination by the SREMP radiated field in the determination of initial system size. For example, a surge coupled to the end of a long transmission circuit within the source region can propagate hundreds of kilometers down the line to impact the remote substation. Another issue addressed in later elements of the methodology is that the localized impact of the event on a large, interconnected system may cascade into a regional problem due to stability concerns.

The initial "state" of the system is necessary, but not sufficient to exercise the methodology. Detailed facility and line data is required to perform both the radiated field and the source region surge elements of the assessment.

### 5.3 SREMP Radiated Field Analysis

The initial EMP threat environment evaluated under the total methodology is the interaction of the power system grid and the SREMP radiated field outside the source region. Since the basic nature of the environment is a propagating "free field," the applicable methodology is identical to that required for HEMP research. This methodology is developed in Volume 2 of this report series and is not duplicated here. Although the same process, questions and concerns are applicable to both phenomena, there are significant qualitative differences between early-time HEMP and SREMP radiated field environments. Key distinctions are shown in Table 8.

Preliminary calculations of the transient overvoltage, at an arbitrary location of interest on an overhead line, strongly indicate that the time to crest and the decay to the first time constant can be represented by existing lightning impulse waveform definitions [22]. The degree of correlation is sufficient such that existing power system equipment design statistics based on lightning basic insulation levels (BIL) can be applied in the estimation of grid response.

Although the protective relaying schemes, and communications/control aspects of the utility system have not been intentionally designed with respect to EMP fields, the general question of electromagnetic interference (EMI) and electromagnetic compatibility (EMC) of subsystems has long been a concern to power system engineers. Within a transmission substation, normal operation of breakers and disconnect switches can produce intense, local transient fields. Recent measurements of this environment [23] has been conducted by Texas A&M University on behalf of the Electric Power Research Institute (EPRI). The incorporation of electromagnetic shielding for digital computer systems at selected control centers located in substations has also been documented [24].

Since the SREMP radiated field is a spatially local environment when compared to the possible extent of system HEMP coverage, it would be useful, from an analysis point of view, to estimate the distance away

Table 8

## RADIATED ELECTRIC FIELD COMPARISON

<u>Parameter</u>	<u>Early-Time HEMP</u>	<u>SREMP</u>
Base Definition	Canonical waveform in public domain	No canonical waveform
Peak Amplitude	50-kV/m	10-kV/m
Spatial Variance	"Smile" diagram model	1/r attenuation $r > r_0$
Polarization	Horizontal and vertical spatially dependent	Vertical Model
Rise Time	$3 \times 10^{-9}$ seconds	$5 \times 10^{-7}$ seconds
Duration	$10^{-8}$ seconds	$10^{-5}$ seconds
Energy Content	Significant at megahertz frequencies	Significant at kilohertz frequencies

from the burst origin beyond which the field amplitude is no greater than normal system noise. Preliminary calculations suggest that vertical electric field strengths of less than 500 volts per meter for power equipment and 100 volts per meter for protection and control circuits may bound the area. In context with the assumptions of the methodology, i.e. a 1/r attenuation, these perimeter locations can be obtained. For example, an initial field magnitude of 2000 volts per meter at a source region boundary 5 kilometers from the burst would place the 500 volt per meter boundary at 25 kilometers and the 100 volt per meter boundary at 100 kilometers. It is anticipated that spatial estimates of this type will be validated as part of the Phase II research.

At the conclusion of this element of the total methodology, the system "state" is characterized to include the effect of the radiated field. The next process is the incorporation of the source region surge exiting the region boundary.

#### 5.4 Source Region Surge Assessment

Under the defined set of initial conditions, EMP interaction with lines intersecting the source region boundary are simulated by formed surges propagating out of the region. Therefore, this element of the total methodology is not concerned with transient field coupling phenomena or free field illumination of facilities. The focus is now on the interaction of the surge and the power system.

As discussed in Section 4 of this report, applicable representations of the waveform indicate a rise time of hundreds of microseconds and a decay with a time constant of several milliseconds. This waveshape is quite similar to that defined for power system switching impulse [22]. Thus, an existing methodology can be adapted to develop the system response. An overview of this methodology is shown as Figure 37. The initial "state" of any line or facility is the "state" after the interaction of that element and the radiated field.

Given that the waveshape of the surge is similar to that defined for switching impulse, the prospective crest and the energy contained in the surge far exceed anything experienced by the system in normal operation. For example, a 500-kV transmission circuit may theoretically experience a peak transient overvoltage of 4.0 per-unit of operating voltage (high-speed reclosing without breaker pre-insertion resistors), while the overvoltage found in the source region surge may be an order of magnitude above this level.

Once the "initial state" of the line is known, the peak overvoltage along the line is calculated out to the first substation. Any station arrester may operate; this operation tends to reduce the transient overvoltage over the entire system. However, in operating, an individual arrester energy capability may be exceeded. The mitigating effect of arresters is a function of: 1) the type of arrester (silicon carbide or metal oxide), 2) the number of arresters installed on the line and/or in the station and, 3) the degree in which the arresters share the total available current.

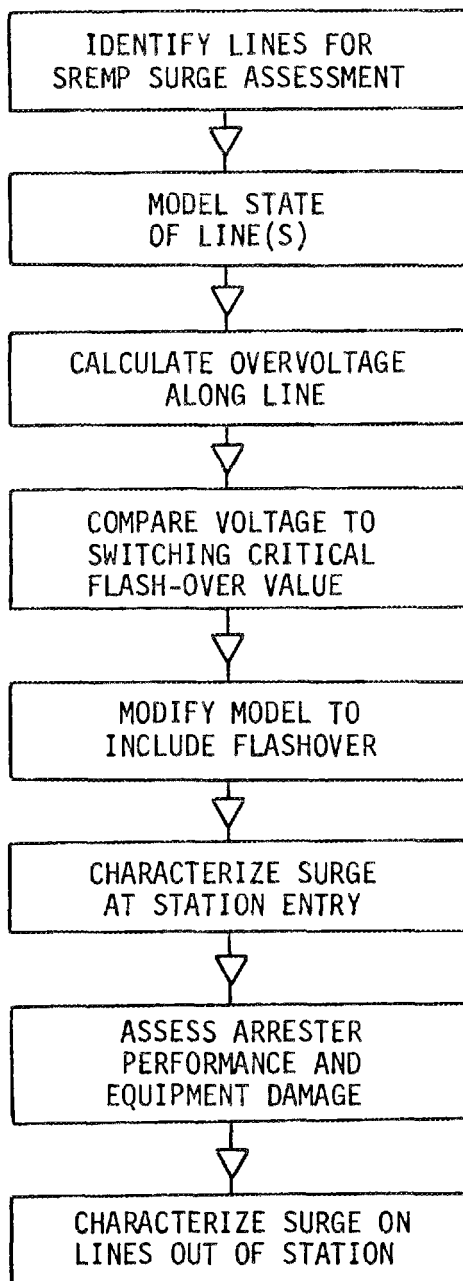


Fig. 37. Overview of source region surge assessment methodology.

Arrester operation does not necessarily eliminate the possibility of line flashover. Voltages on the line must be monitored to determine if the switching impulse critical flashover (CFO) of the line is still exceeded.

The methodology must then address the transient overvoltage experienced by equipment within the substation. Power transformers are of special concern since 1) if the basic switching level (BSL) of the transformer is exceeded transformer damage may occur and 2) transformer winding connection will determine if the surge will propagate through the transformer.

Source region surges encountering ungrounded winding configuration (wye, delta or star) will see an effective common mode open circuit configuration regardless of the secondary winding configuration. If the surge side winding is grounded, but the secondary is delta connected, the common-mode surge will not propagate beyond the transformer. The current flowing in the delta connection must be calculated in order to assess the probability of transformer damage due to short-circuit type mechanical forces.

In the case of wye grounded primary and wye secondary connections, the surge will couple through the transformer and further analysis is required to define the limit of propagation. For transformers containing delta connected tertiary windings, a special concern is of note. The tertiary is usually designed only to withstand 30 to 40% of short circuit currents (on the transformer rating base). Failure to monitor the current in this winding may lead to mis-assessment of the possible transformer damage.

The analysis is recursive for each line intersecting the source region boundary. This portion of the methodology concludes with an assessment of the damage and "state" change of these lines.

### 5.5 System Stability Analysis

At the conclusion of the source region surge analysis, the real-time of the system is several milliseconds after the burst. The system state at this time is known based on: 1) estimates of EMP damage/misoperation and 2) fault conditions requiring system protective operation. In addition, the methodology now acknowledges the non-EMP damage associated with the surface burst. Such damage cannot be assumed to occur all at the same time. As discussed in Section 2 of this report, above-ground lines and facilities located at the 3.5 psi boundary may not experience direct damage until several seconds after the burst.

For the purpose of this methodology, such damage may be divided into two areas, one established by the fireball radial distance plus an outer perimeter established by peak-overpressure greater than 3.5 psi. Systemic damage to the power grid out to the fireball radius is added to the post-EMP system state to form the input data simulation case for a transient stability study. An overview of this methodology is shown as Figure 38. The study simulates a few seconds of elapsed time. If the system remains stable; 1) a new load flow is computed, 2) peak overpressure damage is added and 3) a new stability run is accomplished. A practical limit to this study may be out to ten seconds after the event. The stability analysis is terminated and the system state is characterized.

If the system does not remain stable during the initial stability run, a concluding assessment is made of system state.

### 5.6 Summary

The methodology presented herein considers the first ten seconds of a nuclear surface burst as a set of three distinct threat environments, separated by time. The assessment process incorporates known power system analysis techniques combined with a parallel methodology developed for HEMP assessment.

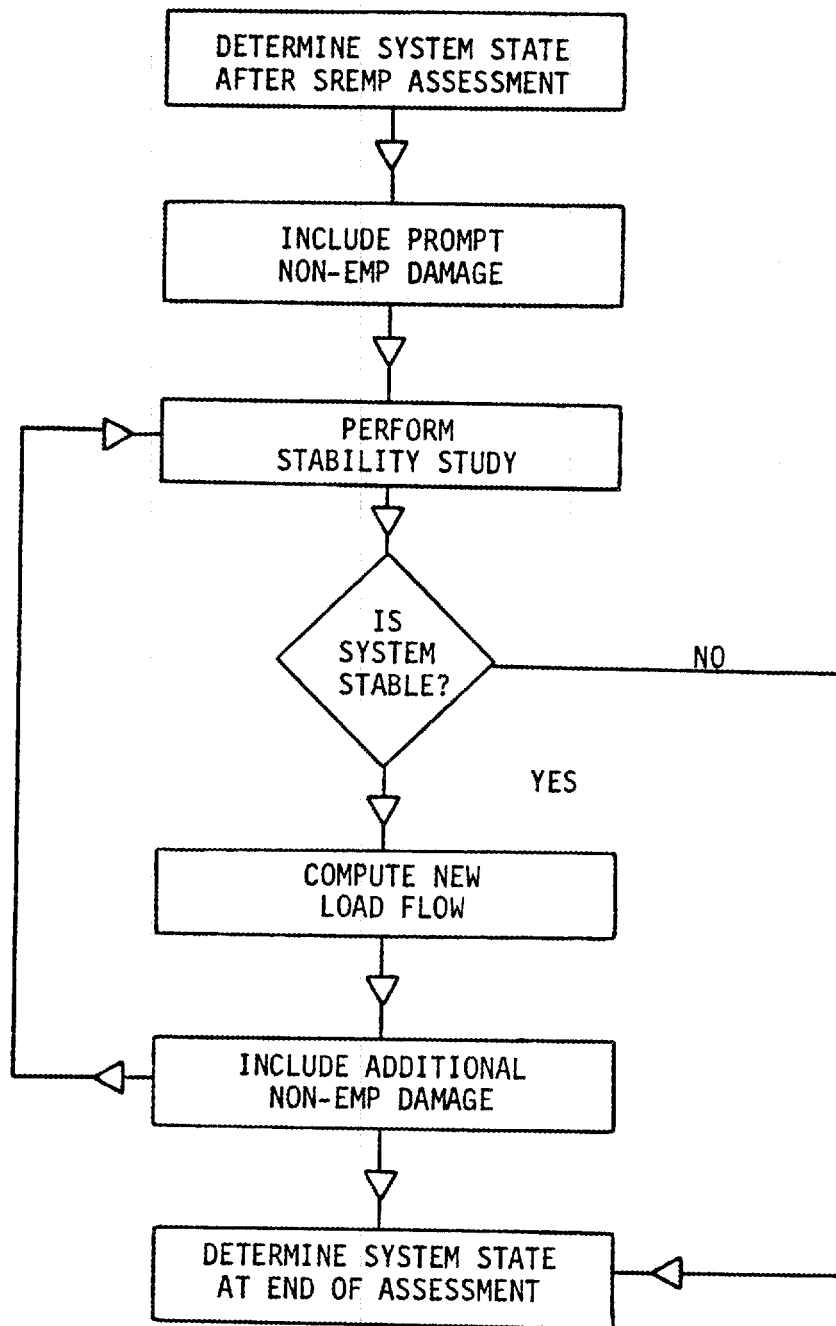


Fig. 38. Overview of system stability assessment methodology.

The initial impact of the nuclear surface burst is a strong function of location, i.e., what portion of the grid can undergo initial non-EMP damage and/or source region surge exposure. Although distribution systems near the burst origin can expect to undergo extensive damage, perhaps more severe than the transmission network. From a systemic viewpoint, the methodology focuses on loss of generation capacity and the transmission network.

The methodology does not extend in time long enough to address system manned restoration at some period of time after the event. Determination of the system state and facility status 10 seconds after the burst can be extrapolated in time with the inclusion of other weapon effects. From a long term perspective, the utility grid near the burst location may very well be abandoned and a new grid will be formed to: 1) bypass the affected area and 2) service new load centers. In this context, the methodology presented herein serves as a prelude to such a total assessment.

## 6. SREMP COMPUTER CODES AND MODELS

### 6.1 Introduction

The methodology divides the total assessment of nuclear surface burst SREMP into three distinct phases: 1) radiated field assessment, 2) source region surge assessment and 3) system stability assessments incorporating physical damage. From a power system analysis perspective, each of the three phases requires different sets of digital simulation codes and models.

In contrast to early-time HEMP simulation, where the coupling of the radiated field to the system produces very high frequency surges, the coupled responses, expressed in terms of open-circuit voltages (short-circuit currents) due to the SREMP radiated field, at a point of interest has a time dependence in the same range as lightning phenomena. Thus, the models required on the simulation can be directly adapted from conventional lightning models. This similarity greatly facilitates the simulation since the models and strength data have been previously validated in lightning research.

A complimentary analysis can be drawn with respect to the waveshape of the source region surge and surges generated by breaker operation(s) on power systems. Study techniques and system models developed for switching surge analysis can be applied to SREMP surges.

The fact that the system disturbance is generated by a nuclear surface burst environment(s) develops a different set of initial conditions, but does not change the use of conventional system assessment techniques such as short-circuit, stability, and load flow studies.

This section describes the requirements of additional digital codes and models needed to perform the total assessment described above. However, since most models required, by virtue of the similarity of SREMP induced waveforms to lightning and switching transients, are well documented [25,26,27] only a few are presented here.

## 6.2 Simulation Codes

Three different types of computer codes are needed to assess the impact of SREMP on civilian power systems. These are:

- Program to compute the excitation of electrical conductors by SREMP radiated field. (Field Excitation Program)
- Program to propagate source region surges into networks. (Transients Program)
- Program to evaluate power system response(s) following the SREMP effects. (Load Flow, System Stability, and Short-Circuit Analysis Programs)

The Field Excitation Program (FEP) determines the open-circuit voltage (Thevenin source) at locations of interest beyond the source region boundary. The coupling algorithms can be developed from the relevant equations presented in Section 4 of this report. The program should have the following capabilities:

- Simulate the incident electric field at any facility and along any line physically located beyond the source region boundary.
- Model propagation constants  $\delta=\alpha+j\beta$  for different types of lines and feeders, where  $\alpha$  and  $\beta$  are the respective attenuation and phase constants.
- Model multi-conductor lines including neutral and overhead ground wires.
- Incorporate corona effects on the propagation of the voltage waves.
- Include frequency dependent grounds.
- Include the dependence of line spatial orientation.
- Model the terminating impedance of the line, at both ends, by any arbitrary load.

A computer code has been developed in Phase I of this project to evaluate the open-circuit voltages due to radiated fields along a single conductor above earth. This program forms the basis for the FEP assessment code to be completed in the Phase II research.

A transients program is needed for simulation of the propagation of the source region surge in the power system as well as for the assessment of damage to station equipment by the radiated field transient overvoltages. The Electromagnetic Transients Program (EMTP) [28,29] is adaptable to fill this requirement. This program is recommended due to wide use and acceptance among electric utility companies. Section 6.3 of this report describes some of the models needed in conjunction with this program.

The load flow and stability programs needed to simulate the operational impact of SREMP on power systems can be accomplished by existing computer codes, e.g. WESTCAT™. In contrast to MHD-EMP investigation, no special model need to be added to these programs. A short-circuit program is also needed to evaluate the system equivalents required as an input to load flow and stability codes. Existing codes can be used without modification.

### 6.3 Simulation Models

Network models are required to match the frequency response of the elements they represent. The prospective size of the systems to be studied inhibits the use of extremely detailed models for every element in the analysis of large power systems. Hence, adequate but approximate models are needed. As examples to the above, this section describes some of the well known models for power transformers, distribution loads, and transmission/distribution lines.

#### 6.3.1 Transformer Models

The voltages which appear on the secondary (or tertiary) terminals of transformers due to surges on the primary terminals are composed of four components [30].

- Electrostatic component.
- Electromagnetic component.
- Oscillatory component in the primary winding which initiates a corresponding oscillation in the secondary and tertiary windings.
- Second oscillatory component produced in the secondary and tertiary winding.

Figure 39 depicts a transferred surge through a transformer. The initial spike (A) is the electrostatic component, the dashed line (B) is the electromagnetic component and the solid line oscillation is due to the oscillatory components.

The magnitude and shape of the voltage transferred by the electrostatic coupling is dependent on: 1) the front of the SREMP induced open-circuit voltage at the primary terminals of the transformer, 2) the nature and impedance of the load connected to the secondary and 3) the capacitance distribution within the transformer. A few tenths of a microfarad capacitance added to the secondary terminals, a low ohmic load, or static plates (internal shields) all act to reduce this component.

The magnitude of the oscillatory components are usually small compared to the electromagnetic component and can be neglected in most practical cases. However, they should be included for a complete assessment of SREMP.

The value of the coupled electromagnetic component is a function of: 1) transformer turns ratio, 2) leakage impedance, and 3) the connected impedances to winding terminals, and 4) the waveshape of SREMP induced open circuit voltage. It has been shown through field and laboratory measurements [30] that the maximum overvoltage obtained through the electromagnetic coupling on the unsurged winding cannot exceed  $E_1 N$ , where  $E_1$  is the magnitude of the surge on the surged winding and  $N$  is the turns ratio of the unsurged to the surged windings.

The electrostatic coupling, as mentioned above, is limited by and is a function of the capacitance distribution in the transformer. Hence, the overvoltage on the unsurged winding can be much greater than  $E_1 N$ .

High frequency models for transformers, necessary for radiated field assessment, can be very complex. Detailed derivations of these power transformer models have been documented [25]. In addition to these "classical" models, Vance [33] indicates that additional elements, such as winding assymetry and bushing inductance need to be incorporated for the analysis of EMP (more typically HEMP) induced voltages. The usefulness of any model is a strong function of available, measured data developed by the equipment manufacturer or electric utility.

For network analysis, approximate models for radiated field/transformer analysis can be the elementary circuit shown as Figure 40. In many digital simulation studies performed by Westinghouse it has been shown that such models duplicate the transformer behavior in the frequency range associated with the radiated field. When the electromagnetic circuit is added to the capacitive model, the composite model, shown as Figure 41 is obtained. A refinement of the composite model should allow resistances  $R_1$  and  $R_2$  to be frequency dependent to reflect higher losses at higher frequencies. Although this frequency dependence has not been used for typical lightning studies, it is recommended for this research program.

For source region surge simulation, it is anticipated that transformer electromagnetic coupling plays a major role in surge transfer across the windings. Standard models now used to represent transformers for switching studies on transient network analyzers (TNA) or digital programs are applicable. Transformer core saturation should be modeled. The inclusion of capacitances, while preferable, is not essential since, in this case, the electrostatic component is of secondary importance compared to the electromagnetic component. Figure 42 depicts a typical model for a three-winding transformer applicable for studying the electromagnetic transfer of the source region surge.

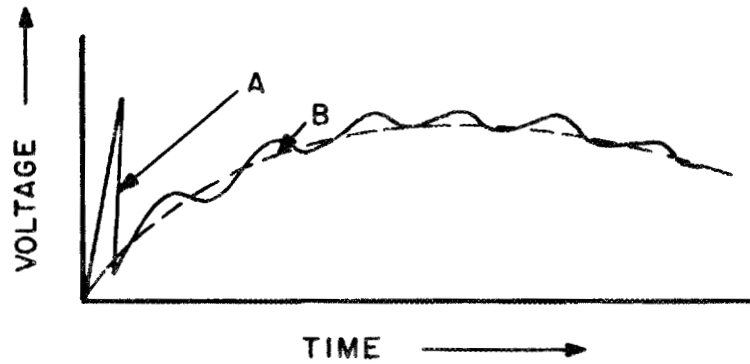


Fig. 39. Typical surge voltage transferred through the transformer.

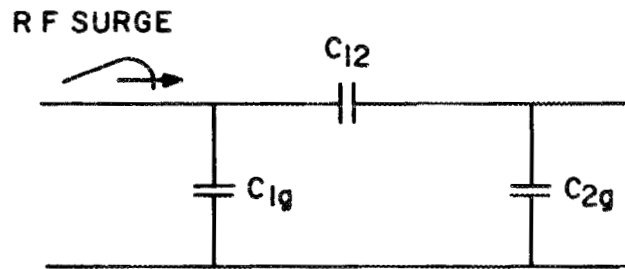


Fig. 40. Electrostatic model for a transformer for the analysis of the radiated field effects.

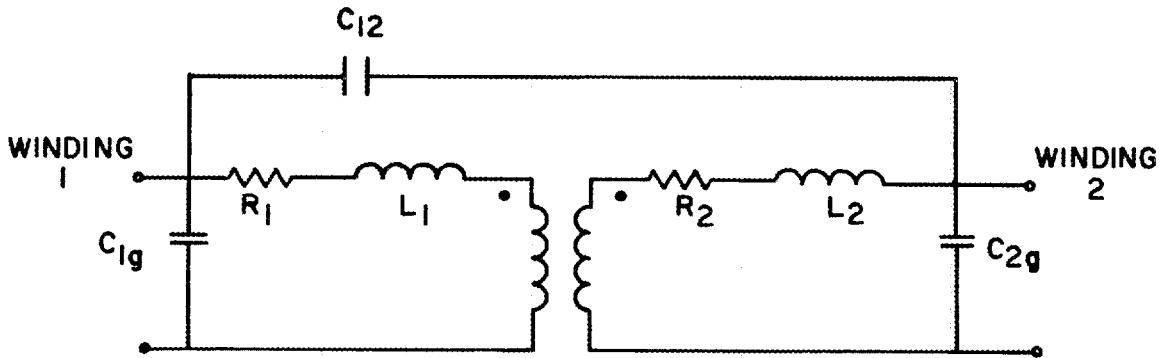


Fig. 41. Complete model of a transformer for the analysis of the radiated field effects.

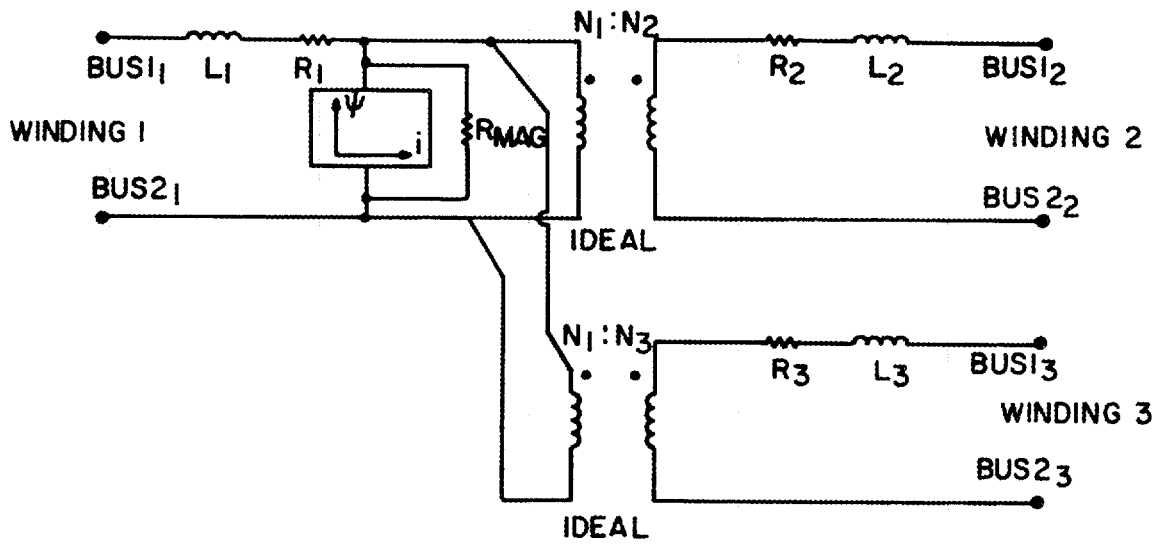


Fig. 42. Model for a three winding transformer for the analysis of the source region surge effects.

### 6.3.2 Representation of Loads

Alternate circuit models have been developed for the representation of system loads for digital transient studies. Some of these models are shown as Figure 43. Previous Westinghouse experience has shown that the series-parallel circuit (model 3) yields the best results for high frequency simulation.

### 6.3.3 Frequency Dependence of Line Parameters

Frequency dependent line models have been developed and implemented on the EMTP [34,35]. Validation of these models has shown good correlation with actual field measurements. It is recommended that select use of these models be incorporated for SREMP assessments of utility systems. Preliminary assessments may employ frequency independent line models to obtain a first estimate of interaction.

### 6.3.4 Corona and Ground Mode Propagation

The practical effect of corona and ground mode propagation is to retard the front of the wave and, dependent on the wave-tail, decrease the crest magnitude of voltage surges propagating over electrical conductors. For source region surge simulation, preliminary calculations and knowledge of switching surge propagation strongly suggests that little mitigation will result even over long lines. For example, simulation of a 300/3000  $\mu$ s surge was placed in common mode on each of the phase conductors of a 132-kV transmission line. For this surge waveshape, a ground mode surge impedance of 632 ohms and a resistance of 53 ohms were used. At a distance of 100-km the surge voltage was attenuated by 9% while the front was retarded by 70  $\mu$ s. In conventional switching surge simulations, the combined attenuation and retardation are small and can be normally neglected.

The same results cannot be expected for surges induced by the radiated field. Simulations of lightning surges having short fronts and tails, and preliminary calculations performed as part of this research

program indicate a significant reduction in magnitude by the inclusion of simplified corona models on lines of interest. It is recommended that corona be included as part of the radiated field simulations, but may not be significant for source region surge mitigation.

#### 6.3.5 Surge Arrester Models

Two arrester technologies are incorporated in the utility system grid: metal or zinc-oxide (ZnO) and traditional silicon-carbide (SiC). Models of both technologies are required to perform transient simulations.

The SiC design has a non-linear SiC block in series with a gap structure, as shown in Figure 44. Flashover of the gap is a function of both the magnitude and rate-of-rise of the voltage to ground. Models for SiC arresters consist of the voltage dependent flashover gap in series with a non-linear resistor. Source region surge assessment employ switching surge flashover characteristics. Lightning characteristics are applicable for radiated field assessment.

Some ZnO arresters are modeled by nonlinear resistors with or without a gap depending on the manufacturer. The volt/current (VI) characteristic for the model of ZnO arrester for the radiated field studies are taken directly from the manufacturer's data. For the source region surge studies, one may extrapolate the VI characteristic from the VI characteristics given for 8x20 impulse and the singular switching impulse protective level supplied by the manufacturer for the 45x90 surge.

#### 6.3.6 Rotating Equipment

The transient equivalent circuits of generators and motors are complex combinations of inductance and capacitance which represent not only the impedance of windings to ground, but also the coupling between coils and turns. These circuits can and have been altered to less complex circuits when considering different applied waveshapes.

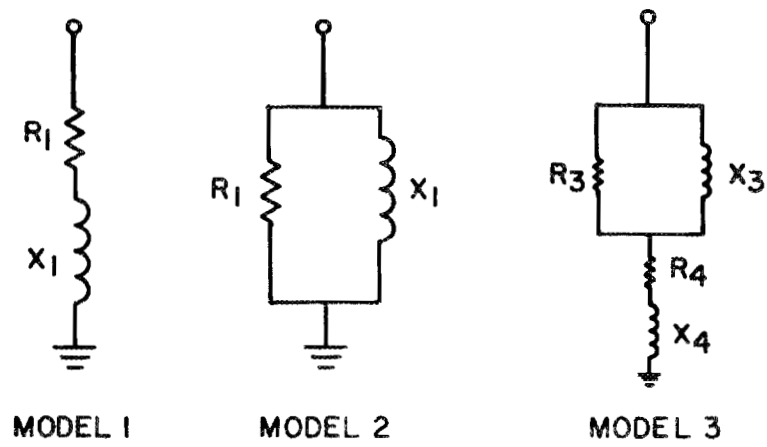


Fig. 43. Models used for distribution loads.

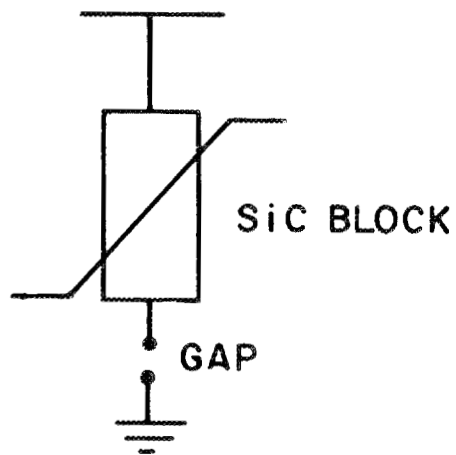


Fig. 44. Model for a SiC arrester.

In a power system, two transient events are presently studied to analyze the required machine protection:

- Lightning, where the surge voltage arrives at the machine terminals through a transformer, or is directly transmitted to the machine by cables or lines [30,31,32].
- Switching, where the surge is created by a circuit breaker located adjacent to the machine at the same voltage level.

Originally, only the lightning event was studied, since it was assumed that lightning would produce the worst electrical stress on machine turn and ground wall insulation. More recently, it has been found that the switching produced by the circuit breaker can produce steeper fronts (0.1 to 0.2  $\mu$ s) than lightning. The machine equivalent circuit required when a steep wavefront surge impinges on a machine is complex and presently is being investigated through tests and theoretical development [36,37].

For machines connected through transformers to the system, surge arresters on the high-voltage side of the transformer provide protection for both the lightning surge and for switching surges generated on the high-voltage system. Machines directly connected (through cables or lines) usually have surge arresters and possibly capacitors applied at the machine terminals.

The two types of surge voltages produced by the nuclear surface burst require different types of equivalent circuits. For the long-front, long-tail source region surge, the usual method of presenting the machine by its subtransient reactance can be used. However, for the surge produced by the radiated field, which somewhat resembles lightning impulse, a more detailed circuit is required. In the past, the machine has been successfully modeled simply by its surge impedance [38]. This same external representation can be employed for radiated field assessment.

### 6.3.7 Line Insulation

An important aspect of EMP assessment of civilian electric utility systems is the study of line insulation performance in response to EMP surges. Line flashover culminating in a fault condition requires the power system to undertake an immediate protective action; i.e., circuit breaker or fuse operation to clear and/or isolate the affected portion of the grid.

For line insulation systems, the insulation strength is normally expressed in terms of the Critical Flashover Voltage (CFO). By definition, CFO is not a deterministic value; the voltage corresponding to CFO is the 50% probability statistic associated with a distribution of insulation strength. For any given insulation system, the basic knowledge of the strength distribution for a given stress has been determined from test programs.

For switching surge study, the switching CFO is a strong function of the physical condition of the line (wet or dry, degree of contamination) as well as the polarity and waveshape of the surge. These effects are depicted in Figure 45 for a 500-kV line design [39]. This figure shows the effect of the wavefront on the CFO for wet and dry conditions, positive and negative polarity. It is important to note that the U-shape curves indicate a critical wavefront exists which results in a minimum insulation strength. Wet conditions decrease the CFO more for negative than positive polarity. Wet, positive polarity produces the lowest CFO values.

It is also important to recognize the difference in insulation performance between lightning and switching surges with respect to CFO. Figure 46 shows, for dry, positive polarity and critical wavefront the respective performance as a function of horizontal strike distance.

Test research in the area of switching surge flashover phenomena [39] has shown that insulation strength distribution (flashover distribution) can be approximated by a cumulative Gaussian distribution of two parameters. The mean forms the definition of CFO

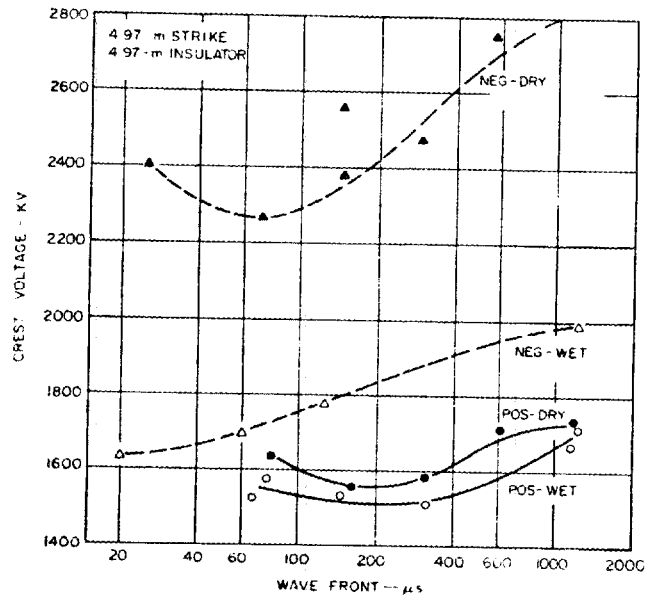


Fig. 45. Effect of wavefront on switching CFO [39].

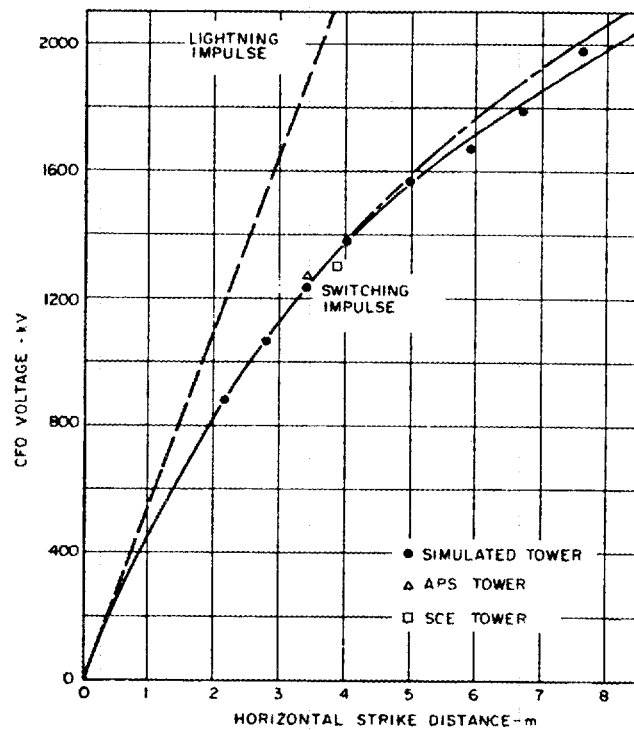


Fig. 46. Comparison of lightning and switching CFO [39].

and the coefficient of variation normally expressed in percent of the CFO. The term "withstand voltage" ( $V_3$ ) is defined at three standard deviations below the CFO. This concept is shown as Figure 47. As shown, the probability of flashover for a crest voltage equal to the withstand voltage is 0.135%.

When the statistical distribution of the stress is known, in addition to strength data, the probability that the stress will exceed the strength can be evaluated. This technique is graphically shown as Figure 48. This approach forms the basis of current insulation system designs based on probabilistic methods.

#### 6.4 Summary

Embedded within the methodology described in this report are necessary assumptions, applicable to civilian power system assessments, based on the nature of the SREMP associated with nuclear surface bursts. Preliminary calculations of the respective transient overvoltages due to the source region surge and radiated field excitation strongly indicate that existing power system analysis techniques can be used to assess SREMP effects on utility systems.

Additional code development is required to fully develop the field excitation program for radiated field assessment. The Electromagnetic Transients Program (EMTP) can be used with the addition of corona models and specific equipment models drawn from the existing "building-block" format of the program. The EMTP is directly applicable to the simulation of source region surge propagation.

The ability to perform meaningful nuclear surface burst EMP assessments, in the public domain may be predicated more on the availability of the necessary environmental descriptions (and the uncertainty contained therein) and less on the power system assessment technique required to perform the assessment.

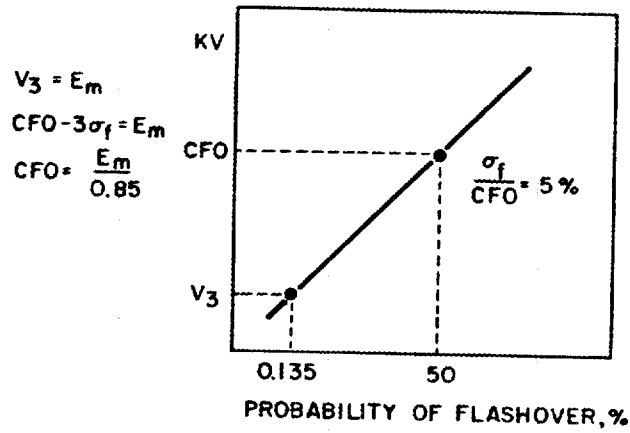


Fig. 47. Comparison of CFO and withstand voltage ( $V_3$ ) [39].

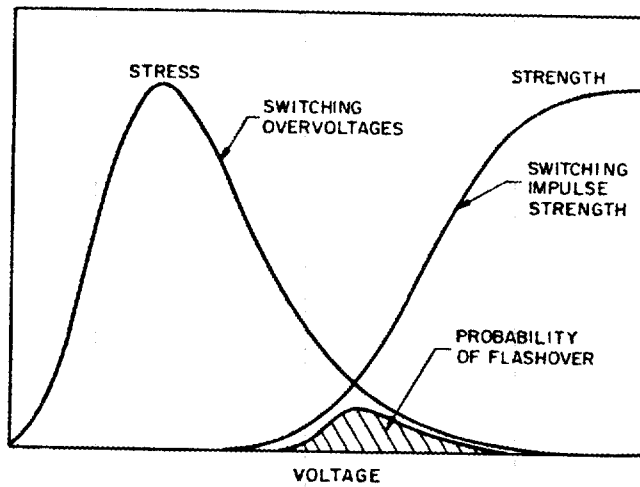


Fig. 48. Graphic depiction of stress-strength analysis used to determine the probability of flashover [39].

## 7. CONCLUSIONS AND RECOMMENDATIONS

Phase I research to investigate the effects of nuclear surface burst SREMP on the civilian electric utility system suggests that the SREMP environment alone may place the directly illuminated portion of the system at some risk. Such risk is in addition to the impact of non-SREMP effects due to the burst. The nature of the SREMP threat can be understood in terms of transient surges induced on the system within the source region, and of the transient electromagnetic field that illuminates the system for some distance beyond the source region. In preparation for Phase II preliminary risk assessment, a methodology applicable to electric power systems has been developed. This methodology anticipates the necessary environmental and power system data bases, coupling response mechanisms, and power system analysis techniques necessary to conduct quantitative assessments.

In the areas of SREMP environmental definitions, power system response, methodology development, and system analysis, the following conclusions are reached:

1. A nuclear surface burst will produce significant transient electromagnetic environments in addition to other direct blast effects. Based on a principle of "balanced survivability," power system assessment must consider all initial aspects of the burst since, for a given radial distance from the burst, the power system will be destroyed and/or damaged by burst effects other than SREMP.
2. Within the source region, transient electrical surges will be coupled to and propagate via overhead lines and underground cable systems penetrating or traversing this region. These physical interconnections for surge propagation will result in surge interaction with the remaining power system prior to destruction of the grid located within the region. Preliminary investigation suggests that, for weapons of interest, the radial distance of the source region may be less than or equal to the radius of direct physical damage. Specific threat distances are a strong function of weapon design and deployment.

3. Phase I research suggests that a practical and reasonable location to define the source region transient surge is at the source region boundary. Previous investigations, published in the public domain, indicate that the time-domain waveform for such surges, defined at this boundary, may exhibit a time to crest greater than 250 microseconds and a fall to half-value on the order of several milliseconds. Such a time domain waveform has great similarity to switching surge phenomena experienced on existing power systems. The peak magnitude of the surge, defined at the source region boundary, may be on the order of 100 kiloamperes to 300 kiloamperes of short-circuit current. For power system simulation, the source region surge may be modelled by a Norton equivalent source located at the boundary of the region.
4. In addition to the above surges, formed within the source region, the electric utility system will be illuminated for some distance beyond the region by a radiated, transient electromagnetic field. This radiated field is characterized by vertical polarization and radial propagation outward from the burst. Previous investigations, published in the public domain, indicate that the radiated field time-domain waveform may exhibit an initial time to crest on the order of a microsecond with an initial zero crossing within tens of microseconds. The initial peak magnitude of the electric field at the source region boundary may be on the order of several kilovolts per meter. Beyond the source region, the peak voltage decreases as  $1/r$  for increasing distance.
5. Preliminary calculations, performed as part of the Phase I research effort, indicate that, for lines radially directed to and outside of the source region, there may exist some critical length of line at which the peak open-circuit voltage is maximum. Based on the radiated field example presented in this report, a maximum open-circuit voltage at an approximate distance of 5 kilometers beyond the source region boundary was noted. Calculations also indicate that for a given distance the coupling is maximum for the radial line and decreases for all other angles of incidence.
6. For overhead lines exposed to surges formed within the source region and illuminated by the radiated field beyond the region, the source region surge may dominate line and system initial response.

7. Existing power system analysis codes, such as EMTP and WESCAT™, can be modified and/or directly incorporated within the SREMP assessment methodology. Additional digital code development will be required to translate the SREMP radiated field environment to system initial transient response.

The Phase I investigation of SREMP interaction with the electric power system has revealed several areas of additional research required to perform preliminary risk assessments. The investigations should be accomplished as an early part of the Phase II research effort prior to such assessments.

The recommendations for additional research are:

1. Detailed development of SREMP and other applicable nuclear surface burst effects in the form of a unified environmental definition directly applicable for civilian electric utility system analysis. This report suggests that a practical spatial location for the SREMP characterization is at the source region boundary. The above development should be a coordinated effort of the Defence Nuclear Agency and Oak Ridge National Laboratory with assistance from the Phase I research team.
2. Research as to the appropriate source region terminating impedance for applicable lines and cables. Present assumptions range from a short-circuit termination to representation by the appropriate characteristic impedance. It is recognized that the best assumption may be a time-dependent value for this impedance.
3. Additional research as to an integrated EMP environmental description applicable to investigations which consider simultaneous or time-spaced, joint high-altitude and surface burst events.

## 8. BIBLIOGRAPHY

1. United States Department of Defense, The Effects of Nuclear Weapons, 1977, Washington, D.C., Government Printing Office, 1977.
2. Institute of Electrical and Electronic Engineers, National Electric Safety Code-1984 Edition, ANSI C2-1984, IEEE, New York, New York 10017.
3. United States Department of Energy, Office of Electric Energy Systems, Electrical and Mechanical Design Criteria for EHV and UHV Overhead Transmission Lines, DOE/RA/2133-01.
4. Ricketts, L. W., et all, EMP Radiation and Protective Techniques, New York, John Wiley and Sons, 1976.
5. Congress of the United States Office of Technology Assessment. The Effects of Nuclear War, Washington, D.C., Government Printing Office.
6. DNA EMP Course, BDM/W-82-305-TR, prepared by the BDM Corporation, January 1983.
7. EMP Engineering and Design Principles, Whippany, New Jersey, Bell Laboratories, 1975.
8. United States Air Force Weapons Laboratory, EMP Interaction: Principles, Techniques and Reference Data - EMP Interaction 2-1, AFWL-TR-80-402 AFWL, Kirtland AFB, New Mexico, 1980.
9. Longmire, C. L., "On the Electromagnetic Pulse Produced by Nuclear Explosions," IEEE Trans. Antennas and Propagation, Volume AP-26, January 1978.
10. Crevier, W. F. and E. Pettus, "Approximate Methods for Calculating the Early Time EMP from Surface Bursts at the Ground In, and Near the Source Region," IEEE Trans. on Nuclear Science, Volume NS-26, December 1979.
11. Crevier, W. F. and E. Kalasky, "Improvements In the Analytical Treatment of Source Region EMP," 5th Symposium on Electromagnetic Compatibility, Zurich, 1983.
12. Graham, W. R., "The Electromagnetic Coupling of Nuclear Explosions to Above Ground Conductors Traversing the Source Region," Defense Nuclear Agency Report No. 5702 P-2, 1981.

## BIBLIOGRAPHY (CONT'D)

13. Lee, K. S. H., "EMP Propagation Over Imperfectly Conducting Ground," Air Force Weapons Laboratory Report AFWL-TR-81-122, November 1981.
14. Radasky, W. A. and K. S. Smith, "An Examination of the Characteristics of the Radiated Nuclear Electromagnetic Pulse from a Ground Burst (U)," (SECRET) DNA Report DNA-4884T, March 1979.
15. C. Jones, Kaman Sciences Corporation, Private correspondence to F. M. Tesche, LuTech, Inc., May 16, 1984.
16. Longmire, C. L. and J. L. Gilbert, "Theory of EMP Coupling in the Source Region," Defense Nuclear Agency Report No. 5687F, February 1980.
17. "Source Region EMP Coupling to Long Lines," Defense Nuclear Agency Report No. 6269F, June 1981.
18. Barnes, P. R., Klein, K. W. and H. W. Zaininger, "Electromagnetic Pulse and The Electric Power System," Technical Paper No. 84SM702-7 presented at the PES Summer Meeting, Seattle, Washington, July 16, 1984.
19. Higgins, D. F., O'Dean, D. E. M. and K. S. Smith, "SREMP Coupling to Long Buried Lines -- A Comparison of Transmission Line and Finite-Difference Solutions," IEEE Trans. on Nuclear Science, Vol. NS-29, No. 6, December 1982.
20. Shen, L. C. and R. W. P. King, "The Cylindrical Antenna with Non-Reflecting Resistive Loading," IEEE Trans. on Antennas and Propagation, AP-13, November 1965.
21. C. L. Longmire, "History and Physics of EMP," presentation at the Fourth NEM Symposium, Baltimore, Maryland, July 2, 1984.
22. IEEE Standard Techniques for High Voltage Testing; ANSI/IEEE Std. 4-1978.
23. Electric Power Research Institute, Measurement and Characterization of Substation Electromagnetic Transients, EPRI EL-2982, March, 1983.
24. Harvey, S. M. and W. J. Ponke, "Electromagnetic Shielding of a System Computer in a 230-kV Substation," IEEE Trans. on Power Apparatus and Systems; Vol. PAS-95, January 1976.

## BIBLIOGRAPHY (CONT'D)

25. Beverly, L. V., Traveling Waves on Transmission Systems, Dover Publications, New York, 1951.
26. Peterson, H. A. Transients in Power Systems, Dover Publications, New York, 1951.
27. Greenwood, A., Electrical Transients in Power Systems, John Wiley & Son, Inc., New York, 1971.
28. Dommel, H. and W. S. Meyer, "Computation of Electromagnetic Transients," Proc. IEEE, Vol 62, pp 988-993, July 1974.
29. Rule Book - Electromagnetic Transients Program (EMTP), Bonneville Power Administration, Portland, Oregon, March 1983.
30. A. R. Hileman, "Surge Transfer Through 3-Phase Transformers," AIEE Trans. on PA&S, February 1959.
31. Powell, R. W., Hileman, A. R. and M. Maxwell, "Lightning Protection of Rotating Machines Directly Connected to Overhead Lines," AIEE Trans. on PA&S, 1962.
32. Dillard, J. K. and A. R. Hileman, "Lightning Protection of Unit-Connected Turbine Generators - Field and Laboratory Studies," AIEE Trans. on PA&S, February 1957.
33. Vance, E. F., Electromagnetic-Pulse Handbook for Electric Power Systems, Stanford Research Institute, Menlo Park, CA.
34. Marti, S. R., "Accurate Modelling of Frequency - Dependent Transmission Lines in Electromagnetic Transients Simulations," IEEE Trans. on PA&S, Vol. PAS-101, January 1982.
35. Semlyen, A. and R. Brierley, "Stability Analysis and Stabilizing Procedures for a Frequency Dependent Transmission Line Model," Paper No. 84-T&D367-9, IEEE/PES 1984 Transmission and Distribution Conference, Kansas City, April 29 - May 4, 1984.
36. Orace, H. and P. G. McLaren, "Surge Voltage Distribution in Line-End Coils of Induction Motors," Paper 84-SM676-3, presented at 1984 Summer Meeting of the IEEE Power Engineering Society.
37. O. M. Nassar, "Effect of Surge Wave Reflections Inside a Motor on Voltage Distribution Across Stator Windings," 84-SM6785-5, presented at 1984 Summer Meeting of the IEEE Power Engineering Society.

## BIBLIOGRAPHY (CONT'D)

38. Dillard, J. K., and A. R. Hileman, "Lightning Protective Requirements of Generators Connected to the System Through Y-Grounded-Delta Transformers, "AIEE Trans. on PA&S, February 1959.
39. A. R. Hileman, "Transmission Line Insulation Coordination," Trans. South African Institute of Electrical Engineers, Vol. 71, Part 6, June 1980.

INTERNAL DISTRIBUTION

- |       |                     |        |                               |
|-------|---------------------|--------|-------------------------------|
| 1-24. | P. R. Barnes        | 36.    | B. W. McConnell               |
| 25.   | R. B. Braid         | 37.    | J. W. Michel                  |
| 26.   | R. S. Carlsmith     | 38-58. | M. C. Miller                  |
| 27.   | F. C. Chen          | 59.    | M. O. Pace                    |
| 28.   | L. G. Christophorou | 60.    | R. A. Stevens                 |
| 29.   | R. I. Crutcher      | 61.    | J. P. Stovall                 |
| 30.   | S. J. Dale          | 62-63. | Central Research Library      |
| 31.   | W. Fulkerson        | 64.    | Document Reference Section    |
| 32.   | P. A. Gnad          | 65-66. | Energy Information Library    |
| 33.   | T. L. Hudson        | 67.    | Laboratory Records - RC       |
| 34.   | J. M. MacDonald     | 68-69. | Laboratory Records Department |
| 35.   | F. W. Manning       | 70.    | ORNL Patent Section           |

EXTERNAL DISTRIBUTION

- 71-80. N. C. Abi-Samra, Westinghouse Electric Corporation, Advanced Systems Technology, 777 Penn Center Boulevard, Pittsburgh, PA 15232
81. W. E. Adams, Director for Radiation, Defense Nuclear Agency, Washington, DC 20305
82. V. D. Albertson, Department of Electrical Engineering, 123 Church Street, S.W., University of Minnesota, Minneapolis, MN 55455
83. H. W. Askins, Jr., The Citadel, Charleston, SC 29409
84. C. E. Baum, NTYEE, Kirkland AFB, NM 87117
85. D. W. Bensen, Federal Emergency Management Agency, Research Division, 500 C Street, S.W., Washington, DC 20472
86. T. Bolt, ED-SD, U.S. Army Engineering, USAEDH, P.O. Box 1600, Huntsville, AL 35087
87. J. N. Bombardt, R&D Associates, 105 E. Vermijo Street, Suite 450, Colorado Springs, CO 80903
88. G. E. Brackett, Code H25, Navy Surface Weapons Center, 1091 New Hampshire Avenue, Silver Springs, MD 20903-5000
89. E. H. Brehm, Department GK/CN32, Brown, Boveri, and Cie, Aktiengesell Schaft, Postfach 351, D-6800 Mannheim 1, West Germany

90. F. C. Buchholz, Pacific Gas & Electric Co., 77 Beale Street, Room 2933, San Francisco, CA 94106
91. J. F. Buck, Wisconsin Electric Power Company, 231 W. Michigan, Milwaukee, WI 53201
92. L. M. Burrage, McGraw-Edison, P.O. Box 100, 11131 Adams Road, Franksville, WI 53126
93. H. S. Cabayan, Lawrence Livermore Laboratory, P.O. Box 5504, Livermore, CA 94550
94. F. L. Cain, Georgia Institute of Technology, Engineering Experiment Station, Atlanta, GA 30332
95. R. N. Carlile, Department of Electrical and Computer Engineering, University of Arizona, Tucson, Arizona 85721
96. I. J. Carney, Nuclear Survivability Organization, Boeing Aerospace Company, P.O. Box 3999, Seattle, WA 98124
97. V. L. Chartier, Bonneville Power Administration, P.O. Box 491-ER, Vancouver, WA 98666
98. K. K. Chen, Sandia National Laboratory, Drawer 1333, P.O. Box 5800, Kirkland AFB, NM 87185
99. H. E. Church, Aluminum Company of American, 1501 Alcoa Building, Pittsburgh, PA 15219
100. B. Cikotas, DNA/RAEE, 6801 Telegraph Road, Alexandria, VA 22310
101. C. F. Clark, Bonneville Power Administration, P.O. Box 3621, Portland, OR 97208
102. R. E. Clayton, Power Technologies, P.O. Box 1058, 1482 Erie Boulevard, Schenectady, NY 12301-1058
103. A. Clerici, Sanelmi, Via Pergolesi 25, 20124 Milano, Italy
104. H. W. Colborn, North American Electric Reliability Council, Research Park, Terhume Road, Princeton, NJ 08540-3573
105. D. E. Cooper, Southern California Edison Company, P.O. Box 800, 2244 Walnut Grove Avenue, Rosemead, CA 91770
106. R. Cortina, ENEL-Centro Ricerca, Automatica, VIA Volta 1, Cologno Monzese (MI), Italy
107. G. Dahlen, Royal Institute of Technology, S-100-44, Stockholm, Sweden

108. J. Darrah, Headquarters NORAD/G5, Peterson AFB, CO 80914
109. Defense Technical Information Center, Cameron Station, Alexandria, VA 22314
110. J. J. Dougherty, Electric Power Research Institute, P.O. Box 10412, Palo Alto, CA 94303
111. W. M. Druen, 8200 South Memorial Parkway, Suite D, Huntsville, AL 35802
112. J. C. Engimann, Commonwealth Edison, 1319 S. First Avenue, Maywood, IL 60153
113. D. M. Ericson, Jr., Sandia National Laboratory, Division 6414, Kirkland AFB, NM 87185
114. W. E. Ferro, Electric Research and Management, Inc., P.O. Box 235, Thomaston, ME 04861
115. W. G. Finney, Project Manager, Stanley Consultants, Inc., Stanley Building, Muscatine, IA 52761
116. M. Fitzgerald, MITRE Corp., P.O. Box 208, Bedford, MA 01730
117. F. Fisher, General Electric Corporation, Electric Utility Systems Engineering Department, Building 5, Room 306, Schenectady, NY 12345
118. P. B. Fleming, Science and Engineering Associates, Inc., Mariners Square, Suite 127, 1900 North Northlake Way, P.O. Box 31819, Seattle, WA 98103
119. R. Fullwood, Science Applications, Inc., 5 Palo Alto Square, Suite 200, Palo Alto, CA 94304
120. M. R. Gent, North American Electric Reliability Council, Research Park, Terhume Road, Princeton, NJ 08540-3573
121. S. M. Gillis, Economic and Public Policy, Department of Economics, Duke University, Durham, NC 27706
122. W. Graham, R&D Associates, P.O. Box 9695, Marina Del Rey, CA 90291
123. J. J. Grainger, 5004 Hermitage Drive, Raleigh, NC 27612
124. I. S. Grant, Power Technologies, Inc., 1482 Erie Blvd., Schenectady, NY 12305
125. A. R. Gritzke, U.S. Department of Navy, Theater Nuclear Warfare Project Office, Washington, DC 20360

126. J. Gut, Research Intitute for Protective Construction, Auf der Mauer 2, CH-8001 Zurich, Switzerland,
127. V. Guten, R-52, National Security Agency, Fort G. Mead, MD 20755
128. R. J. Harrington, George Washington University, Department of Electrical Engineering and Computing Science, Washington, DC 20052
129. M. F. Hebb, Florida Power Corp., P.O. Box 14042, Mail Code AB, St. Petersburg, FL 33733
130. M. H. Hesse, JEC 5008, Rennselear Polytechnic Institute, Troy, NY 12181
131. D. Higgins, JAYCOR, Santa Barbara Facility, P.O. Box 30281, 360 South Hope Avenue, Santa Barbara, CA 93105
132. D. W. Hilson, Tennessee Valley Authority, 1100 Chestnut Street, Tower 2, Chattanooga, TN 37402
133. F. C. Holdes, Pacific Gas & Electric Company, 3235-18th Street, San Francisco, CA 94110
134. W. S. Howington, Noranda Aluminum, Inc., P.O. Box 70, New Madrid, MO 63869
135. R. Hutchins, BDM Corporation, 1801 Randolph, S.W., Albuquerque, NM 87106
136. J. Hunt, Emergency Preparedness Administrator, San Diego Gas and Electric Company, P.O. Box 1831, San Diego, CA 92112
137. V. Inkis, Ontario Hydro, U7E1, 700 University Avenue, Toronto, Canada M5G1X6
138. Wasy1 Janischewskyj, Electrical Engineering Dept., University of Toronto, Toronto, Canada M5S1A4
139. H. P. Johnson, Georgia Power Company, 270 Peachtree Street, 11th Floor, Atlanta, GA 30303
140. V. K. Jones, Science and Engineering Associates, Inc., Mariners Square, Suite 127, 1900 North Northlake Way, P.O. Box 31819, Seattle, WA 98103
141. F. R. Kalhammer, Director, Energy Management and Utilization Division, Electric Power Research Institute, 3412 Hillview Avenue, P.O. Box 10412, Palo Alto, CA 94303
142. W. Karzas, R&D Associates, P.O. Box 9695, Marina Del Rey, CA 90291
143. K. W. Klein, Chief of Power Delivery Branch, Department of Energy, CE-143, Division of Electric Energy Systems, Forrestal Building, Room 5E-052, 1000 Independence Avenue, S.W., Washington, DC 20585

144. N. Kolcio, American Electric Power, 1 Riverside Plaza, Columbus, OH 43216
145. J. Labadie, IRT, 6800 Poplar Place, McLean, VA 22131
146. H. T. Lam, South Carolina Public Service Authority, 1 Riverwood Dr., Monks Corner, SC 29461
147. T. R. LaPorte, Professor, Political Science, Institute of Government Studies, University of California, 109 Moses Hall, Berkeley, CA 94720
148. R. C. Latham, Duke Power Company, P.O. Box 33189, Charlotte, NC 28242
149. A. Latter, R&D Associates, P.O. Box 9695, Marina Del Rey, CA 90291
150. J. S. Lawler, Department of Electrical Engineering, University of Tennessee, Knoxville, TN 37916
151. K. S. H. Lee, Dikewood Division of Kaman Science Corp., 2800 28th Street, Suite 3780, Santa Monica, CA 90405
- 152-161. J. R. Legro, Westinghouse Electric Corporation, Advanced Systems Technology, 777 Penn Center Boulevard, Pittsburgh, PA 15235
162. M. Lessen, Consulting Engineer, 12 Country Club Drive, Rochester, NY 14618
163. Library, JAYCOR, 205 S Whiting Street, Alexandria, VA 22304
164. J. Locasso, Rockwell International, 3370 Meraloma Avenue, P.O. Box 4192, Mail Code 031-BB17, Anaheim, CA 92803
165. C. L. Longmire, Mission Research Corporation, P.O. Drawer 719, Santa Barbara, CA 93102
166. W. C. Maklin, IRT Corporation, 6800 Poplar Place, McLean, VA 22101
167. R. M. Maliszewski, American Electric Power Service Corp., 1 Riverside Plaza, P.O. Box 16631, Columbus, OH 43216-6631
168. J. N. Mallory, Southern California Edison Co., P.O. Box 800, Rosemead, CA 91770
169. J. D. Martin, Harris Corporation, PRD Electronics Division, 6801 Jericho Turnpike, Syosset, NY 11791
170. P. S. Maruvada, Hydro-Quebec Institute of Research, 1800 Montee Ste-Julie, Varennes, Quebec, CANADA J0L2P0
171. R. G. McCormack, CERL, Corps of Engineers, P.O. Box 4005, Champaign, IL 61820
172. G. F. Meenaghan, Vice President for Academic Affairs and Dean of the College, The Citadel, Charleston, SC 29409

173. C. Menemenlis, University of Patras, Patras, Greece
174. A. S. Mickley, Philadelphia Electric Corp., 2301 Market Street, Philadelphia, PA 19101
175. I. N. Mindel, IIT Research Institute, 10 West 35th Street, Chicago, IL 60616
176. D. L. Mohre, Cajun Electric Power Corp., P. O. Box 15440, Baton Rouge, LA 70895
177. B. B. Mrowca, Baltimore Gas & Electric Co., P.O. Box 1475, Baltimore, MD 21203
178. K. Muller, IABG, Einsteinstrasse 20, 8012 Ottobrunn, West Germany
179. Este-M Murtha, Booz Allen and Hamilton, General Services Administration, 18th & F Streets, N.W., Washington, DC 10405
180. H. P. Neff, Department of Electrical Engineering, University of Tennessee, Knoxville, TN 37916
181. B. O. Nettles (Code 203), Naval Electronic Systems Engineering Center, Charleston, 4600 Marriott Drive, North Charleston, SC 29418
182. D. R. Nevius, North American Electric Reliability Council, Research Park, Terhume Road, Princeton, NJ 08540-3573
183. G. B. Niles, Baltimore Gas & Electric Company, Principal Eng. Room 1020, P.O. Box 1475, Baltimore, MD 21203
184. B. Noel, Los Alamos National Laboratory, Mail Station 5000, P.O. Box 1663, Los Alamos, NM 87545
185. B. Nowlin, Arizona Public Service Company, P.O. Box 21666, Phoenix, AR 85036
186. R. Oats, Atomic Weapons Research Establishment, Building D57, Aldermaston, Reading, RG74PR, England
187. G. Orrell, Dep. Associate Director for National Preparedness, Federal Emergency Management Agency, 500 C Street, S.W., Washington, DC 20555
188. L. Paris, University of Pisa, Via Diotisalvi 2, 56100 PISA
189. R. Parker, RDA, P.O. Box 9335, Albuquerque, NM 87119
190. R. Parkinson, Science Applications, Inc., 5150 El Camino Real, Suite B-31, Los Altos, CA 94022
191. A. Pigini, CESI-Via Rubahimo 59-Milano, Italy

192. J. B. Posey, Ohio Brass Co., 380 N. Main Street, Mansfield, OH 44903
193. M. Rabinowitz, Electric Power Research Institute, 3412 Hillview Avenue, P.O. Box 10412, Palo Alto, CA 94303
194. W. A. Radaski, Metatech Corp., 358 South Fairview Avenue, Suite E, Goleta, CA 93117
195. J. J. Ray, Bonneville Power Administration, P.O. Box 3621, Portland, OR 97208
196. T. J. Reed, Westinghouse Electric Corporation, Advanced Systems Technology, 777 Penn Center Boulevard, Pittsburgh, PA 15235
197. R. L. Retallach, American Electric Power, 1 Riverside Plaza, Columbus, OH 43216
198. J. Richardson, National Academy of Science, 2101 Constitution Avenue, Washington, DC 20418
199. F. Rosa, Nuclear Regulatory Commission, Division of Systems Integration, MS P1030, Washington, DC 20555
200. D. H. Sandell, Harza Engineering Co., 150 South Wacker Drive, Chicago, IL 60606
201. J. A. Sawyer, MITRE Corp., MS-H070, P.O. Box 208, Bedford, MA 01703
202. R. A. Schaefer, Metatech Corp., 20 Sunnyside Avenue, Suite D, Mill Valley, CA 94941
203. M. Schechter, A.D.A., P.O. Box 2250(81), Haifa, 31021, Israel
204. H. Singaraju, Air Force Weapons Laboratory, Kirkland AFB, NM 87117
205. A. C. Smith, Jr., Beam Research Program, Lawrence Livermore National Laboratory, P.O. Box 808, Livermore, CA 94550
206. J. C. Smith, 1 Adams Avenue, P.O. Box 44, Canonsburg, PA 15317
207. R. Smith, DNA, RAEE, 6801 Telegraph Road, Alexandria, VA 22310
208. W. Sollfrey, RAND Corp., 1700 Main Street, Santa Monica, CA 90406
209. H. Songster, Electric Power Research Institute, Electrical Systems Division, 3412 Hillview Avenue, P.O. Box 10412, Palo Alto, CA 94303

210. G. K. Soper, Defense Nuclear Agency, Washington, DC 20305
211. S. Spohn, DB4C2, Defense Intelligence Agency, Washington, DC 20301
212. J. R. Stewart, Power Technologies, Inc., P.O. Box 1058, 1482 Erie Boulevard, Schenectady, NY 12301-1058
213. R. L. Sullivan, Department of Electrical Engineering, College of Engineering, University of Florida, Gainesville, FL 32611
214. I. O. Sunderman, Lincoln Electric System, P.O. Box 80869, Lincoln, NE 68501
215. R. W. Sutton, Science Applications, Inc., 1710 Goodridge Drive, P.O. Box 1303, McLean, VA 22102
- 216-225. F. M. Tesche, LuTech, Inc., 3742 Mt. Diablo Boulevard, Lafayette, CA 94549
226. L. Thione, CESI-Via Rubattino 54 20734, Milano, Italy
227. R. J. Thomas, 302 Phillips Hall, Cornell University, Ithaca, NY 14853
228. R. Torres, BDM Corporation, 1801 Randolph, S.W., Albuquerque, NM 87106
229. W. Tyler, NT, Kirkland AFB, NM 87117
230. M. A. Uman, Department of Electrical Engineering, University of Florida, Gainesville, FL 32611
231. E. F. Vance, Route 3, Box 268A, Fort Worth, TX 76140
232. D. R. Volzka, Wisconsin Electric Power Company, 231 West Michigan Street, Milwaukee, WI 53201
233. J. Vora, Nuclear Regulatory Commission, MS 5650 NL, Washington, DC 20555
234. C. D. Whitescarber, Martin Marietta Orlando Aerospace, Sandlake Road Complex (SLRC), Mail Point 399, P.O. Box 5837, Orlando, FL 32855
235. W. P. Wigner, 8 Ober Road, Princeton, NJ 08540
236. M. W. Wik, Forsvarets Materielverk, S-11588 Stockholm, Sweden
237. C. B. Williams, IRT Corp., 7650 Convoy Court, P.O. Box 80817, San Diego, CA 92138

- 238. W. H. Williams, Division Manager, AT&T Information Systems, Building 83, Room 1B23, 100 Southgate Parkway, Morristown, NJ 07960
- 239. D. D. Wilson, Power Technologies, Inc., P.O. Box 1058, Schenectady, NY 12301
- 240. U. P. Wissmann, AEG-Telefunken, General Electric Company, 1 River Road, Building 36-444, Schenectady, NY 12345
- 241. H. W. Zaininger, Zaininger Engineering Company, 3408 Vance Court, San Jose, CA 95132
- 242. Institute for Energy Analysis, ORAU - Library
- 243. Assistant Manager for Energy Research & Development, DOE/ORO Oak Ridge, TN 37830
- 244-897. Given for distribution as shown in DOE/TIC-4500 under Category UC-97a,b,c (Electric Energy Systems)